

INFORMATION TO USERS

This material was produced from a microfilm copy of the original document. While the most advanced technological means to photograph and reproduce this document have been used, the quality is heavily dependent upon the quality of the original submitted.

The following explanation of techniques is provided to help you understand markings or patterns which may appear on this reproduction.

1. The sign or "target" for pages apparently lacking from the document photographed is "Missing Page(s)". If it was possible to obtain the missing page(s) or section, they are spliced into the film along with adjacent pages. This may have necessitated cutting thru an image and duplicating adjacent pages to insure you complete continuity.
2. When an image on the film is obliterated with a large round black mark, it is an indication that the photographer suspected that the copy may have moved during exposure and thus cause a blurred image. You will find a good image of the page in the adjacent frame.
3. When a map, drawing or chart, etc., was part of the material being photographed the photographer followed a definite method in "sectioning" the material. It is customary to begin photoing at the upper left hand corner of a large sheet and to continue photoing from left to right in equal sections with a small overlap. If necessary, sectioning is continued again – beginning below the first row and continuing on until complete.
4. The majority of users indicate that the textual content is of greatest value, however, a somewhat higher quality reproduction could be made from "photographs" if essential to the understanding of the dissertation. Silver prints of "photographs" may be ordered at additional charge by writing the Order Department, giving the catalog number, title, author and specific pages you wish reproduced.
5. PLEASE NOTE: Some pages may have indistinct print. Filmed as received.

Xerox University Microfilms

300 North Zeeb Road
Ann Arbor, Michigan 48106

75-542

BUCKLE, David Charles, 1941-
NEGATIVE MUON DEPOLARIZATION IN LIQUID
HELIUM AND SEVERAL HYDROCARBONS.

The College of William and Mary in Virginia,
Ph.D., 1974
Physics, elementary particles

Xerox University Microfilms, Ann Arbor, Michigan 48106

**NEGATIVE MUON DEPOLARIZATION
IN LIQUID HELIUM AND SEVERAL HYDROCARBONS**

**A Dissertation
Presented to
The Faculty of the Department of Physics
The College of William and Mary in Virginia**

**In Partial Fulfillment
Of the Requirements for the Degree of
Doctor of Philosophy**

**by
David C. Buckle**

1974

APPROVAL SHEET

This dissertation is submitted in partial fulfillment of
the requirements for the degree of

Doctor of Philosophy



David C. Buckle

Approved, August 1974



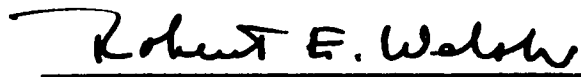
Robert T. Siegel




John B. Delos



William J. Kossler



Robert E. Welsh



Richard L. Kiefer
Department of Chemistry

TABLE OF CONTENTS

	Page
ABSTRACT	vi
I. THEORY	2
A. Introduction	2
B. Muon Decay	3
C. Muon Spin Precession	7
D. Depolarization of the Muon Spin	10
1. Slowing to $v \approx ac$	10
2. Initial Capture and Cascade to the state $n_0 l_0 j_0$	11
3. Atomic Cascade From $n_0 l_0 j_0$ to 1s State	14
E. Further Depolarization Mechanisms	16
1. Depolarization Due to Nuclear Spin	16
2. Electron Shell	18
3. Formation of Mesic Molecular Systems	20
II. EXPERIMENTAL METHOD	21
A. General	21
B. Counters	23
1. Plastic Scintillators	23
2. Helium Counter	24
C. Beam Selection	24
D. Logic and Electronics	25
1. Fast Timing	25
2. Slow Logic or "Digitron"	27

E.	Magnetic Field	28
F.	Target Configurations	29
G.	Data Accumulation	30
III.	HELIUM TARGET - COUNTER	32
A.	Introduction	32
B.	Dewar Development	32
1.	Target Vacuum Seals	33
2.	Filling Procedure	34
C.	Counter Operation	35
IV.	DATA ANALYSIS	38
A.	Introduction	38
1.	Data Presentation	39
2.	Non-Linear Multiparameter Analysis	39
3.	Linear Multiparameter Analysis	40
4.	Frequency Search Analysis	41
5.	Time Dependence of Asymmetry	42
6.	Corrections to Asymmetry	43
7.	Analysis of Random Data	43
B.	Carbon and Magnesium	44
1.	Lifetimes	44
2.	Multiparameter Non-Linear Analysis	46
3.	Frequency Search-Contour Plot	47
4.	Asymmetry Results	48

C.	Hydrocarbons and Water	49
1.	Lifetimes	49
2.	High Fields	49
3.	Time Dependence of Asymmetry - High Fields	51
4.	Low Fields	52
D.	Liquid Oxygen	55
1.	Lifetimes and Stainless Steel Background	55
2.	Frequency Search - Asymmetry Results	57
E.	Liquid Helium	57
1.	Lifetimes	59
2.	Frequency Search	59
3.	Asymmetry Results	59
V.	DISCUSSION OF RESULTS	61
A.	Summary	61
B.	Liquid Helium	64
C.	Hydrocarbons and Water	71
D.	Liquid Oxygen	75
E.	Conclusions	76
VI.	TABLES	78
VII.	APPENDICES	86
VIII.	REFERENCES	96
IX.	ACKNOWLEDGEMENTS	99
X.	FIGURES	100

ABSTRACT

The asymmetry a_0 in the angular distribution of electrons from the decay of polarized negative muons bound in atomic states has been measured in several pure substances: C, Mg, O, and He; in H₂O; and in several hydrocarbons: toluene, polyethylene, paraffin, and plastic scintillant. The angular distribution was sampled by precessing the muon magnetic moment and observing the time dependence of the decay distribution given by $N(t) = N_0 e^{-\lambda t} (1 + a_0 \cos \omega t)$.

Measurements made at the Larmor precession frequency of the muon spin in C and Mg gave:

$$a_0^C = -0.048 \pm 0.003$$

$$\text{and } a_0^{Mg} = -0.044 \pm 0.004.$$

These results are in agreement with theoretical predictions. The result for liquid He was consistent with complete depolarization of the muon spin, in disagreement with theoretical predictions, and was:

$$a_0^{He} = -0.003 \pm 0.005.$$

The hydrocarbons and H₂O all yielded values for a_0 of approximately $\frac{1}{2}$ the value measured in C. This represents the first observation of reduced residual polarization in these hydrocarbons. The results are compared with theoretical predictions based on the formation of large mesic molecules in the muon atomic capture process. Qualitative agreement is found. Several depolarizing mechanisms for muons in liquid He are discussed and compared to the experimental result.

A search was also made for evidence of the formation of a spin coupled system of an atomically bound muon and electron in the total angular momentum $F = S_e + S_\mu = 1$, $m_F = 1$ state. Measurements were made in liquid He, liquid O₂, polyethylene, toluene, and plastic scintillant. No asymmetry was seen, for any target, which could be attributed to the formation of this system.

**NEGATIVE MUON DEPOLARIZATION
IN LIQUID HELIUM AND SEVERAL HYDROCARBONS**

I. THEORY

A. Introduction

The behavior of negative muons (μ^-) in condensed matter is of interest for several reasons. The spin-dependent weak interaction processes can be investigated through μ^- nuclear capture reactions if the μ^- spin orientation before capture is known. The magnetic moments of μ^- atomic systems might be used as probes to study basic molecular structures. For this reason experiments have been performed to measure the residual polarization of μ^- bound in muonic atoms. These measurements have indicated a strong dependence on molecular processes which occur at the time of atomic capture. Measurements made in liquid He^{1,2} have shown the μ^- to be completely depolarized on reaching the ground state of the He muonic atom. The predictions made by Shmushkevich³ and Mann and Rose⁴ for μ^- stopping in targets with zero nuclear spin were found to be correct for several metals. The straightforward atomic cascade depolarization mechanisms in liquid He, the simplest available spin zero nucleus, cannot account for this total depolarization. This experiment was undertaken to investigate some possible mechanisms which might explain this result. In this section we discuss the basic decay process from which the μ^- polarization can be determined, and several mechanisms which lead to depolarization of the μ^- spin.

In Section II and in Section III the experimental procedure is described. The analysis procedure for the data is presented in Section IV, and Section V is a discussion of the results of our experiment as they relate to several depolarizing mechanisms.

Throughout this paper frequent reference is made to the precession of the "free" muon magnetic moment. This is defined as the condition in which the μ^- is free of any magnetic influence other than the externally applied magnetic field. The magnetic moments of the μ^+ and μ^- are assumed to have the same magnitude.

B. Muon Decay

The postulation by Lee and Yang⁵ that the weak interaction processes of β decay and muon (μ) decay did not conserve parity was followed by prompt confirmation in experiments by Wu, et al.,⁶ and by Garwin, et al.⁷ The β decay ($n \rightarrow p + e^- + \bar{\nu}_e$) of oriented nuclei⁶ and the muon decay process ($\mu^\pm \rightarrow 2\nu + e^\pm$)⁷ both gave a strong spatial asymmetry about the spin direction of the decaying particle. Lee and Yang proposed that the neutrinos (ν) accompanying these processes were representable by two component spinors. These two components are each characterized by a definite value for the spin projection along the momentum vector. This quantity, referred to as the helicity of the particle, is either -1 or $+1$, depending on whether the assignment of particle or antiparticle is made for a given neutrino. Measurements of the polarization of electrons from β decay and of the neutrino helicity by Goldhaber, Grodzins and Sunyar^{8,9} determined the presently accepted

helicity assignments for the leptonic particles. Feynman and Gell-Mann¹⁰ formulated the presently accepted form of the interaction as a vector (V) and Axial vector (A) interaction in which the coupling constants have opposite sign (V-A). Burgy, et al.,¹¹ measured the correlation between the γ , e^- and recoil protons from polarized neutron decay and the results were consistent with the V-A assignment. The leptonic portions of the wave functions involved in the weak decay process are assumed to participate only through their left handed components. We define the helicity projection operators as,

$$\begin{aligned}\gamma^+ &= 1/2 (1 + i\gamma_5) \\ \text{and } \gamma^- &= 1/2 (1 - i\gamma_5),\end{aligned}$$

where $\gamma^{+(-)}$ is the right handed (left handed) projection operator, and

$$i\gamma_5 = \begin{pmatrix} 1 & 0 & 0 & 0 \\ 0 & 1 & 0 & 0 \\ 0 & 0 & -1 & 0 \\ 0 & 0 & 0 & -1 \end{pmatrix}.$$

The familiar commutation relations for the gamma matrices are given by,

$$\begin{aligned}\gamma_5 \gamma_\mu &= -\gamma_\mu \gamma_5 \\ \gamma_\mu \gamma_\nu &= \gamma_\nu \gamma_\mu.\end{aligned}$$

The μ^- decay interaction is described by the characteristic matrix element,

$$\langle \bar{\chi}_\nu^t | 0_1 | \chi_e^t \rangle \langle \bar{\chi}_\mu^t | 0_1 | \chi_\nu^t \rangle,$$

where χ^L is the left handed projection of the particle wave function,

$$\chi_{\mu}^L = \gamma^{-} \psi_{\mu},$$

and O_1 is the interaction operator. The commutation relations result in the survival of only the vector $O_1 = g_V \gamma_{\mu}$ and axial vector $O_2 = g_A \gamma_5 \gamma_{\mu}$ forms of the interaction. The predicted form of the e^{-} spatial distribution from μ^{-} decay at rest is given by,

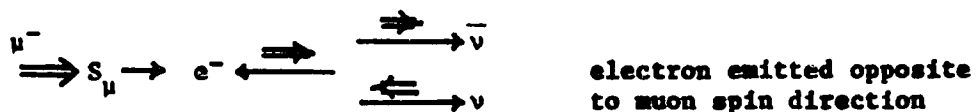
$$dN_e = 2x^2 \{ (3-2x) - \xi(1-2x)\cos\theta \} \cdot dx d\Omega_e / 4\pi.$$

Here the electron mass is neglected and x is the ratio of the electron energy to the maximum allowed energy in the decay process $\mu^{-} \rightarrow e^{-} + \bar{\nu}_e + \nu_{\mu}$. θ is the angle between the muon spin and the electron momentum direction, and ξ is given by,

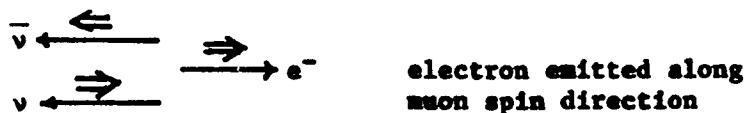
$$\begin{aligned} \xi &= (g_A g_V^* + g_V g_A^*) / (|g_A|^2 + |g_V|^2) \\ &= -1, \text{ for V-A, } (g_A = -g_V). \end{aligned}$$

This angular dependence can be understood simply by observing the relative spin orientations when the electron obtains maximum energy.

Two possibilities are diagramed below.



or



The helicity of the e^- can now be seen to be the important factor leading to the asymmetry in the decay process. Since the two ν 's are emitted parallel in the maximum energy decay, their spins are anti-aligned and therefore the e^- must carry the original μ^- spin in order to conserve angular momentum. Electrons emitted in the direction with the μ^- spin must therefore have a positive helicity or be right-handed, while e^- emitted opposite to the μ^- spin will be left-handed. Since the e^- is a particle it has a negative helicity of $-v/c$. Therefore the e^- will be emitted preferentially opposite to the μ^- spin direction. The e^- distribution from the decay of μ^- at rest having polarization P is then given by,

$$dN_e = 2x^2 \{ (3-2x) + P(1-2x) \cdot \cos\theta \} dx d\Omega_e / 4\pi. \quad (1)$$

A review of weak interaction processes is given by Wu and Moszkowski¹² and by DeBenedetti,¹³ among many others.

Under experimental conditions a detection threshold x_0 for the electron energy existed such that $x_0 \leq x \leq 1$. In addition, the detection element for e^- was of finite dimensions. When equation (1) is integrated over all detectable energies, $x_0 \leq x \leq 1$, and averaged over the detection solid angle the expected distribution becomes:

$$N(\bar{\theta}) = N_0(1 + a' \cdot \cos\bar{\theta}), \quad (2)$$

where $a' = F(x_0) \cdot F(\Omega_e) \cdot a_0$. Here $F(x_0)$ is a correction due to non zero threshold ($F(x_0) = 1$ for $x_0 = 0$), $F(\Omega_e)$ is the reduction due to

finite solid angle, and $a_0 = P\delta$, where $\delta = -1/3$ is the result for integration from $0 \leq x \leq 1$, a point detector, and $P = 1$. N_0 is the fraction of the μ^- decay events which will be seen by the detection system, and $\bar{\theta}$ is the angle between the μ^- polarization direction and the center of the detection system.

C. Muon Spin Precession

The interaction of the magnetic moment of a μ^- at rest in a static magnetic field \vec{H}_0 is given by the simple interaction Hamiltonian,

$$H_{int} = \vec{\mu}_\mu \cdot \vec{H}_0$$

$$\text{where } \vec{\mu} = \frac{-e\hbar}{m_\mu c} \cdot \vec{S}_\mu = -\gamma\hbar\vec{S}_\mu.$$

The energy eigenvalues are:

$$E_m = -\gamma\hbar H_0 m.$$

Since the μ^- spin can have only two orientations there are just two eigenvalues:

$$E^+ = \frac{-\gamma\hbar H_0}{2} = \frac{-\hbar\omega}{2}$$

$$E^- = \frac{\gamma\hbar}{2} \cdot H_0 = \frac{\hbar\omega}{2},$$

where $\omega = \gamma H_0$.

The time dependent wave function for a μ^- of arbitrary polarization is a sum of the eigenstates $\chi_{\frac{1}{2}}$ and $\chi_{-\frac{1}{2}}$.

$$\psi(t) = a \cdot \chi_{\frac{1}{2}} e^{\frac{i\omega t}{2}} + b \chi_{-\frac{1}{2}} e^{\frac{-i\omega t}{2}}.$$

The expectation value for the components of the spin are then given by:

$$\begin{aligned} \langle \sigma_x \rangle &= \frac{1}{2} \{ \bar{\psi}(t) | \sigma^+ + \sigma^- | \psi(t) \} \\ \langle \sigma_y \rangle &= \frac{1}{2} i \{ \bar{\psi}(t) | \sigma^+ - \sigma^- | \psi(t) \} \\ \text{and } \langle \sigma_z \rangle &= \{ \bar{\psi}(t) | \sigma_z | \psi(t) \}. \end{aligned}$$

Here σ^+ and σ^- are the familiar step up and step down operators defined as:

$$\begin{aligned} \sigma^+ &= \sigma_x + i\sigma_y, \\ \text{and } \sigma^- &= \sigma_x - i\sigma_y. \end{aligned}$$

When these operate on the χ spinors we have:

$$\begin{aligned} \sigma^+ \chi_{\frac{1}{2}} &= 0, \\ \sigma^+ \chi_{-\frac{1}{2}} &= 2\chi_{\frac{1}{2}}, \\ \sigma^- \chi_{\frac{1}{2}} &= 2\chi_{-\frac{1}{2}}, \\ \sigma^- \chi_{-\frac{1}{2}} &= 0. \end{aligned}$$

The result is:

$$\begin{aligned}\langle \sigma_x \rangle &= (a^* b e^{-i\omega t} + a b^* e^{i\omega t}) \\ &= 2\text{Re}(a^* b e^{-i\omega t})\end{aligned}$$

$$\begin{aligned}\langle \sigma_y \rangle &= (a^* b e^{-i\omega t} - a b^* e^{i\omega t}) \\ &= 2\text{Im}(a^* b e^{-i\omega t})\end{aligned}$$

$$\text{and } \langle \sigma_z \rangle = |a|^2 - |b|^2.$$

Normalisation requires that $|a|^2 + |b|^2 = 1$. If we represent the constants as $a = a e^{i\alpha}$ and $b = b e^{i\beta}$ where a , b , α , and β are real, the expectation values become:

$$\langle \sigma_x \rangle = 2ab \cdot \cos(\beta - \alpha - \omega t)$$

$$\langle \sigma_y \rangle = 2ab \cdot \sin(\beta - \alpha - \omega t)$$

$$\text{and } \langle \sigma_z \rangle = a^2 - b^2.$$

It is easily seen that these are the components of a vector of unit magnitude precessing about the z axis with an angular frequency $\omega_\mu = \gamma H_0$. For the free muon $\gamma = \frac{e}{m_\mu c} = 8.506 \cdot 10^4$ radians/(gauss sec.).

The angle $\bar{\theta}$ in equation (2) is now time dependent. If the beam polarization direction at $t = 0$ is such that $\bar{\theta} = \phi_0$ then we set $(\beta - \alpha) = \phi_0$ and we have, putting the x direction along the detection axis:

$$\cos \bar{\theta} = \cos(\phi_0 + \omega t).$$

The remaining time dependence for the distribution results from the disappearance rate of the muon governed by the processes of nuclear

capture and muon decay.

The time dependent distribution is then given by:

$$\frac{1}{\lambda_d} \cdot \frac{dN_e(t)}{dt} = N_0 e^{-\lambda t} \{1 + a' \cdot \cos(\omega t + \phi)\}. \quad (3)$$

Here λ_d is the muon decay rate and λ is the total disappearance rate

$$\lambda = \lambda_d + \lambda_{\text{capture}}.$$

D. Depolarization of the Muon Spin

Shmushkevich⁶ and Mann and Rose⁴ dismissed the phenomena leading to muonic atom formation and calculated the expected μ^- polarization in the $1s$ atomic state. We follow the arguments of Shmushkevich. When polarized μ^- are slowed and brought to rest in matter the process can be separated into several stages. These include (1) the slowing of the μ^- from $v = c$ to $v = ac$; (2) initial capture of the μ^- into a bound atomic level characterized by quantum numbers n_0 , l_0 , and j_0 ; and (3) the atomic cascade of the μ^- to the ground state ($1s$) of the target atom.

1. Slowing to $v = ac$

Ford and Mullin¹⁴ demonstrated that the μ^- undergoes very little depolarization during stage 1 where the primary energy loss mechanism is one of Coulomb scattering and ionization of the surrounding atoms. The μ^- reaches an energy low enough so that no further ionizations are possible. Then through elastic scattering the μ^- reaches thermal

energies. The momentum direction becomes random while the spin direction is unaltered. These energy loss mechanisms are due to electric fields only and do not significantly affect the polarization.

2. Initial Capture and Cascade to the state n_0, l_0, j_0

At this point the μ^- will fall into a bound state of the muonic atom with the simultaneous Auger ejection of one of the outer atomic electrons. The initial level n_1, l_1, j_1 is assumed to be populated on a statistical basis where the probability P of forming an initial state of orbital angular momentum l_1 is, $P(l_1) = 2l_1 + 1$. The μ^- then makes rapid Auger transitions to the level n_0, l_0, j_0 where the following condition holds:

$$\Delta_{n_0 l_0} > \Gamma_{n_0 l_0} \quad (4)$$

Here $\Delta_{n_0 l_0}$ is the fine structure splitting of the state $n_0 l_0$ and $\Gamma_{n_0 l_0}$ is the total width or rate out of the state for all processes. For He and C this occurs at a principal quantum number $n_0 = 5, 6$. The μ^- is not considered to be depolarized during the previous transitions to this level. At this point following Shmushkevich³ we write the wave function for the bound muon as:

$$\begin{aligned} \psi_0 &= \sum_m a_m \cdot \phi_{n_0 l_0} \cdot \chi_{l_2} \\ &= \sum_{j_0, m} a_m \cdot C_{l_0 m, l_2}^{j_0, m+l_2} \cdot \phi_{n_0, l_0, j_0, m+l_2} \end{aligned}$$

Here $\phi_{n_0 l_0 m}$ is the mesic wave function for angular momentum l and principal quantum number n_0 and χ is the spin part of the wave function.

The total angular momentum j_0 has the values $j_0 = l_0 \pm \frac{1}{2}$ and,

$$\phi_{n_0 l_0 j_0 m \pm \frac{1}{2}} = \sum_{r\lambda} \cdot C_{l_0 r, \frac{1}{2}}^{j_0 m \pm \frac{1}{2}} \cdot \phi_{n_0 l_0 r} \cdot \chi_\lambda$$

is the mesic atomic wave function with the quantum numbers $n_0 l_0 j_0$ and $m_j = m \pm \frac{1}{2}$. If the condition in equation (4) is met then the states $j_0^+ = l_0 + \frac{1}{2}$ and $j_0^- = l_0 - \frac{1}{2}$ may be considered separately. We make use of the randomness of the initial angular momentum in assuming that all values of m are equally probably and obtain the probability P_{j_0} of forming a state with a given value of j_0 .

$$P_{j_0} = \frac{2j_0 + 1}{2(2l_0 + 1)}$$

$$= P_{j_0}^+ = \frac{l_0 + 1}{2l_0 + 1} \text{ for } j_0 = l_0 + \frac{1}{2} \quad (5)$$

$$\text{and } = P_{j_0}^- = \frac{l_0}{2l_0 + 1} \text{ for } j_0 = l_0 - \frac{1}{2}.$$

We now compute the mean value $\langle \sigma_z \rangle$ for a state with a definite value of j_0 and obtain:

$$\langle \sigma_z \rangle_{n_0 l_0 j_0} = \frac{1}{P_{j_0}} \cdot \sum_{\substack{m m' \\ r r' v v'}} \cdot a_m a_{m'} \cdot C_{l_0 m, \frac{1}{2}}^{j_0 m \pm \frac{1}{2}} \cdot C_{l_0 m', \frac{1}{2}}^{j_0 m' \pm \frac{1}{2}} \cdot C_{l_0 r, \frac{1}{2}}^{j_0 m \pm \frac{1}{2}} \cdot C_{l_0 r', \frac{1}{2}}^{j_0 m' \pm \frac{1}{2}} \langle v' | \sigma_z | v \rangle.$$

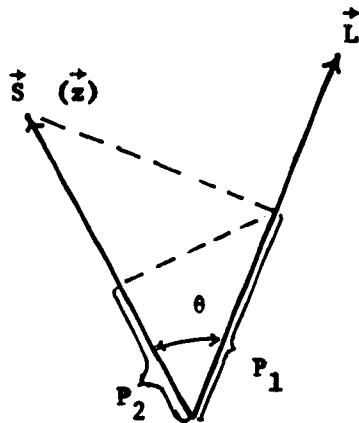
Summation over the magnetic quantum numbers yields:

$$\langle \bar{\sigma}_z \rangle_{n_0 l_0 j_0} = \frac{2l_0 + 3}{3(2l_0 + 1)} \text{ for } j_0 = l_0 + \frac{1}{2} \quad (6)$$

$$\frac{2l_0 - 1}{3(2l_0 + 1)} \text{ for } j_0 = l_0 - \frac{1}{2};$$

and for large l_0 this is approximately $1/3$ for both j_0^+ and j_0^- .

This is seen classically by observing the following vector diagram:

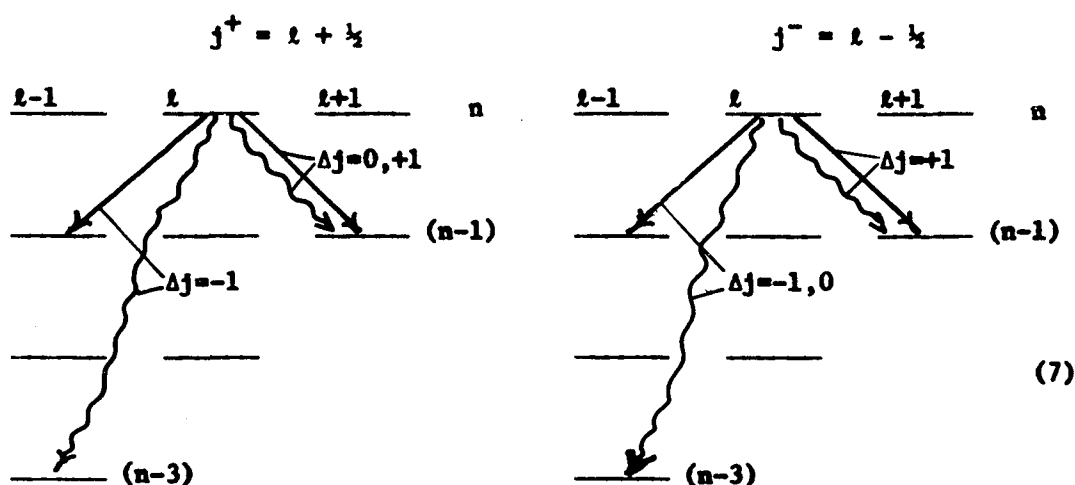


where P_1 is the projection of the spin vector onto the angular momentum vector \vec{L} , and P_2 is the projection of P_1 back onto the original spin direction which is taken as the z axis. The muon spin will precess about the angular momentum vector \vec{L} preserving the projection $P_1 = |S| \cos \theta$. The polarization is the projection $P_2 = P_1 \cos \theta = |S| \cos^2 \theta$ back onto the original z axis, averaged over all possible orientations of the

angular momentum vector \vec{L} . Since $\overline{(\cos^2 \theta)} = 1/3$, the resulting polarization is given by $|S|/3$ or $1/3$. This is the limit of equation (6) for large values of l_0 .

3. Atomic Cascade From $n_0 l_0 j_0$ to $1s$ State

Once the condition given in equation (4) is met the fine structure splitting allows depolarizing transitions to occur. To illustrate some of the possible transitions the following level diagram is presented:



In Auger transitions, shown by the straight arrows, the most probable transition is to lower l and $\Delta n = -1$. For the radiative process the most probable transition is to the lowest possible final principal quantum number n or a so called "circular orbit". We deal first with the states having $j^+ = l + \frac{1}{2}$. It is seen that for the most probable

transitions the only allowed value for Δj is $\Delta j = -1$. Such a transition therefore will preserve the projection of the spin angular momentum and not depolarize the μ^- . For transitions to the right or $\Delta l = +1$, however, there exists the possibility of change in the spin projection in going to an allowed final state ($\Delta j = 0$, transition). Such transitions will partially depolarize the muon. These transitions with $\Delta l = +1$ occur with low probability, less than 10% for both Auger and radiative processes except for high p states and s states. For states with $j^- = l - \frac{1}{2}$, however, the most probable transitions now include possible transitions with $\Delta j = 0$. Shmushkevich has defined a polarization parameter β_k which represents the polarization which remains after a given cascade path k.

$$\beta_k = \prod P_{n_0 n_1} \cdot P_{n_1 n_2} \cdots P_{n_{i-1} n_i}$$

where $P_{n' n''}$ is the probability for a given transition of maintaining the spin projection at its initial value. Clearly in a particular product chain the later $P_{n'' n'''}$ can be dependent on what transitions have preceded. For the most part it is seen, however, that those states with $j^+ = l + \frac{1}{2}$ will follow paths k where β_k^+ is approximately 1 since the most probable transitions maintain the spin projection, while transitions from states with $j = l - \frac{1}{2}$ have low values of β_k^- of approximately 0. We then have from equations (5) and (6):

$$\begin{aligned}
 P &= p_{j_0}^+ \langle \bar{\sigma}_z \rangle_{n_0 l_0 j_0^+} \cdot \beta_k^+ + p_{j_0}^- \langle \bar{\sigma}_z \rangle_{n_0 l_0 j_0^-} \cdot \beta_k^- \\
 &= \frac{l_0+1}{2l_0+1} \cdot \frac{(2l_0+3)}{3(2l_0+1)} = 1/6 \cdot \frac{(2l_0+2)(2l_0+3)}{(2l_0+1)^2},
 \end{aligned} \tag{8}$$

which approaches 1/6 for large l_0 .

Measurements were made by Ignatenko, et al.,^{15,16} of the μ^- residual polarization for the substances C, Mg, Zn, Cd, Pb, S and H₂O which gave results for a_0 of approximately -0.05 in agreement with the prediction (8). A result was obtained for the nuclear spin $I = \frac{1}{2}$ target of P. The result was $a_0 = 0.025$ which is explained by the muon-nuclear spin hyperfine interaction.

E. Further Depolarization Mechanisms

The preceding discussion of depolarization caused by fine structure interactions and initial capture should be applicable for all atoms of arbitrary nuclear spin. The discussion here follows closely those given by H. Uberall¹⁷ and E. Lubkin¹⁸ for systems of total angular momentum $F = I \pm \frac{1}{2}$.

1. Depolarization Due to Muon Interaction with Nuclear Spin

For a muon arriving in the K shell the probability of forming one of the two hyperfine states, $F^+ = I + \frac{1}{2}$ or $F^- = I - \frac{1}{2}$, can be found from

$$N_+(m_F) = \frac{I + m_F + 1/2}{(2I + 1)^2} \quad \text{and} \quad N_-(m_F) = \frac{I - m_F + 1/2}{(2I - 1)^2} \quad \text{such that,}$$

$$N_+ = \sum_{m_F} N_+(m_F) = \frac{I + 1}{(2I + 1)},$$

$$N_- = \sum_{m_F} N_-(m_F) = \frac{I}{(2I + 1)},$$

and $N_+ + N_- = 1$. Here N_+ includes all states with $F = I + 1/2$ and N_- includes all states with $F = I - 1/2$. The polarization of the spin in either state is given by:

$$P_+ = \frac{1}{3} \cdot \frac{2I + 3}{2I + 1}, \text{ for } F = I + \frac{1}{2},$$

$$\text{and } P_- = \frac{1}{3} \cdot \frac{2I - 1}{2I + 1}, \text{ for } F = I - \frac{1}{2}.$$

The magnetic moments of the two states are given by:

$$\mu_+ = \mu_\mu + \mu_N,$$

$$\text{and } \mu_- = - \frac{2I - 1}{2I + 1} \left(\mu_\mu - \frac{I + 1}{I} \cdot \mu_N \right).$$

The two states will therefore be characterized by two different gyro-magnetic ratios, $h\gamma = \mu/F$:

$$h\gamma_+ = \frac{1}{I + 1/2} \left(\mu_\mu + \mu_N \right)$$

$$\text{and } h\gamma_- = - \frac{1}{I + 1/2} \left(\mu_\mu - \frac{I + 1}{I} \cdot \mu_N \right).$$

For nuclei with zero nuclear spin only the γ_+ survives and $N_+ = 1$ (trivial case of no hyperfine interaction) and we expect the final polarization to be the one obtained in Section I-D with

$$\gamma_+ = \frac{2\mu}{\hbar} = 8.506 \cdot 10^4 \text{ radians/(gauss sec.)}$$

For nuclear spin $I = \frac{1}{2}$, the state of total angular momentum $F = 0$ is completely depolarized. For $F = 1$, $m_F = 1$ the polarization P_+ is $2/3$ and the net polarization is $N_+P_+ + N_-P_- = \frac{1}{2}$ and this state should precess with a gyromagnetic ratio of:

$$\begin{aligned} \gamma_{\hbar} &= \mu_{\mu} + \mu_N \\ &= \mu_{\mu} + \frac{m_{\mu}}{m_N} \cdot \mu_{\mu} \approx \mu_{\mu} \end{aligned}$$

and $P = 1/12$ where we assume that the interaction only occurs in the ground state.

2. Electron Shell

We are interested here primarily in liquid He which is the simplest zero spin nucleus available to us. The possibility that a muonic He atom might recapture an e^- is unlikely because of binding energy considerations. The e^- on neighboring He atoms are bound four times more strongly than an e^- bound to the proton-like $(\text{He } \mu^-)^+$ ion would be. However, should this system form, it might be possible to observe a

spin coupling between the unpaired e^- spin and the μ^- spin.¹⁹ If such a system were to be formed the formalism presented above can be applied; by setting $I = s_e = \frac{1}{2}$ and $\mu_N = \mu_e$ we obtain:

$$P = \frac{1}{2}$$

$$\text{and } \gamma_+ = \frac{\mu_\mu + \mu_e}{\hbar} = \frac{\mu_e}{\hbar} \cdot \left(1 + \frac{m_e}{m_\mu}\right).$$

In He one would not expect this system to form and other explanations for the measured lack of residual polarization in liquid He¹ must be found. The formation of muonic molecular ions like $\text{He}(\mu^- \text{He})^+$, suggested by Hughes,²⁰ might cause disturbances in the μ^- polarization during collisions with other He atoms which are not explained simply as in the hyperfine case.

In insulating materials containing C it might be difficult for the C atom to be resupplied with electrons after the Auger ejection of those available in the molecule. If a single e^- is recaptured and is present on the boron-like $(\mu^- \text{C})^{5+}$ atom the $e-\mu$ spin system might be observable.

The main effort of our experiment was to search for such $\mu-e$ spin-coupled systems especially in liquid He. Before investigating the various insulating hydrocarbons for these phenomena, residual polarization measurements were made for μ^- still essentially free from any electron spin interaction with $\gamma_\mu = 2\mu_\mu$. Should the polarization found

for such targets be the same as in C then a search for further depolarizing mechanisms would be redundant.

3. Formation of Mesic Molecular Systems

Gershtein et al.,²¹ and Ponomarev²² have presented arguments for the formation of large muonic molecules during the initial capture process. The muon is proposed to adiabatically replace one of the valence electrons in a molecular orbital in some cases before being captured into a separated muonic atom. The subsequent transitions from these orbitals to atomic levels could significantly alter the initial statistical angular momentum distribution on which much of the argument in this Section was based. These arguments will be discussed in conjunction with the discussion of the hydrocarbon results in Section V.

II. EXPERIMENTAL METHOD

A. General

The experiment was conducted at the NASA Space Radiation Effects Laboratory in Newport News, Virginia. Protons from the six hundred MeV/c synchrocyclotron were incident on an internal "harp" target, consisting of approximately 100 strands of carbon monofilament stretched across the open end of a C-shaped frame. Pions were produced by this target over the course of multiple proton traversals, enhancing the duty cycle to approximately two. Negative pions (π^-) of nominal momentum 200 MeV/c were extracted by the field of the cyclotron magnet and focussed by a single pair of quadrupole magnets adjacent to the cyclotron. The "muon channel" transport system was not available at the time of this experiment. Instead, a hole, approximately one foot square, was opened in the south shielding wall and a bending magnet was located immediately beyond the wall. Longitudinally polarized muons (μ^-), originating from the decay of π^- in flight, were bent into the experimental area by the bending magnet. For most of this experiment this magnet was tuned to select the "backward" μ^- of approximately 90 MeV/c momentum.

The μ^- passed through a pair of scintillation counters, were slowed by a copper degrader, and brought to rest in the target material.

Figure 1 is a plan view of the He experimental arrangement. The cylindrically-shaped He target was the lower section of an experimental dewar, which was located in the central region of a pair of Helmholtz coils. The axis of the magnetic field was perpendicular to the beam line. This field served to precess the muon magnetic moment about this axis. An array of fast scintillators (Pilot B) coupled to photomultiplier tubes by light pipes (UVT plexiglass) (counters 1, 2, 4 and 5 in Figure 1) signaled the arrival of the μ^- at the target, and detected the decay e^- . A detailed description of these counters is given in Section II-B-1. The He counter labeled 3 in Figure 1 is described in Section II-B-2, and in Section III.

A system of fast coincidence circuitry performed the basic logic operations on counter signals in order to identify stopping μ^- and decay e^- . Signatures μ^- and e^- were presented to a time interval meter, or "Digitron," which digitized the time interval between the arrival of the μ^- and the detection of its decay e^- . This digital time information was stored in the memory of a 400 channel pulse height analyzer. The logic is described in Section II-D.

Two types of measurements were made during the experiment. Each type was characterized by the magnitude of the precession field employed. High fields (approximately 100 gauss) were used to study the precession of the magnetic moment of the "free" muon, whose frequency was given by:

$$\frac{\omega_{\mu}}{H} = \frac{e}{m_{\mu} c} = 8.506 \cdot 10^4 \text{ radians/(gauss sec.)}.$$

Low fields (approximately 1.5 gauss) were used in a search for evidence of a spin-coupled state linking a μ^- to an unpaired e^- in the $F = 1$, $m_F = 1$ state. Such a system would be characterized by a frequency,¹⁷

$$\frac{\omega_{\mu-e}}{H} = 8.836 \cdot 10^6 \text{ radians/(gauss sec.)}.$$

B. Counters

1. Plastic Scintillators

In Figure 2 the five plastic counters labeled 1, 2, 3, 4, and 5 are shown. The light pipes were bonded directly to the scintillant at one end and were coupled to the glass envelope of the phototube (56 AVP) by a thin layer of optical grease at the other end. The light pipes and scintillant assemblies were wrapped with 0.0005" aluminized Mylar, and rendered light-tight with a wrapping of black masking tape. Soft iron tubes surrounded the phototubes to provide magnetic shielding.

Beam defining counters 1 and 2 were identical 8" x 8" x $\frac{1}{4}$ " scintillators and were located before and after a 5" x 5" opening in a secondary shield wall following the bending magnet.

Target defining counter 3 in the Figure 2 configuration was $5\frac{1}{2}$ " x $5\frac{1}{2}$ " x $\frac{1}{4}$ ". This counter was slightly smaller than any of the C or hydrocarbon targets in lateral extent and therefore defined the active stopping areas of these targets.

Counters 4 and 5 which served as both muon veto and electron telescope counters were both 10" x 10" scintillants. Counter 4 was $\frac{1}{4}$ " thick

and employed a straight light pipe arrangement. Counter 5 was $\frac{1}{2}$ " thick and the light pipe was curved to give a 30° bend so that scintillants 4 and 5 could be mounted flush against each other. In practice, counter 5 was maintained a constant distance from the center of the target while counter 4 was positioned as close as possible to the target. This was done in order to optimize the veto efficiency of 4 in the muon stop signature.

2. Helium Counter

Figure 1 is a plan view of the experimental arrangement showing the He counter designated as counter 3. The counter is given a complete description in Section III. In order to minimize the number of μ^- stopping in high-Z material the vacuum walls surrounding the target cylinder were only 0.020" along the beam line and the walls of the radiation jacket were replaced with 0.005" Cu foil shown as dashed lines in the Figure. Muons traversing or stopping in the He promoted scintillation pulses²³ which were viewed through a sapphire window by a single phototube (Amperex 56 AVP). The phototube was positioned approximately at the radial location of the precession coil windings in order to minimize the amount of magnetic shielding required by the tube.

C. Beam Selection

Muon differential range curves and decay event, ("STORES"), range curves were taken with the C target arrangement shown in Figure 2 and with a special plastic target counter inserted into the He target cylinder

in Figure 1. This latter target is described in Section III. The thickness of Cu degrader used during the experiment was determined from the maximum in the decay event curve shown in Figure 3(b). Due to π^- decay kinematics, the μ^- entering the bending magnet had a range of momentum of approximately 90 MeV/c ("backward directed") to 210 MeV/c ("forward directed") for a pion of nominal 200 MeV/c central momentum. Figure 3(a) is a plot of beam rate vs. bending magnet current. Selection of the "forward" μ^- necessarily admitted a large number of π^- into the experimental area. The accidental event rates in the time spectra were strongly influenced by this pion flux. The accidental event rates for two C runs, one taken with "forward" μ^- (run 10) and the other with "backward" μ^- (run 11) can be compared in Table I. B is the accidental rate per channel and N_0 the decay event rate per channel at $t = 0$. Because of the much lower background, "backward" μ^- were selected for all remaining runs. In all runs except 22 during which the stainless steel dewar was in place, the background remained below 2% of N_0 , and for the He runs was 1.8% or less.

D. Logic and Electronics

1. Fast Timing

Figure 4 is a block diagram of both the fast and slow logic. The slow logic is singled out by the dashed envelope and labeled "Digitron". The upper portion is separated into two parts, the "Start" and "Stop" legs of the (μ -e) time interval. The circuit configuration shown was

used for the experimental arrangement shown in Figure 2, where counter 3 is the plastic target defining counter. Pulses from the phototubes triggered Chronetics Model 101 discriminators and these discriminator outputs served as inputs to several Chronetics Model 103 AND/OR coincidence units. YES inputs were shaped to five nsec width and NO inputs to 20 nsec.

The fast coincidence (12) was designated a beam monitor and recorded for each run. A μ^- which stopped in the target material satisfied the coincidence ($\overline{12345}$), where the bar signified the anti-coincidence mode of operation. This signal became the START input for the time interval meter or "Digitron". A decay e^- signature was defined by ($\overline{2345}$) and this signal, delayed by 1 $\mu\text{sec.}$, served as the "Digitron" STOP input. This fixed delay permitted the system to accept and monitor 1 $\mu\text{sec.}$ of uncorrelated or "negative time" events. The use of plastic counter 3 in the anti-coincidence mode in the e^- signature insured that decay e^- resulting from μ^- stopped in 3 would not contribute to the final spectrum. When the He counter was in place the logic was modified to include it in the signature of both the stopping μ^- and the decay e^- . The He counter in Figure 1 is labeled 3 and the e^- signature became ($\overline{12345}$) instead of ($\overline{2345}$). Typical counting rates for C and He were:

	Carbon	Helium
(12)/sec.	$4.82 \cdot 10^3/\text{sec.}$	$5.87 \cdot 10^3/\text{sec.}$
μ^- stop/(12)	0.410	0.260
e^-/μ^- stop	0.090	0.025.

2. Slow Logic or "Digitron"

A detailed description of the time interval meter used in this experiment is given elsewhere;²⁴ only its basic features are described here. The block labeled GATE and 2ND MUON in Figure 4 consisted of modular Lecroy logic units. The GATE unit was opened by the μ^- signal and closed by the electron signal, its width therefore a measure of the (μ -e) time interval. The system also incorporated 2ND MUON protection, which prevented an event from being recorded if another μ^- triggered the START input during the maximum range of analysis. The analysis time was the same for every event and was slightly larger than 8 μ sec. The timing gate was fed to one input of a Chronetics Model 102 coincidence unit modified to accept a DC signal. The second input to this unit was a continuous train of 50 MHz pulses from a temperature stabilized crystal oscillator. This oscillator was stable to better than one part in 10^5 throughout the experiment. The output of the 50 MHz coincidence unit was, therefore, a gated train of 50 MHz pulses representing the (μ -e) time interval in digital form. These pulses were then fed to a 100 MHz scaler (RIDL Model 49-48-001) for counting and buffer storage. A valid event or "STORE" was registered if an e^- was detected within 7.8 μ sec. after a μ^- signal, and no 2nd μ^- was detected. The timing gate was artificially closed 7.8 μ sec. after the arrival of a μ^- , if an e^- signal at the STOP input had not already done so.

When the event was identified as a "STORE" the number in the 100 MHz scaler was transferred to the address register of a 400 channel

analyzer (TMC-Model 401) and one count was added to this channel. At an oscillator frequency of 50 MHz, at most 8 μ sec. could be handled by the analyzer. With an artificial 7.8 μ sec. closing of the timing gate and with 1 given to negative time events, 6.8 μ sec. was available for the longest (μ -e) interval. Typical "STORES" and 2ND MUON rates for C and He were:

	Carbon	Helium
"STORES"/ μ^- stop	0.040	0.020
2ND MUONS/ μ^- stop	0.045	0.045.

E. Magnetic Field

The precession field was generated by a pair of Helmholtz coils of mean diameter 23", in combination with the vertical fringing field of the main cyclotron magnet (typically 8G). Transverse "X" and "Y" bucking coils were employed to cancel the horizontal components of the cyclotron field which were less than 4G. These coils were wound on square frames and adjusted for approximate Helmholtz spacing in order to optimize uniformity over a 6" x 6" x 6" central volume. The various coil pairs are shown in place in Figures 1 and 2. The precession coils were water-cooled circular coils of 900 turns each. They were powered by a Sorensen DCR-300-8A DC power supply in the current limited mode and could produce a central axis field of 100 gauss. Their spacing was modified to give the best uniformity for a 6" length along the central axis. Under experimental conditions the stainless steel end plate of the helium target cylinder was removed and a magnetic field mapping was

made within the target volume. Field measurements were made with an incremental gaussmeter and Hall probe (F. W. Bell Model 240). Initially the total field within the chamber was reduced to 0.01 G, and then the precession field was raised to either the low field setting (1.5G) or the high field setting (100 G). The uniformity of the field over the target region was better than 0.2 G at the 100 G setting, except for regions within $\frac{1}{4}$ " of the sapphire-to-metal window seal. This region was excluded from the primary stopping volume by collimation ahead of the cryostat. At the low field settings the uniformity was approximately ± 0.05 G. To confirm the stability of the settings for either high or low fields the Hall probe was moved to a fixed position outside of the dewar or target region but within 6" of the target center. An adjustable feedback circuit in the gaussmeter allowed a 0.1 G change in the field to give a full-scale deflection on an external chart recorder. The field values were then continuously monitored during each run. No fluctuations were seen beyond those attributable to temperature drifts in the probe.

F. Target Configurations

Table II lists the dimensions and thickness for the targets used in the experiment. The C, H₂O and hydrocarbon targets were chosen to have approximately the same stopping power along the beam direction varying from 4.4 to 6.0 g/cm².

The C, polyethylene, paraffin, Pilot B scintillant, and Mg targets were rectangular solids which were suspended in the beam by string.

The liquid targets of distilled H_2O and reagent grade toluene were contained in thin polyethylene bags. The bags were constrained to rectangular shape by a thin wire mesh stretched on a frame of stainless steel wire which could also be suspended in the beam by string.

The liquid O_2 target was contained in a stainless steel cylindrical dewar, 10" high and 4" in inside diameter, giving an average thickness of approximately 11.0 g/cm^2 .

Figure 5 is a cross-sectional view of the He target as viewed along the beam axis. The lower portion of the He reservoir is the 6" right cylinder target volume which contained an average thickness of He of 1.6 g/cm^2 at 4.2° K .

G. Data Accumulation

Each single run included approximately $4 \cdot 10^5$ decay events, including background with accumulation rates from 40 to 100 events per second. The data were taken in three sequences of runs. The first sequence included runs 10 through 19, the second included runs 22 through 28 and the third included runs 102 through 120.

Figure 2 is a plan view of the arrangement used for the first sequence of runs. The magnetic field was set to approximately 100 G and the targets of polyethylene (12), Pilot B (14), and distilled H_2O (16) were run. Carbon was run several times (10, 11, 13, 15) for calibration at the high field setting. The field setting was then reduced to the low value and the Pilot B (18) and polyethylene (19) targets were run.

Sequence two began with the placement of the He counter in the beam as shown in Figure 1. While the dewar was still open, two calibration runs were made at high fields. The C target and the plastic counter 3 were temporarily inserted into the target cylinder of the dewar and data were taken with the logic shown in Figure 4 (run 22). The second calibration included the He counter phototube by inserting the plastic array described in Section III-C (run 23). The dewar was then sealed and filled with liquid He. Three runs at high field settings (24, 26, and 28) and two at low fields (25 and 27) were then taken.

The third sequence of runs were taken in the same manner as the first. Carbon target runs 102, 107, and 117 were interspersed with targets of paraffin (103 and 113), polyethylene (104), Pilot B (106 and 109), Mg (108 and 111), toluene (110 and 115), distilled H₂O (112 and 114), and liquid O₂ (118), all at high fields. The field was then set to its low value and the liquid O₂ target (119) and toluene target (120) were run.

The frequent C runs at high fields served to monitor the performance of the "Digitron" system and the relative values of the beam polarization.

Before and after each sequence of runs data from uncorrelated events were simulated with two radioactive sources. These "random" runs were accumulated to insure that no non-linearities were present in the "Digitron" system.

III. HELIUM TARGET - COUNTER

A. Introduction

The occurrence of scintillations due to the passage of charged particles through liquid He is a well known phenomenon. A review of the development of liquid He as a scintillating material prior to 1965 has been given by Birks.²³ A report on the development of the present counter has been published elsewhere.²⁵ The scintillation property enabled liquid He to serve as both a target and a counter for stopped μ^- . In this experiment the He counter labeled 3 was included in both the identification of stopped μ^- ($\overline{12345}$) and decay e^- ($\overline{12345}$). As considerable time and effort were expended in the development of the He counter, we single it out for further discussion here.

The description of the counter is divided into two parts. Section III-B describes the cryostat assembly and its development, and Section III-C describes the counter operation.

B. Dewar

Figure 5 is a cross-sectional view of the Sulfrian Corp. experimental He dewar used in this experiment. The cryostat consisted of two main sections, (1) a 15-litre reservoir section and (2) a 6" right

cylindrical target cup. The target cup was joined to the bottom of the reservoir section at a 4" diameter neck seal. The He reservoir section was surrounded by a liquid N₂ radiation jacket which, with a demountable Cu extension, provided thermal shielding for the target cup. The scintillation light from the target He was viewed by the photomultiplier tube through a 5" diameter synthetic sapphire window mounted at one end of the target cylinder. A stainless steel plate was mounted at the other end.

1. Target Vacuum Seals

The original design for the neck seal and window seals incorporated In solder joints at all three locations. This type of arrangement proved inadequate because of difficulties encountered in remaking the seals. The three seals were modified to employ pure In metal "O" rings. A special clamp consisting of two split-ring collars served to draw the two original neck seal flanges together. Two concentric "O" rings formed from 1/16" diameter pure In wire (Indium Corporation of America) were positioned between these flanges and crushed by tightening the screws joining the two collars.

Figure 6 is an exploded view of the final window seal configuration. A receiving flange was present at each end of the target cup. These flanges were recessed to accept the window assemblies, and were threaded on their outside diameters. Retaining rings were machined from non-magnetic 316 stainless steel and threaded to mate with the flanges. Eight compressing screws were threaded through the front

surface of each retaining ring and came to bear on the stainless steel window flange. A single "O" ring formed from 3/32" diameter pure In wire was formed to fit between the target flange and window flange. All of the In rings were compressed in two or three successive steps of tightening. A He mass spectrometer leak detector was used to check the vacuum seals before, during, and after cool-down and no detectable leaks were found. Ultimate pressures measured at the pumping station, consisting of a 4" diameter CVC oil diffusion pump backed by a (Walsh 1397) two-stage mechanical pump, were approximately $2 \cdot 10^{-6}$ Torr with the dewar warm and $2 \cdot 10^{-7}$ Torr when cold. For the purpose of extracting the windows, four blind holes were tapped into the window flanges and matching clearance holes were cut in the retaining rings. Screws were threaded into these holes and nuts were brought to bear on the outer surface of the retaining ring permitting the windows to be withdrawn. Finally, all exposed parts of these seals as well as the screws were silver plated to minimize radiation heat input to the liquid He.

2. Filling Procedure

A special top hat covered the 2" diameter filling neck of the reservoir and was fitted with several "O" ring sealed ports of 1/8" and 1/4" diameter. One of the ports accepted the liquid He transfer line which replenished the reservoir from a 100-litre storage container. A 1" diameter pumping port in the side of this top hat was coupled to a separate mechanical pump for evacuation of the reservoir and target in preparation for a cool-down. Cooling the dewar from room to liquid He

temperature was accomplished gradually. Temperatures at the reservoir-target neck seal, sapphire window, nitrogen jacket extension, and phototube were monitored by copper-constantan TC junctions. The TC leads were brought out through a feedthrough in the vacuum wall to a 12-station sequential chart recorder. While filling the liquid N_2 reservoir the temperature on the phototube was monitored to insure a gradual cooling of the glass envelope of the tube. The reservoir and target section were then cooled to just above liquid N_2 temperatures by the admission of cold N_2 gas through a top hat port. The N_2 was evacuated and the reservoir was purged with cold He gas from the storage dewar and again evacuated. The remaining cool-down was accomplished with cold He gas from the storage dewar until finally liquid He began to fill the target. Two 1/10 watt, 56 ohm resistors, separated by 1" and mounted at the lower end of a 1/8" diameter thin walled stainless steel tube, served as a level probe. The resistors formed one side of a resistance bridge and a sharp level indication was obtained when the top resistor just entered or exited the liquid He.

Initial filling and cool-down from room temperature took approximately eight hours and refilling the dewar about one hour. Boil-off rates during the experiment was 0.75 l/h so that approximately twelve hours of counter operation were permitted before refilling was required.

C. Counter Operation

The lower portion of Figure 5 includes the assemblies required for operation of the dewar as a counter. Figure 1 shows a top view of the

lower section in place during the experiment. The scintillation light was initially wave-shifted by an Al foil liner prepared in the following manner. The foil was spray-coated with 25 mg/cm^2 of white Tygon paint followed by the deposition of approximately $100 \text{ }\mu\text{g/cm}^2$ of the wave shifter, p, p' diphenylstilbene (DPS). A thin transparent layer of DPS, approximately $25 \text{ }\mu\text{g/cm}^2$ thick was also deposited on the inside surface of the sapphire window. A study of various combinations of paints and thicknesses of DPS indicated that the values used here were near optimum for maximum light collection. A single 2" diameter phototube (Amperex 56 AVP) viewed the scintillation light through a vacuum light pipe constructed from Al foil spray-painted with white Tygon paint. The phototube was separated from the 5" diameter window by approximately 10" in order to position the cathode at the radial location of the Helmholtz coil windings. This had the effect of minimizing (1) the amount of magnetic shielding required by the phototube, and, (2) the magnetic distortion in the target region caused by such shielding. The phototube was wrapped with Cu wool and supported by two Lucite discs in a Cu tube extending from the liquid N_2 jacket. This served to cool the phototube to a temperature of approximately 120° K which reduced the radiant heat input into the He target. The voltages and signal were carried by stainless steel wire to the tube base located outside of the cryostat. A 0.004" diameter stainless steel wire was electroplated with ^{210}Po and attached to the end of a 1/8" diameter stainless rod. The rod was passed through one of the ports at

the top of the dewar and allowed the ^{210}Po α source to be lowered into the target volume through a 1/2" diameter opening in the top of the target liner. The phototube performance was monitored during the cooling procedure by observing its response to a fast light pulser. A voltage pulse from a pulser (Hamner Model 961-D) fired the pulser bulb mounted at the base of the phototube, and a 1/8" diameter Lucite rod carried the light to the photocathode. Once the target began to fill with He one could probe the liquid level with the α source, since large changes in the scintillation pulse height occurred at the liquid-vapor interface.

A calibration of the electronics used in the He experimental configuration was performed in run 23 by inserting a special array of plastic scintillant into the target cylinder. The array consisted of five regularly spaced sheets of 1/8" thick plastic scintillant (Pilot B) whose edges were viewed by the phototube through the sapphire window. The planes of the sheets were perpendicular to the beam direction and their total thickness along the beam axis was approximately 1.8 g/cm^2 . The signal from the phototube was then included in both the μ^- stop and decay e^- signatures to simulate the logical configuration used in the He runs.

IV. DATA ANALYSIS

A. Introduction

Equation (3) gives the form of the expected time distribution of electrons from the decay of partially polarized negative muons at rest in a constant magnetic field perpendicular to their polarization direction.

$$N(t) = N_0 \cdot e^{-t/\tau} \cdot \{1 + a' \cdot \cos(\omega t + \phi)\} + B.$$

Here N_0 is the amplitude in the $t = 0$ channel for zero asymmetry, τ is the mean lifetime of muons against disappearance, a' is the precession amplitude or asymmetry parameter, ω is the precession frequency, ϕ is the direction of the μ^- spin with respect to the e^- detection system at $t = 0$ and B is the accidental rate for uncorrelated events. Figure 7 is a plot of two typical data runs. The C data clearly show the precession signal superimposed on the exponentially decaying spectrum. The Hs data show the presence, at early times, of stainless steel contamination which causes the sudden change in logarithmic slope.

In order to determine the best value for the asymmetry parameter a' , for each data run, a set of best values was also determined for the parameters N_0 , τ , ω , ϕ , and B . This set of values was found by performing a least squares analysis procedure for each data run. The chi squared quantity,

$$\chi^2 = \sum_1 \frac{(y_1 - N(t_1))^2}{\sigma_1^2}, \quad (9)$$

was minimized by a non-linear analysis which represented $N(t_1)$ by a Taylor's series expansion of $N(t)$ to first order in the parameters. A general outline of this multiparameter analysis procedure is given in Appendix A. χ^2 is expressed in the Tables as the normalized value χ_v^2 ,

$$\chi_v^2 = \chi^2 / (\text{number of points} - \text{number of free parameters}).$$

1. Data Presentation

Figures 8-14 are plots of individual data runs with the background subtracted and the lifetime folded out. The data were represented by the expression,

$$y(t) = \frac{(\bar{y}_1 - B) \cdot e^{+t/\tau}}{N_0}, \quad (10)$$

where \bar{y}_1 is the average over eight adjacent channels or 0.16 $\mu\text{sec.}$, and t is the time at the center of the eight channel interval. The curves are the plotted values of the expression,

$$f(t) = 1 + a' \cdot \cos(\omega t + \phi),$$

where the values of a' , ω , and ϕ were the final best fit results from the analysis procedure.

2. Non-Linear Multiparameter Analysis

The number of parameters which could be successfully simultaneously fit, depended on the magnitude of the precession amplitude a' , and on

how well the complete set of initial values for all of the parameters approximated the final best fit. This procedure required that initial values be assigned for all of the parameters which described the data. Any number of the parameters from one to six could be considered free by the analysis procedure. The selection of which parameters were to be free was governed by their interaction in the fitting procedure. It was not usually possible to include the lifetime, τ , as a free parameter simultaneously with the frequency, ω . The particular form of the analysis for each data run will be discussed in the following sections. In general, four separate types of analysis were performed using the non-linear approach: (1) lifetime τ , as a free parameter; (2) frequency ω as a free parameter; (3) phase angle ϕ as a free parameter; and (4) both phase and frequency as free parameters.

This procedure yielded corrections which were applied to each free parameter. The iterative procedure was repeated until the corrections for all of the parameters were less than one part in 10^4 . Normally four or five iterations were sufficient to reach this convergence requirement.

3. Linear Multiparameter Analysis

It is pointed out in Appendix A that the same procedure for calculating the minimum chi squared approximations could be used in both non-linear and linear approaches. When τ , ω , and ϕ are not considered as free parameters, an approximately linear expression for $N(t)$ can be written as:

$$N(t) = N_{ss} e^{-t/\tau_{ss}} + N_0 e^{-t/\tau} + A' e^{-t/\tau} \cos(\omega t + \phi) + B. \quad (11)$$

where N_{ss} is the amplitude of decay events arising from muons stopping in stainless steel, τ_{ss} is the mean lifetime of muons in stainless steel and $A' = a'N_0$.

This approach was used when possible to reduce the amount of computer running time required by the iterative procedure. In the linear form the expression given for $N(t)$ was exact and only one iteration was required.

4. Frequency Search Analysis

This method of analysis is similar to that described in other experiments^{26,27} where precession signals in muon decay were observed. The parameters τ , ϕ , and B were assigned values based on the following: τ was taken from the compilation presented by Eckhause et al.,²⁸ for the particular target material; ϕ was assigned the value of either 0.0 or π depending on whether forward or backward muons were being stopped, and B was calculated based on the negative time information included in each data run. A range of values (0.05 to 3 MHz) for the frequency, ω , was selected and ω was assigned a value equal to the lower end of the range.

A two-parameter linear least squares procedure was then performed with this set of values for the parameters τ , ω , ϕ , and B . The two free parameters were N_0 and $a'N_0 = A'$.

An increment $\Delta\omega$ was added to the assigned value for ω (usually $\Delta\omega = 0.05$ MHz) and the fitting procedure was repeated. The procedure was complete when the current value for ω had reached the end of the previously assigned range of values. The resulting series of values for χ_v^2 , asymmetry $a' = A'/N_0$ and N_0 were plotted against the corresponding values for the parameter ω . Figure 15 shows the results for the parameter a' , plotted for a range of frequency values from 0.05 MHz to 3.0 MHz, for several of the data runs. The location of the peak in a' corresponded to the location of a resonance dip in the plotted values of χ_v^2 .

5. Time Dependence of Asymmetry

All of the procedures described above were performed for some selected region of data in each run. The Σ in the definition of χ^2 was performed for values of i such that $I1 \leq i \leq I2$ where $I1$ and $I2$ were specified before the particular analysis procedure was begun. The region of analysis was defined by a data window which was $(I2 - I1 + 1) \cdot \Delta t$ wide. With an oscillator frequency of 50 MHz, Δt was 20 ns per channel. In most of the analysis a fixed window width was selected and the starting point was varied in order to observe the dependence of the results on early times. It was found from this procedure that the first ten channels exhibited some slight systematic errors and for this reason these were not included in any of the reported results. In each data run 330 channels or 6.6 μ sec. of decay information was available for

analysis. For most analysis procedures the data interval included 200 or more channels and the size of this interval is normally expressed in μsec . (50 channels = 1 μsec .)

6. Corrections to Asymmetry

In equation (3) the asymmetry parameter a' is expressed as:

$$a' = P \cdot F(x_0) \cdot F(\Omega_e) \cdot a_0,$$

where P is the muon polarization, $F(x_0)$ is a correction factor for electron energy loss in the target and telescope elements and $F(\Omega_e)$ is a correction factor for the finite geometry of the detection system. Appendix B gives the development of the calculations for these correction factors. The correction factors for each target are given in Table III which is summarized well by:

$$F(\Omega_e) \approx 0.85;$$

$$\Omega_e/4\pi \approx 0.13;$$

$$F(x_0) \approx 1.01.$$

7. Analysis of Random Data

Data runs with uncorrelated random start and stop inputs to the time interval meter were made before and after each experimental sequence of runs. These "random" data runs were analyzed by a linear least squares fitting procedure for N_0 and slope. The expected distribution was given by:

$$N(t) = N_0 + m \cdot t.$$

Here N_0 is a constant amplitude for each channel and m is the slope in counts per time interval. The value for the absolute slope, m/N_0 , was determined for each "random" data run. For all random runs the result was:

$$|m/N_0| \leq 3 \cdot 10^{-5} \text{ per channel.}$$

These data runs were also analyzed by the frequency search procedure with the substitution of $N(t) = N_0 \cdot \{1 + a' \cos(\omega t + \phi)\}$ for the functional form of the data. The range of the frequency was (0.05 to 3.0) MHz and ϕ was varied over a range of values from 0 to π . For all values of ϕ and ω the result was $|a'| \leq 0.001 \pm 0.001$. N_0 was as small as 800 and as large as 10,000 for different random data runs.

B. Carbon and Magnesium

Carbon was used as the primary calibration target during this experiment. It was well suited for this purpose because the mean lifetime was long enough to give seven clear precession cycles at fields of approximately 100 gauss. Figures 8-14 each include a plot of a C data run for comparison.

Magnesium was included as a target since it was also expected to give a large μ^- decay asymmetry. Due to the shorter lifetime, however, only three precession cycles were available for analysis.

1. Lifetimes

The lifetime fitting procedure was applied to all of the C runs and the hydrocarbons, polyethylene, Pilot B, paraffin, and toluene.

These are grouped here since the μ^- are expected to form a muonic C atom in all of the targets, and this should govern the mean lifetime.

The lifetime fitting for the C runs was made difficult by the large precession signal present. If the asymmetry were neglected and the distribution fit by an expression of the form,

$$N(t) = N \cdot e^{-t/\tau} + B,$$

a large value for χ^2_{ν} resulted. The lifetimes used in the initial fitting procedures were therefore taken from Eckhause, et al.²⁸ Once an approximate set of values for the parameters a' , ω , and ϕ were obtained, the expression,

$$N(t) = N_0 e^{-t/\tau} \{1 + a' \cdot \cos(\omega t + \phi)\} + B, \quad (12)$$

could be used to represent the data. An iterative non-linear fitting procedure was then used allowing N_0 , τ , and B to be free parameters. The values for χ^2_{ν} for each data run fit in this manner were then nearly equal to one. All of the hydrocarbon targets gave fitted values for τ which were within statistical errors of the expected lifetime given by Eckhause, et al.,²⁸ for C $\{\tau = (2.034 \pm 0.004) \mu\text{sec.}\}$.

Table IV gives the results for the fitted values of lifetimes measured in this experiment. The value for C,

$$\tau = (2.027 \pm 0.004) \mu\text{sec.},$$

is a weighted mean of the lifetime result for each C and hydrocarbon data run.

Magnesium, because of the much shorter lifetime and large precession signal did not yield as reliable a value for τ . The mean for two separate data runs was:

$$\tau = (1.10 \pm 0.04) \text{ } \mu\text{sec.}$$

2. Multiparameter Non-Linear Analysis

For all of the C calibration runs a convergent iterative procedure which included N_0 , a' , ω , ϕ , and B as free parameters was performed. The data window was 5.8 $\mu\text{sec.}$ and the results for this procedure are given in Table I. No errors are given for the parameter B due to the good agreement with negative time data from each run. This parameter is presented as a fraction of N_0 to show the factor of seven improvement in background when "backward" μ^- were stopped. The first entry is for run 10, taken with "forward" μ^- . All other runs were taken with "backward" μ^- .

The frequency is presented as ω/H in order to show the good agreement with:

$$\gamma_{\mu} = \omega/H = 8.506 \cdot 10^4 \text{ radians/(gauss sec.)},$$

the gyromagnetic ratio for the "free" μ^- . The average value for all of the C runs was:

$$\omega/H = 8.50 \begin{matrix} +0.04 \\ -0.02 \end{matrix} \text{ radians/(gauss sec.)}.$$

For the "backward" μ^- the phase ϕ was expected to be π . The phase result for run 117 is attributed to the changes made in the target

support when liquid O_2 was used. For the high fields, an error in phase angle of 0.17 radians was equivalent to an uncertainty of one channel in the location of $t = 0$, and the period for the precession was approximately 37 channels. The results for a' do not include corrections for solid angle and electron energy loss.

3. Frequency Search-Contour Plot

In order to investigate the dependence of asymmetry on the value chosen for the phase in any fitting procedure, a series of frequency search procedures were performed for C run 117. A range of values for the phase ϕ was selected, and ϕ was set to the low end of the range. The range for the frequency was selected to be approximately $\pm 30\%$ of the previously determined frequency for this C run, and a frequency search procedure was initiated. After the complete range of values for frequency had been exhausted, the value for the phase ϕ , was incremented by 0.2 radians and the procedure was repeated.

Figure 16 is a contour plot of the resulting values of the asymmetry a' vs. phase ϕ and frequency ω . The dependence on frequency is clearly the most important, while changes in phase as large as 0.5 radians or approximately 30° still allowed the frequency search to find a near maximum value for a' . The χ^2_{ν} quantity, however, showed a minimum value only for the selection of ϕ and ω consistent with the results yielded by the multiparameter analysis.

The stability of the beam polarization in magnitude and direction, as evidenced by Table I, coupled with the weak dependence of asymmetry

a' on ϕ , allowed the frequency search technique to serve as the primary analysis procedure for the remaining targets. Magnesium run 108 was analyzed by the frequency search procedure and results are shown in Figure 17(b).

4. Asymmetry Results

After the precession parameters ω , and ϕ , were determined for each data run a final two parameter linear procedure which included N_0 and a' only as free parameters was performed. This fitting procedure was identical to the procedure used in the frequency search. It was the only procedure which could be used for all data runs in the experiment and was therefore used as the standard method for determining the value of asymmetry to be reported. The data window was 4.0 μsec . wide and began at $t = 0.4 \mu\text{sec}$. This selection was made for consistency in comparing results. The He data, to be discussed later, contained significant background from μ^- stops in stainless steel, and for this reason the first 0.4 μsec . ($t = 2 \cdot \tau_{Fe}$) was omitted from the analysis.

The results of this procedure, corrected for solid angle and electron energy loss are given in Table V, and were:

$$a_0 = -0.048 \pm 0.003 \text{ for C}$$

and $a_0 = -0.044 \pm 0.004 \text{ for Mg.}$

The values given in Table V are the weighted means of the results for each individual data run of the same target material.

C. Hydrocarbons and Water

Figures 8 and 9 present data from distilled H₂O and paraffin taken at high fields. Figures 10, 11, and 12 present data for Pilot B, polyethylene, and toluene taken at high fields and at low fields. Each Figure includes a C data run for comparison.

1. Lifetimes

The mean lifetime τ used in the hydrocarbon runs was the same as that used in C and the analysis is described there. The result of the lifetime fitting procedure was:

$$\tau_{\text{mean}} = (2.027 \pm 0.004) \text{ } \mu\text{sec.}, \text{ for hydrocarbons.}$$

The H₂O runs were treated in the same manner as C. The initial value for asymmetry a' was taken from the two-parameter linear analysis procedure where the values of ω , and ϕ , were taken from the C calibration run. The result, given in Table IV, is the weighted mean of the lifetime results from the liquid O₂ target runs as well as the H₂O runs. The muons stopping in H₂O are assumed to decay from the ground states of muonic oxygen atoms. The fitted lifetime for negative muons stopped in liquid O₂ was:

$$\tau = (1.816 \pm 0.008) \text{ } \mu\text{sec.}$$

2. High Fields

The most important feature of these targets is a uniformly low value of a' . All of the hydrogenous targets gave residual polarization

values of approximately $\frac{1}{2}$ or less than that found for C, when run at high fields.

The frequency search procedure was used for the preliminary determination of the best value for the precession frequency in each high field data run. Figure 15 shows the results of the frequency search analysis procedure for Pilot B scintillant (run 109), toluene (115), paraffin (113), and polyethylene (104), all at high fields. Figure 17(c) displays the results for H₂O (run 112). The peaks at $\omega \approx 1.38$ MHz are at the expected frequency for the "free" μ^- precession at fields of approximately 100 G. A C run (107) analyzed in the same way is presented in Figure 15(a). The general result of $a'_{\text{HN}} \approx \frac{1}{2}a'_C$ is clear, where a'_{HN} is the asymmetry value for a hydrogen-containing compound and a'_C is the asymmetry found in C. Each data run gave the lowest value for χ^2_{v} at the same frequency value at which a peak in asymmetry was indicated. All data runs at high fields of H₂O, Pilot B, toluene, polyethylene, and paraffin contained sufficient precession amplitude to allow a five-parameter non-linear fitting procedure to be used. The initial assignments for the parameters N_0 , a' and ω were taken from the results of the frequency search procedure. The initial value for the phase angle ϕ was determined by a C calibration run taken in the same geometrical arrangement. The assignment for B was estimated from the negative time information contained in each run. The value of the lifetime τ was fixed at the value given in Section IV-C-1. The results for the iterative fitting procedure for N_0 , ω , ϕ , B, and a' for all of the high field hydrocarbon and H₂O runs are given in Table VI.

3. Time Dependence of Asymmetry - High Fields

For any analysis procedure used the data window could be varied. In order to investigate a' and its dependence on the location of this window it was most convenient to keep its length fixed and change only the time at which it began. In order to look at possible time dependence over a long range of starting times the window was shortened to eighty channels or 1.6 μsec . Each data run was analyzed separately by the two-parameter linear procedure for N_0 and a' . The parameters ω , ϕ , and B were fixed at the values obtained from the multiparameter non-linear fitting procedure. The starting time for the analysis was varied through a range of values from 0.2 μsec . to 5.0 μsec . and the resulting values for a' were plotted vs. the first channel used in the fitting procedure. Figures 18, 19 and 20 show these results. Figure 18 includes two C runs which were analyzed in this manner to show the lack of any time dependence. The results at each value of initial channel for all high field runs of the same target material were averaged before plotting. The data taken with H_2O shown in Figure 18 and toluene and paraffin (Figure 19) show no time dependence beyond the statistical errors. Both Pilot B and polyethylene, however, seem to demonstrate some relaxation or loss of polarization with increasing time. In the values reported here this relaxation has not been included. Some discussion of the possible implications of such relaxation will be given in Section V.

All runs were analyzed by the same two-parameter linear fit employed in the frequency search program in order to present the results given

in Table V. The data window was from 0.4 to 4.0 μsec . The value for ϕ was obtained from the C calibration run made during the same sequence of runs, and the frequency, background and lifetime were taken from the results of the multiparameter analysis procedure.

The final values for asymmetry were weighted means of the results from all data runs of the same target material. Corrections for solid angle and electron energy loss were included and the values as given in Table V were:

H ₂ O	$a_0 = -0.019 \pm 0.002$
Polyethylene	-0.022 ± 0.002
Toluene	-0.021 ± 0.003
Paraffin	-0.026 ± 0.002
Pilot B	$-0.016 \pm 0.002.$

4. Low Fields

The loss of polarization, indicated by the weak precession signal for the "free" muon, in the hydrocarbons was investigated for three of the hydrocarbons, Pilot B, polyethylene and toluene, by searching for evidence of the formation of a μ -e spin-coupled system. Such a system would have been characterized by a frequency, $\omega = \mu_e (1 + m_e/m_\mu) \cdot H$. We would expect at most a 1% signal since, in general, these targets displayed about $\frac{1}{2}$ of the "free" μ^- asymmetry of C.

If we identify N_f as the number of muons which do not form a μ -e hyperfine system and $N_{\mu-e}$ as the number which are so coupled, we may

make the following simple statement. The number of particles which will show precession at the "free" muon frequency is less than the number formed in C. If we then express the asymmetry, a' , in terms of the carbon value, a'_C , we write:

$$a'(\text{free}) = \frac{N_f}{N_o} \cdot a'_C,$$

where $N_o = N_f + N_{\mu-e}$ and we assume no other depolarizing mechanisms. Since the observed values for a' in the hydrocarbon and H_2O data were $1/3a'_C < a' < 2/3a'_C$, we may write:

$$\frac{1}{3} < \frac{N_f}{N_o} < \frac{2}{3};$$

and since $N_f = N_o - N_{\mu-e}$, we obtain also:

$$N_{\mu-e} < \frac{2}{3} \cdot N_o.$$

In Section I-D-2 the depolarization due to the formation of the spin-coupled $\mu-e$ system was shown to be $1/2$, due to the loss of signal for $m_F = 0$ states. We combine the results to yield:

$$a'_{\mu-e} = \frac{N_{\mu-e}}{N_o} \cdot a'_C \cdot \frac{1}{2} \tag{13}$$

$$\leq \frac{a'_C}{3} = 0.013.$$

This is the largest signal that was expected to be present for the hydrocarbons and H₂O at low fields. Because of the very small signal expected the non-linear fitting procedures which included either ϕ or ω as free parameters were not used. For these low field runs the values for ϕ were taken from the C calibration runs as a starting point and a frequency search analysis was performed. The weak dependence on ϕ shown in the high field runs and the stability of the phase angle ϕ throughout each sequence of runs made a search for ϕ unnecessary. The results of the frequency search procedure for the low field runs of Pilot B, polyethylene, and toluene are shown in Figure 21, where asymmetry a' is plotted vs. the value of the frequency ω . No peaks in the region of 2.1 MHz were seen for any run. This frequency corresponded to the approximate value expected for the μ -e system. The deviations from zero at low values of frequency were caused by small errors in the background B. The values for χ^2_{ν} showed no change over the full range of frequency for any of these runs. A single run with a C target was made at low fields in order to observe any systematic errors which might be produced by the slowly precessing "free" μ^- signal known to be present in C. No μ -e signal was expected since the depolarization is accounted for by the atomic capture and cascade mechanisms alone. The results of the frequency search procedure for this low field C run are shown in Figure 21(a).

The results for asymmetry are quoted for the standard two-parameter linear analysis with the value of ω fixed at the calculated frequency

of precession for the hypothetical μ -e system. The results for the low field hydrocarbon runs as given in Table V for the $F = 1$, $m_F = 1$ state of the spin-coupled μ -e system were:

Pilot B	$a_0 = -0.001 \pm 0.003$
Toluene	-0.001 ± 0.004
Polyethylene	$0.0 \pm 0.004.$

D. Liquid Oxygen

Liquid O_2 was also used as a target. It was expected that muons stopped in this strongly paramagnetic substance would give no "free" signal. Runs at both high and low fields were made in order to : (1) confirm the expected result of $a_0 = 0.0$ at the "free" muon frequency; and, (2) to investigate the possibility of formation of the μ -e system. If this system were formed by all stopped muons, after the atomic cascade to the ground state the largest signal expected for O_2 at $\omega_{\mu-e}$ would be approximately 2%.^{3,17}

Figure 13 includes plots of both high and low field data for liquid O_2 .

1. Lifetimes and Stainless Steel Background

The liquid O_2 data and the liquid He data both included contamination from μ^- stopping in Fe. The lifetime for muons in Fe is $0.2057 \mu\text{sec}.$ ²⁸ The presence of this contamination did not contribute any significant errors in the analysis if the first $0.4 \mu\text{sec}.$ of decay information were omitted from the fitting procedures. For this reason a time interval

of 0.4 to 4.4 $\mu\text{sec.}$ was chosen as the standard interval for data analysis for the asymmetry results reported in Table V. The precision was improved, however, by first subtracting the stainless steel background. A multiparameter linear analysis procedure was performed for the O_2 data using the expression,

$$N(t) = N_{\text{ss}} e^{-t/\tau} + N_0 e^{-t/\tau} + B, \quad (14)$$

to represent the data. No large precession signal was present in the data and therefore reasonably good values for χ^2_{ν} were obtained with this representation. The parameters N_{ss} , N_0 and B were free, and a data window of 0.2 to 6.5 $\mu\text{sec.}$ was used. The results of this procedure for N_{ss} and B without errors are included in Table VII. The uncertainty for N_{ss} was approximately $0.25 \cdot N_{\text{ss}}$ and for B was approximately $0.05 \cdot B$.

The same representation (14) was used in the lifetime fitting procedure. This procedure was a three-parameter non-linear analysis for the best values of the parameters N_0 , τ , and B where N_{ss} was taken from the previous background analysis. The resulting values for τ for both the high field run and the low field run were included in the weighted mean lifetime result for O_2 . This mean result also included the lifetime values from the H_2O data and was:

$$\tau = (1.816 \pm 0.008) \mu\text{sec.}, \text{ for } \text{H}_2\text{O} \text{ and liquid } \text{O}_2.$$

2. Frequency Search - Asymmetry Results

The same method of analysis was used for both high and low fields due to the low values of the precession signal. The frequency search procedure was used to analyze the data for the presence of a signal at a frequency in the range of (0.05 to 3.0) MHz. The results for the high field run (O_2 118) are shown in Figure 17(d). A signal exists at the "free" μ^- frequency but is only one standard deviation away from a null result. The low field run (O_2 119) was analyzed in the same manner and gave a small signal approximately two standard deviations from the null result. However, when the analysis data window was increased to 6 μsec . instead of the 4 μsec . interval used in the frequency search procedure, both results were consistent with no residual polarization.

The results for liquid O_2 for both high and low fields are given in Table VII. The procedure used was the standard two-parameter fit to N_0 and a' used in the frequency search procedure and the data interval was 0.28 to 6.28 μsec . The stainless steel background was subtracted during the analysis, and the results for the asymmetry a' were:

$$a' = +0.001 \pm 0.002, \text{ for "free" } \mu^- \text{ precession,}$$

$$\text{and } a' = -0.003 \pm 0.002, \text{ for } (\mu-e), F = 1, m_p = 1.$$

E. Liquid Helium

The He was contained in the stainless steel target cylinder and the surrounding vacuum walls were also of stainless steel construction.

This material in the back walls was not eliminated from the μ^- stop signal and it was the main contribution to the background in the He runs. The three-parameter linear fitting procedure for N_{ss} , N_0 , and B that was used for the liquid O₂ data was also used here. The results for N_{ss} and B are given in Table VII for both high field and low field runs.

Figure 14 presents the He data for both values of precession field. The background, B, in the expression,

$$\{N(t) - B\}e^{+t/\tau}/N_0,$$

included the best estimate for the stainless steel background, and B was actually time dependent.

$$B(t) = N_{ss}e^{-t/\tau_{ss}} + B.$$

The Figure also includes data from C. For this single C data run the target was located inside of the He dewar and also included some stainless steel background. The large precession signal found for C is apparent in the Figure. This run served as the calibration for the frequency and phase angle of the "free" μ^- spin precession. One other calibration target, an array of thin Pilot B sheets, was run in the dewar configuration. This run included the same phototube and electronic arrangement which were used in the liquid He runs. The results for the C run (22) are given in Table I and for the Pilot B array (23) in Table VI. The plastic array target gave an asymmetry result consistent with runs made with a thicker target of Pilot B at high fields.

1. Lifetimes

After the subtraction of the stainless steel background a three-parameter non-linear procedure for N_0 , τ , and B was used to determine the best value for the μ^- lifetime in He. The result for He as given in Table IV was:

$$\tau = (2.186 \pm 0.014) \mu\text{sec.}$$

Since the precision of this value was about five times worse than that of the tabulated value,²⁸ $\tau = (2.1982 \pm 0.0026) \mu\text{sec.}$, the latter value was used in the asymmetry fitting procedure.

2. Frequency Search

Figure 17 includes a plot of the asymmetry results from the frequency search procedure for the high field liquid He data. There is no precession signal evident at the "free" μ^- frequency. The large excursions at low frequencies were due to the uncorrected stainless steel background present in all He data. Figure 21(b) shows the results for a low field He run and the same lack of any precession signal is apparent.

3. Asymmetry Results

The frequency search analysis for liquid He runs gave no apparent peaks for any frequency when the stainless steel background was taken into account. The χ^2_{ν} values from the frequency search were constant for all values of frequency. The runs at high fields were also analyzed by

the two-parameter linear fitting procedure with N_0 and a' as free parameters. The frequency and phase angle were taken from the C calibration run (22). The stainless steel background was included in the functional representation of $N(t)$ and the amplitude N_{ss} was taken from the background analysis procedure described above. The functional form of $N(t)$ was given by equation (11).

The stainless steel lifetime ($\tau_{ss} = \tau_{Fe} = 0.2057 \mu\text{sec.}$) and the helium lifetime ($\tau = \tau_{He} = 2.1982 \mu\text{sec.}$) were taken from Eckhause, et al.,²⁸ and the data interval was (0.28 to 6.28) $\mu\text{sec.}$, or 6.0 $\mu\text{sec.}$ wide.

The results of this procedure and the values used for N_{ss} and B are given in Table VII. The weighted mean for the high field results was:

$$a' = -0.002 \pm 0.004.$$

The weighted mean of the low field results was:

$$a' = 0.0 \pm 0.003 \quad (F = 1, m_F = 1; \mu\text{-e}).$$

Both of these results are consistent with total depolarization of the muon spin at the time of decay.

V. DISCUSSION OF RESULTS

A. Summary

The mechanisms proposed by Mann and Rose,⁴ and by Shmushkevich,³ are sufficient to explain the depolarization of μ^- in metals having nuclear spin $I = 0$. Experimentally^{1,15,29} measured e^- asymmetries from μ^- decay in C and Mg and other nuclear spin zero targets have shown good agreement with the predicted value $a_0 = -0.055$, corresponding to a residual muon polarization of ~ 0.17 . Here a_0 is the asymmetry parameter in the expression,

$$N(t) = N_0 e^{-\lambda t} \cdot \{1 + a_0 \cos(\omega t + \phi)\}.$$

All measurements of the asymmetry parameter a_0 in equation (2) include a factor P , the polarization of the muon at the instant of decay. Since the quantity of theoretical interest is the asymmetry parameter a_0 (or equivalently the final muon polarization at the instant of decay) it is necessary to remove the beam polarization factor P_b in order to compare our results with theoretical prediction. To deduce the value of P_b we compare our observed asymmetry in C (cf. Table V) of $a_0 = -0.048 \pm 0.003$ with the "accepted value" $a_0 = 0.055$, attributing the lower value measured in this experiment to a beam

polarization of $P_b = 0.87 \pm 0.05$. In the remainder of this Section, however, we have not removed this polarization factor from the observed asymmetries, on the grounds that even the "accepted value" has some uncertainties associated with earlier measurements of beam polarization. This is equivalent to an assumption of 100% beam polarization, or to placing an emphasis on the relative asymmetries rather than on their absolute values.

In this experiment³⁰ we have confirmed the results of Ignatenko, et al.,^{15,16} for C and Mg but have found contradictory results for measurements in H₂O and in several hydrocarbons. The earlier experiments reported values of a_0 in H₂O, paraffin, Mg and polyethylene¹⁹ all in good agreement with the C value. Our experiment and one performed simultaneously by Evseev, et al.,²⁹ show significantly reduced values for a_0 for the hydrogenous materials. Table V gives the best values for a_0 measured in this experiment. The high field results are asymmetries for the electron distribution attributed to the decay of a bound muon whose spin precesses at its characteristic Larmor precession frequency.

$$\omega_\mu = \gamma_\mu H_0 = 8.506 \cdot 10^6 \text{ radians/sec.},$$

for a 100 G field. Here $\gamma_\mu = e/m_\mu c$. The results for the hydrogenous targets all show low values for a_0 of approximately one-half the value measured in C. The low value for O₂ (in H₂O) of $a_0 = -0.019 \pm 0.002$ was noted in earlier experiment by other investigators.³¹

The expected total depolarization in strongly paramagnetic liquid O_2 has been confirmed by a result of $a_0 = 0.003 \pm 0.004$ in this substance.

The surprising result of complete depolarization of μ^- stopped in liquid He reported by Kane¹ and Hughes² was also confirmed in this experiment. For high field data our result was:

$$a_0 = -0.003 \pm 0.005.$$

The possible formation of the neutral atom ($\mu^-He e^-$) was investigated by using low precession fields and searching for a precession signal at the frequency expected for the $F = 1, m_F = 1$ state of the spin-coupled $\mu-e$ system. This frequency was given by:

$$\omega = \gamma_{\mu-e} \cdot H_0,$$

$$\text{where } \gamma_{\mu-e} = \frac{\mu_B}{h} (1 + m_e/m_\mu).$$

The results for this frequency were also consistent with total depolarization and were:

$$a_0 = -0.002 \pm 0.003.$$

The results for the hydrogenous materials and for liquid He are in disagreement with the predicted polarization and further mechanisms are required to explain the depolarization. Some possible mechanisms for

the total depolarization in liquid He are discussed in Section V-B. The low results for the hydrogenous materials are discussed in Section V-C.

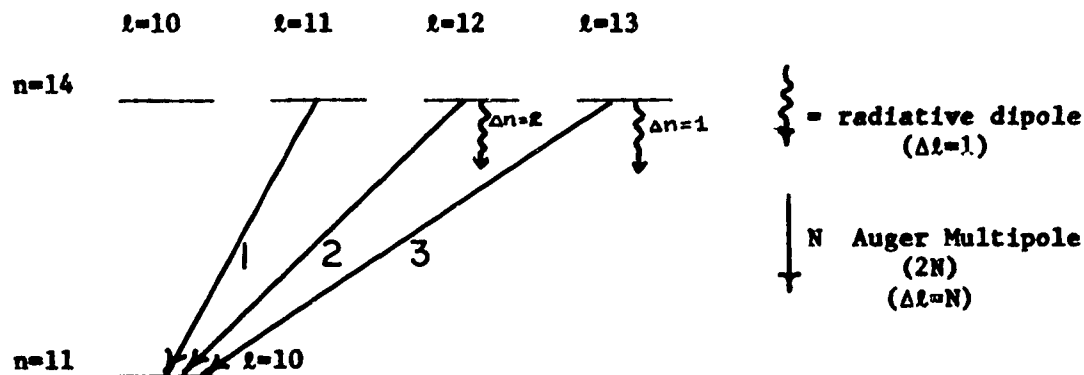
B. Liquid Helium

The results for this material are particularly puzzling because of the simplicity of the atomic system. However, there are significant differences between the cascade mechanisms for muonic He atoms and muonic C. The initial capture may proceed in the same way by the Auger ejection of an e^- from the capturing atom. After thus arriving at an initial level characterized by the quantum numbers n'' , l'' , and j'' , the μ^- then makes a series of transitions through various intermediate levels n' , l' , j' , and finally arrives in the $1s$ state from which it decays. In C the first five successive transitions are probably made by the Auger ejection of the remaining e^- . At this point the μ^- in C will have reached a level with $n = 6$. These stages are characterized by Auger rates³² given by:

$$\Gamma (\text{Auger}) \quad 10^{13-14} \text{ sec.}^{-1}$$

The subsequent transitions from $n = 6$ to $n = 1$ proceed by both radiative transitions and by further Auger ejection of e^- which have been resupplied to the C atom. In conductors the resupply rates are greater than $10^{12}/\text{sec.}$ so that the atom remains neutral throughout most of the cascade process. In He, however, several differences arise. After being captured the μ^- may make only one internal Auger transition.

Because of the tightly bound e^- in surrounding He atoms no neutralization is expected to take place. The radiative rates at levels of large principal quantum number n are characteristically 10^8 sec.^{-1} and much slower than the collision rates with surrounding He atoms ($> 10^{12} \text{ sec.}^{-1}$ at 4.2 K). The cascade then may proceed by the ejection of an e^- from a neutral He atom during a collision. During these collisions it is expected that Stark mixing of adjacent levels of the angular momentum l for the same principal quantum number n will occur. The following diagram is a representation of some of the possible transitions which can occur from "circular" ($l = n-1$) and near "circular" orbits for principal quantum number $n = 14$.



The Auger transition rates of higher multipole order have been calculated by Russell³² and can be generally described by:

$$\Gamma (2N \text{ Auger}) = 10^{-3 \cdot N} \Gamma (\text{Auger-dipole}),$$

where the $2N$ represents the multipole order and the transitions are to the same final value for n . It is energetically forbidden for the $n = 14$

level to undergo Auger transitions with $\Delta n < 3$ and for this reason the levels of $n = 12$, and 13 have been omitted from the diagram. The radiative transitions are dipole and proceed to final states with the minimum possible value of n . At this level in liquid He ($n = 14$, $l = 13$) the radiative rate to (13, 12) is $6.9 \cdot 10^7 \text{ sec.}^{-1}$ and the $\Delta l = 3$ Auger rate as calculated by Russell is approximately $2 \cdot 10^6 \text{ sec.}^{-1}$, while the rates out of the state (14, 12) are $8.1 \cdot 10^7 \text{ sec.}^{-1}$ for radiative dipole and $2 \cdot 10^9 \text{ sec.}^{-1}$ for $\Delta l = 2$ Auger. The Auger transitions are to the same final state (11, 10). The transition from (14, 11) to (11, 10) is an Auger dipole transition with a rate of $5.2 \cdot 10^{11} \text{ sec.}^{-1}$. The rates given here are calculated in the manner used by Michael³³ with the substitution of the μ^- mass for the K^- mass. Were it not for Stark mixing during collision with other He atoms, these high angular momentum states would not rapidly depopulate. This would lead to a small fraction of "trapped" muons as suggested by Condo³⁴ in an attempt to explain the long cascade time of π^- in liquid He ($t_{\pi^-} = 3.19 \cdot 10^{-10} \text{ sec.}$).³⁵ If the Stark mixing occurred at a rate on the order of $10^{12} \text{ sec.}^{-1}$ to adjacent levels the cascade should proceed at least an order of magnitude faster than the experimentally measured value. The pions should arrive in an s state within a few $\times 10^{-11} \text{ sec.}$ If Stark mixing is reduced by the same order as the high multipole Auger transition from the $l = 13$ to the $l = 11$ level then the rate out of the state (14, 13) would be approximately,

$$\Gamma \{ \text{Stark } (l=13 \rightarrow l=11) \} + \Gamma \{ \text{Auger } (14, 12) \rightarrow (11, 10) \}$$

$$\approx 5 \cdot 10^9 \text{ sec.}^{-1}$$

If all of the mesons were to initially form high angular momentum states instead of the small fraction suggested by Condo, then the long π^- cascade time could be explained. If the Stark rates to adjacent levels are reduced by two orders of magnitude then the (14, 13) level is again metastable and "trapping" of only a small fraction of π^- will explain the cascade time.

The initial distribution of the μ^- in the initial (n, l) levels has been a subject of interest in explaining the measured X-ray yields in liquid He.^{36,37} Computer coded cascade simulations have been used to study the dependence of the relative yields K_α/K_β and $K_\alpha/\text{all } K$ for pionic and muonic atoms. The initial l distribution was varied according to $P(l) = (2l + 1)e^{\alpha l}$ where α was found to be negative for the muonic He³ data. The Stark mixing rates were not varied but were sufficient to depopulate the trapped high angular momentum states.

If we do not consider the possibility of Stark mixing then the two highest angular momentum states for n = 14 are "trapped" and must proceed by radiative transitions or slow Auger transitions. Muons with n = 14, l = 11 will make a fast dipole Auger transition to the state (11, 10) which is also metastable with an estimated rate for combined $\Delta l = 2$ Auger transition to (9, 8) and radiative dipole to (10, 9) of $\Gamma_{\text{tot}} \approx 5 \cdot 10^8 \text{ sec.}^{-1}$ ($\Gamma_{\text{rad}}(11-10) \rightarrow (10, 9) = 1.5 \cdot 10^{+8} \text{ sec.}^{-1}$).

If the initial population of the angular momentum states is assumed to be statistical then 38% of the stopped muons would remain at these high n levels for times characteristic of the radiative rates or $t = 0.6 \cdot 10^{-8}$ sec. We now consider the effect of the remaining e^- . For this discussion we must neglect the state (14, 12) which is assumed to have ejected the second e^- in making the allowed dipole Auger transition. The μ^- trapped in the initial levels may now form a spin-coupled angular momentum system with the remaining e^- . As noted before, the characteristic frequency of precession of the system is:

$$\omega_{\mu-e} = 8.79 \cdot 10^6 \text{ rad/(gauss sec.)} \cdot H_0,$$

and for 100 G fields would be approximately $8.8 \cdot 10^8$ rad/sec. The phase contributed by this coupling, lasting for $t = 0.6 \cdot 10^{-8}$ sec., to the initial μ^- spin direction would be $\phi' \approx 5$ radians. The system will remain until the μ^- falls to a level where Auger ejection of this e^- is allowed and the μ^- will subsequently reach the ground state of the positively charged muonic He atom. The fact that such μ^-e^- precession was not observed in this experiment does not counter this argument since, in this scheme, the system exists for only 10^{-8} sec. If this mechanism were allowed it would require that 80% of the initially captured muons reach these trapped levels in order to account for the total depolarization noted here. Since we have turned off the Stark mixing for this argument, and since the atomic capture process of both π^- and μ^- should be nearly identical, this formation would predict π^- cascade times of

approximately 10^{-8} seconds which is in obvious disagreement with the measured value of $3.19 \cdot 10^{-10}$ sec.^{38,35} We must then argue for either increased Stark mixing rates or a large shift toward lower values of angular momentum in the initial capture populations. The cascade times for μ^- in liquid He from levels of $n = 14$, assuming no trapping, are approximately $5 \cdot 10^{-11}$ seconds. Negative pions begin their cascades from slightly higher initial values of the principal quantum number n , but the rates for the allowed transitions are still $> 10^{12}$ sec.⁻¹ Condo pointed out that only a few such "traps" could explain the long cascade time results if they were trapped appreciably longer than 10^{-10} seconds. It has been found that in order to explain the relative yields of the pionic K_β/K_α and $K_\alpha/\text{all K X-rays}$ in liquid ^3He and ^4He , a large shift toward low values of l was required.³⁶ This is inconsistent with the arguments presented above which would tend to fill "circular orbits".

The He-muonic ion $(\mu^-\text{He})^+$ is not likely to be neutralized by the recapture of an e^- . The e^- of neighboring He atoms are bound by approximately 4 times the energy as in the proton-like $(\mu^-\text{He})^+$ ion. The e^- which might possibly be captured by this ion would be those ejected from neighbors during the early stages of the cascade. During the final stages while Auger deexcitation is still the dominant mechanism, the energy given to the external e^- is sufficient to insure their disappearance from the region of the muonic helium ion.

The possible formation of large clusters in liquid He $(\mu^-\text{He})^+\text{He}_n$ has been suggested but it is not expected that these aggregations would

have any net magnetic influence on the μ^- spin.³⁹

In summarizing these remarks concerning the depolarization in liquid He little can be said of a definitive nature. The cascade and capture mechanisms proposed by Shmushkevich³ are insufficient to explain the depolarization found in liquid He. The possibility of e^- recombination with the muonic ion has been investigated by looking for the spin coupled precession. We have ruled out the possibility of the formation of the $(\text{He}\mu^-e^-)$ neutral atom if the muon is still polarized ($P \geq 6\%$) in the ground state and if the recombination is assumed to take place in less than 10^{-8} sec. A slow recombination rate of the order of 10^{+7} sec.⁻¹ would result in a random initial phase for the μ -e system being investigated.

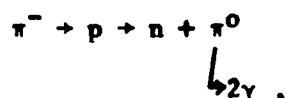
The evidence for low angular momentum populations found in the π^- and μ^- X-ray yields in both liquid ^3He and ^4He strongly suggest that the cascade mechanisms of Shmushkevich are altered and the depolarization may certainly be affected by this change. If the depolarization in liquid He is due to bulk effects, a measurement of the decay electron distribution from μ^- stopped in He gas might yield a detectable asymmetry.

One other noble gas has shown similar properties. Kane¹ observed a complete lack of polarization in liquid Argon. Backenstoss, et al.,⁴⁰ observed the K X-rays in gaseous Argon at 180 atm. The resulting spectra showed no K_β (3P-1s) transitions in the pure gas, but when it served as an impurity in gaseous H this transition became apparent. The simultaneous measurement of the K_α (2P-1s) transition in liquid He and the

decay distribution, might provide some information as to the mechanisms involved in the depolarization.

C. Hydrocarbons and Water

Ponomarev²² has suggested that evidence is strongly in favor of the formation of large mesic molecules when π^- or μ^- are stopped in chemical compounds. Zinov, et al.,⁴¹ have found significant changes in the muonic $K_{\nu}/\text{all } K$ relative X-ray yields when measured first in pure metals and then in oxides. Panofsky, et al.,⁴² found results indicating that a strong deviation from capture rates measured in mixtures was found when measured in compounds of the same materials. The capture process,



for H_2 was identified by the detection of the γ rays emitted in the decay of the π^0 . The "Z law"⁴³ predicts that this process should be simply proportional to the compound ratios or that,

$$W(Z, H_n) = n/mZ,$$

where W = probability for the process $\pi^- + p \rightarrow n + \pi^0$, per stopped π^- . The results for measurements made in LiH, various hydrocarbons, H_2O and other materials, gave results, in disagreement with the Z law, which could be approximated well by:

$$W(Z, H_n) = anZ^{-3}/m.$$

Ponomarev has proposed that some of the negative mesons may be stopped in molecular orbits of the $\bar{\mu}_m H_n$ molecule, by an adiabatic replacement of the valence electrons. The probability for transitions to the states of the isolated $p\mu^-$ atom are small. This is due to the low radiative rates out of the molecular orbitals as compared to the Auger transition rates. The Auger effect requires a large overlap between the final meson state and the initial state of the ejected e^- . Since there are no e^- in isolated H atomic states, no Auger transitions are possible. The only e^- in isolated atomic states are in states of the Z atom. The μ^- will quickly form the $Z\mu^-$ atom by the Auger ejection of one of these atomic e^- . The rates for processes such as $\mu^- \rightarrow$ molecular orbital $+ H \rightarrow Z\mu^-$ are therefore small. Results in hydrocarbons required a modification of the expression for W resulting in:

$$W(C_m H_n) \propto nZ^{-2}/\nu m.$$

Here ν is the number of valence electrons in the C atom. The enhancement of Z/ν is proposed to take into account the two s electrons in the C atom, these form a closed shell and it is argued that they do not participate in the initial capture process. In the picture presented for these disruptions in the capture probabilities only the C-H or Z-H bonds are considered.

If we make the assumption that all e^- in the molecule are equivalent and omit the 1s e^- in C, then the probability for forming molecular states at initial capture W_1 is given by:

$$W_1(C_m H_n) = 2n/(n + vm).$$

If these orbitals lead to total depolarization of the μ^- through some mechanism then the residual polarization would be:

$$\begin{aligned} a_o^{C H n} &= (1 - W_1) \cdot a_o^C = \frac{vm - n}{vm + n} \cdot a_o^C \\ &= \frac{(4m - n)}{(4m + n)} \cdot a_o^C, \text{ where } v = 4 \text{ in C.} \end{aligned}$$

For several hydrogenous materials we obtain:

$$a_o^{CH_2} = 1/3 \cdot a_o^C$$

$$a_o^{CH} = 3/5 \cdot a_o^C$$

$$a_o^{H_2O} = 1/2 \cdot a_o^C$$

if we neglect the $1s e^-$ in O.

For H_2O we might expect similar results although the valence bond structures and chemical behavior of the μ^- are probably quite different. It should be noted that the results of this experiment are not in detailed agreement with these predictions. Our results show a slight increase in asymmetry values for increasing H fractions. In general, the approximately one-half loss in polarization for these targets is at least qualitatively explained by these arguments. The transitions from

molecular orbitals to bound atomic levels in C may be to states with significantly lower values of angular momentum than in the direct atomic capture process. This could then lead to nearly complete depolarization in the subsequent cascade to the ground state.

The two hydrocarbons, Pilot B and polyethylene, which are reported in this experiment gave some indication of a slow (3 μ sec.) relaxation time for the asymmetry parameter a' . Such relaxations might be due to random recapture of some of the e^- into the partially ionized μ^-C atom. A slow recombination rate for these e^- could mean that the μ^- forms the μ^-e^- system only for short times as compared to its lifetime so that at a later time the μ^- is again free from the magnetic influence of the e^- . In this manner the μ^- would gradually lose their polarization. The possibility of a large fraction of the μ^- finding their way first to a H atom and being depolarized by the hyperfine structure and then decaying there is argued against by some recent measurements of asymmetry in hydrocarbons. R. Arlt, et al.,⁴⁴ measured μ^- decay asymmetry in coincidence with a C K_β or higher K transition X-ray. This experiment was performed for the C X-rays in paraffin. The result for the asymmetry was the same for that measured in the paraffin with no X-ray detection or $a_0^{\text{paraffin}} \approx 1/2 \cdot a_0^C$. It might be surprising if this were not so, since we have argued that low angular momentum states can contribute more strongly to the depolarizing mechanisms set forth by Shmushkevich, and it seems that the higher K transition yields would result from a lowering of the initial angular momentum. Because of the fairly large

errors involved in our asymmetry values such a dependence on the exact cascade scheme would be hard to determine. We have proposed earlier that a measurement of the e^- distribution in coincidence with observation of the muonic K_α X-ray transition would be of interest since these events must include the cascade transitions from circular orbits.

In summary, it appears from the hydrocarbon data that the molecular processes suggested by Gershtein²¹ and Ponomarev²² at least have pointed to the most likely sources of depolarization in these substances.

D. Liquid Oxygen

The velocity of a thermalized muonic O atom at liquid O₂ temperatures is approximately 10^5 cm/sec. At this velocity the muonic system experiences approximately $3 \cdot 10^{11}$ collisions per second. The collisional depolarization of the muonic O atom is explained in the following manner. We assume a random orientation of the magnetic moments of the unpaired O valence e^- during these collisions and estimate the fields experienced by the μ^- during each collision by $2\mu_B/a_0 = 1.2 \cdot 10^5$ gauss. We further assume that a statistical variation in the relative number of opposite orientations will yield approximately

$$N = \sqrt{t \cdot 3 \cdot 10^{11}} \text{ sec.}^{-1}$$

net collisions with the fields oriented along some axis. The time of interaction is taken as 10^{-12} sec. and we obtain the following value for the expected random phase accumulation $\bar{\phi}_r$,

$$\bar{\phi}_r = (\sqrt{t \cdot 3} \cdot 10^{11}) \cdot (3 \cdot 10^{-2} \text{ radians}).$$

For $t = 10^{-8}$ seconds $\bar{\phi}_r = 1.5$ radians. And for $t = 10^{-7}$ seconds $\bar{\phi}_r = 5$ radians. This is sufficient to depolarize the muon spin for the purposes of this experiment.

This depolarization is more severe for μ -e coupled system due to the larger magnetic moment. The results of this experiment are consistent with total depolarization of the muon in $< 10^{-6}$ seconds.

E. Conclusions

The search for a precession signal from the spin-coupled (μ^- -e $^-$) atomically bound system yielded no residual polarization for any target substance employed. No evidence was found for the formation of the neutral atom ($\text{He}^{++}\mu^-e^-$). If this neutral system were formed in less than 10^{-8} sec. with a probability $\geq 11\%$ while the μ^- was still polarized, and in the atomic ground state, the low field search would have yielded a measurable polarization result. Other mechanisms must be present for the explanation of the He result. The formation of the $(\mu^- \text{He})^+ \text{He}$ molecular ion may occur, but the binding is through dispersive forces only at an internuclear spacing of several Bohr radii.³² This molecule is therefore not expected to influence the μ^- spin. Other experimental evidence^{36,37} argues against the possible "trapping" of the μ^- in high angular momentum states before the atomic cascade to the ground state, and therefore the depolarizing effects associated with the electrons in the formation of the $(\mu^- \text{He})^+$ atom are assumed to be negligible.

The hydrocarbon and H₂O results are qualitatively explained by the theoretical predictions based on the formation of muonic molecular states preceding the cascade to the ground state.²² No evidence was seen for the formation of the (μ^-e^-) spin-coupled system in the hydrocarbon targets of Pilot B scintillant, polyethylene, and toluene.

The enhanced populations of the low angular momentum states, predicted from the molecular formation²² in the hydrocarbons and required by the X-ray yield measurements in liquid He,^{36,37} may be the cause for the depolarization observed. A large deviation from the statistical $(2l + 1)$ angular momentum distribution would alter the prediction^{3,4} based on the fine structure interaction during the atomic cascade, in a way which would lead to lower polarization of the μ^- .

Since both the depolarization and X-ray yields show strong dependence on the atomic cascade and on the initial populations of the angular momentum states, it would perhaps be useful to perform the cascade calculations with both X-ray yield and final polarization as constraints. It is also possible to measure the residual polarization in these substances in coincidence with the observation of a specific X-ray transition.⁴⁴ These measurements might give some information about the effect of a particular cascade path on the ground state polarization of the μ^- .

VI. TABLES

- I. Carbon Calibration Parameters**
- II. Target Thickness**
- III. Energy and Geometry Correction Factors**
- IV. Negative Muon Lifetimes**
- V. Summary of Experimental Results**
- VI. Results for Hydrogenous Materials at High Fields**
- VII. Asymmetry Results**

TABLE I

CARBON CALIBRATION PARAMETERS (a)
LIFETIME 2.027×10^{-6} SEC.

Run No.	χ^2_{ν}	N_0	ω/H rad/(gauss sec.)	ϕ radians	B/N_0	$-a'$ (b)
10(c)	0.97	3123 ± 8	$(8.54 \pm 0.07) \times 10^4$	-0.11 ± 0.13	0.076	0.034 ± 0.004
11	1.07	6485 ± 10	8.49 ± 0.05	$+3.03 \pm 0.12$	0.010	0.040 ± 0.003
13	0.95	3381 ± 7	8.51 ± 0.05	$+3.07 \pm 0.12$	0.013	0.039 ± 0.003
15	1.06	3990 ± 8	8.48 ± 0.05	$+3.02 \pm 0.12$	0.008	0.042 ± 0.003
22(d)	1.01	2279 ± 10	8.50 ± 0.05	$+3.08 \pm 0.11$	0.026	0.041 ± 0.004
102	1.12	3995 ± 7	8.49 ± 0.05	$+3.02 \pm 0.12$	0.019	0.042 ± 0.003
107	0.88	3870 ± 7	8.52 ± 0.05	$+2.96 \pm 0.11$	0.017	0.042 ± 0.003
117	0.91	3807 ± 7	8.49 ± 0.05	$+3.43 \pm 0.11$	0.017	0.046 ± 0.003

(a) The analysis results are from a five parameter non-linear fit for the parameters N_0 , a' , ω , ϕ , and B . The data interval was from 0.28 μ sec. to 6.08 μ sec. (channels 15-304).

(b) Asymmetry values do not include corrections for solid angle or electron energy loss.

(c) Forward muons were incident for this run, all others were taken with backward muons.

(d) The carbon target was located inside the stainless steel helium dewar and the analysis included subtraction of the background from stops in the dewar walls.

TABLE II
TARGET THICKNESS

Target	Thickness	Dimensions (cm)		
		W	H	T
Carbon	4.41 g/cm ²	15.3	15.3	3.0
Magnesium	1.74	10.2	10.2	1.27
Helium (liquid) ^(a)	1.59	15.3 cm cylinder		
H ₂ O	5.47	15.3	15.3	5.5
O ₂ (liquid) ^(b)	11.0	10 cm cylinder		
Pilot B	5.20	15.3	15.3	5.0
Toluene	4.40	15.3	15.3	5.0
Polyethylene	4.68	15.3	15.3	5.0
Paraffin	5.95	15.3	15.3	6.7

(a) The helium was contained in the target cryostat.

(b) The liquid was contained in a cylindrical stainless steel dewar, of 25 cm height and 10 cm inside diameter.

TABLE III
ENERGY AND GEOMETRY CORRECTION FACTORS

Target	x_0 ^(a)	$F(x_0)$	$\Omega/4\pi$	$F(\Omega)$
Carbon	0.115	1.0054	0.130	0.858
Magnesium	0.078	1.0017	0.130	0.859
Helium (liquid)	0.074	1.0015	0.119	0.858
H ₂ O (distilled)	0.156	1.0129	0.131	0.856
Oxygen (liquid)	0.200	1.0259	0.133	0.850
Pilot B Scintillant	0.142	1.0099	0.131	0.856
Toluene (reagent)	0.125	1.0069	0.131	0.856
Polyethylene	0.139	1.0093	0.131	0.856
Paraffin	0.165	0.0151	0.132	0.854

(a) E_0 is the minimum energy of electrons which will penetrate 1/2 of the target thickness and counter 4 of the telescope. x_0 is the ratio of E_0 to the maximum energy of decay electrons.

TABLE IV
NEGATIVE MUON LIFETIMES

Element	Mean Lifetime	
	This Experiment	Earlier Work ^(a)
He	$(2.186 \pm 0.014) \times 10^{-6}$ sec.	$(2.1982 \pm 0.0026) \times 10^{-6}$ sec.
C	2.027 ± 0.004	2.034 ± 0.004
O	1.816 ± 0.008	1.812 ± 0.010
Mg	1.105 ± 0.040	1.070 ± 0.030

(a) M. Eckhause, R. T. Siegel, R. E. Welsh, and T. A. Filippas, Nucl. Phys. 81, 575 (1966). This paper includes a compilation of Lifetimes measured prior to 1965.

TABLE V
SUMMARY OF EXPERIMENTAL RESULTS ^(a)

	Analyzed Events	$-a_0$ ^(b)
A. <u>High Fields</u> (Analyzed for free muon precession)		
Carbon	1.990×10^6	0.048 ± 0.003 ^(c)
Magnesium	0.433	0.044 ± 0.004
Helium	0.183	0.003 ± 0.005
H ₂ O (distilled)	0.968	0.019 ± 0.002
Oxygen (liquid)	0.332	0.003 ± 0.004
Pilot B Scintillant	0.875	0.016 ± 0.002
Toluene (reagent)	0.543	0.021 ± 0.003
Polyethylene	0.667	0.022 ± 0.002
Paraffin	0.621	0.026 ± 0.002
B. <u>Low Fields</u> (Analyzed for μ-e hyperfine precession)		
Oxygen (liquid)	0.334×10^6	0.008 ± 0.004
Helium (liquid)	0.382	0.002 ± 0.003
Pilot B Scintillant	0.356	0.001 ± 0.003
Toluene (reagent)	0.336	0.001 ± 0.004
Polyethylene	0.296	0.0 ± 0.004

- (a) The results quoted here are for a two parameter fitting procedure for N_0 and a' on each individual data set. The data interval was from 0.4 μ sec. to 4.4 μ sec.
- (b) The value given for a_0 is the weighted mean of the results from each single run of the same target. Corrections for solid angle and electron energy loss are included.
- (c) The errors quoted are not statistical but represent the standard deviation for the weighted mean calculated from all the results of individual runs of the same target.

TABLE VI
RESULTS FOR HYDROGENOUS MATERIALS AT HIGH FIELDS^(a)

Target	χ^2_{ν}	N_0	ω $\times 10^6$ rad/sec.	ϕ radians	B	$-a'$ ^(b)
H₂O						
Run 16	0.96	3662±12	8.27±0.08	2.58±0.34	33±2	0.017±0.003
112	0.92	5282±16	8.69±0.16	2.95±0.42	83±3	0.016±0.003
114	1.01	6010±13	8.78±0.13	3.04±0.27	97±3	0.015±0.002
Pilot B Scintillant						
Run 14	1.02	4547±12	8.35±0.13	2.65±0.28	56±3	0.014±0.003
(c)23	1.10	610±4	8.59±0.30	2.57±0.57	4±1	0.013±0.008
106	0.94	3865±12	9.10±0.15	2.79±0.33	67±3	0.015±0.003
109	1.09	3832±12	8.65±0.19	3.13±0.47	67±3	0.012±0.003
Polyethylene						
Run 12	1.03	5404±12	8.51±0.08	2.66±0.20	50±2	0.019±0.002
104	1.09	3918±10	8.67±0.10	2.90±0.24	58±2	0.019±0.003
Paraffin						
Run 103	0.83	3837±14	8.41±0.10	3.12±0.26	80±3	0.025±0.003
113	0.93	4836±13	8.76±0.11	2.73±0.26	85±3	0.021±0.003
Toluene						
Run 110	0.98	3842±11	8.71±0.10	3.10±0.26	65±2	0.018±0.003
115	0.96	3755±11	8.68±0.10	3.15±0.24	62±2	0.020±0.003

(a) The results reported here are from a five parameter fit for N_0 , a' , ω , ϕ , and B over the data interval 0.28 μ sec. to 6.08 μ sec.

(b) Asymmetry results do not include corrections for solid angle or electron energy loss.

(c) Array of thin sheets inside of stainless steel dewar.

TABLE VII
ASYMMETRY RESULTS^(a)

	N_{ss} ^(b)	B ^(b)	χ^2_{ν} ^(c)	N_0 ^(c)	$-a'$ ^(c,d)
A. <u>High Fields</u> (Analyzed for free muon precession)					
(C-22)^(e)					
Helium 24	318	13	1.04	867 ± 3	0.004 ± 0.005
26	255	19	0.94	903 ± 4	0.002 ± 0.005
28	254	10	0.93	638 ± 3	-0.001 ± 0.006
(C-117)					
Oxygen 118	800	75	0.98	5154 ± 9	-0.001 ± 0.002
B. <u>Low Fields</u>^(f) (Analyzed for μ-e hyperfine precession)					
(C-22)					
Helium 25	1000	22	1.15	3966 ± 7	-0.000 ± 0.003
27	390	10	0.96	1082 ± 4	-0.001 ± 0.005
(C-15)					
Pilot B 18	none	42	1.04	4981 ± 9	-0.001 ± 0.003
Polyethylene 19	none	30	1.09	4134 ± 8	-0.002 ± 0.003
(C-117)					
Oxygen 119	800	76	0.91	5162 ± 9	0.003 ± 0.002
Toluene 120	none	38	0.98	4693 ± 8	0.002 ± 0.003

- (a) These runs were analyzed by a two parameter linear procedure for N_0 and a' .
- (b) These values are results of a three parameter analysis for N_{ss} , N_0 , and B. The amount of stainless steel background is given by its amplitude at $t = 0$, N_{ss} .
- (c) These results are from a two parameter analysis N_0 and a' which used the results from (b) for subtraction of stainless steel background. The data interval was from 0.28 μ sec. to 6.28 μ sec.
- (d) Asymmetry results do not include corrections for solid angle or electron energy loss.
- (e) Values of the precession frequency and phase angle used here were taken from the C calibration run shown in parentheses.
- (f) Here the frequency was calculated from the expected precession rate of the $F = 1$, $m_F = 1$ state of the μ -e system and values for the phase were taken from the indicated C high field calibration run.

VII. APPENDICES

APPENDIX A

Least Squares Analysis Procedure

A complete description of the general fitting procedures for statistical data is given by Bevington.⁴⁵

The expression which describes the data in this experiment is assumed to be in the form shown below.

$$N(t) = N_0 e^{-\lambda t} \cdot \{1 + a' \cos(\omega t + \phi)\} + B, \quad (\text{A-1})$$

where N_0 is the number of counts in the $t = 0$ bin of the spectrum (for $a' = 0$), λ is the total disappearance rate for negative muons, a' is the asymmetry coefficient, ω is the precession frequency, ϕ is the initial phase angle, and B is the accidental background rate. This expression is not a linear combination of the parameters and therefore a non-linear analysis is required. An expansion of the function $N(t)$ in the form of a Taylor's series expansion in the parameters was chosen to give a locally valid linear approximation to $N(t)$.

$$\begin{aligned} N(t) &= N(t) \Big|_0 + \sum_j \frac{\partial N(t)}{\partial P_j} \Big|_0 (P_j - P_j^0) \\ &= N(t) \Big|_0 + \sum_j f_j(t) P_j, \end{aligned} \quad (\text{A-2})$$

where $|_0$ implies evaluation of the function at the initial values of subsequent corrected values of the parameters, $f_j(t)$ is the derivative of $N(t)$ with respect to the parameter P_j , p_j is the difference between P_j and P_j^0 , and P_j^0 is the current value of the parameter P_j . In this analysis the technique of least squares was applied to minimize the quantity Chi squared:

$$\chi^2 = \sum_1 \frac{\{Y_1 - N(t_1)\}^2}{\sigma_1^2}, \quad (\text{A-3})$$

where Y_1 is the data value at $t = t_1$, and $\sigma_1^2 = Y_1$, assuming a Poisson distribution for each point.

Substitution of expression (A-2) for $N(t_1)$ in equation (A-3) yields:

$$\chi^2 = \sum_1 \frac{\{Y_1 - N(t_1)|_0 - \sum_j f_j(t_1)p_j\}^2}{\sigma_1^2}. \quad (\text{A-4})$$

A necessary and sufficient condition for a local minimum in χ^2 is that all of the first derivatives with respect to the p_j vanish.

$$-\frac{\partial \chi^2}{\partial p_j} = \sum_1 \frac{f_j(t_1)\{Y_1 - N(t_1)|_0 - \sum_k f_k(t_1)p_k\}}{\sigma_1^2} = 0. \quad (\text{A-5})$$

The following identifications were made:

$$D_{jk} = \sum_1 \frac{f_j(t_1)f_k(t_1)}{\sigma_1^2} \quad (\text{A-6})$$

$$S_j = \sum_1 \frac{f_j(t_1)(Y_1 - N(t_1)|_0)}{\sigma_1^2};$$

and from expression (A-5) we obtained:

$$D_{jk}P_k = S_j, \quad (A-7)$$

where the repeated subscript k in the product indicates a sum over all possible values for that subscript. If there are N parameters, D_{kj} is an N x N square matrix. If there exists an inverse DI of the matrix D such that

$$\begin{aligned} DI_{jk}D_{kl} &= \delta_{jl} = 1, \text{ if } j = l \\ &= 0, \text{ if } j \neq l, \end{aligned} \quad (A-8)$$

we may operate on (A-7) with the inverse DI to obtain:

$$DI_{lk}D_{kj}P_j = DI_{lk}S_k;$$

or, substituting (A-8) for $DI_{lk}D_{kj}$, we have:

$$\delta_{lj}P_j = P_l = DI_{lk}S_k. \quad (A-9)$$

The expressions (A-9), N in number, are the results for the corrections to the parameters P_l which yield an approximate minimum value for χ^2 . From (A-2) we have $P_j = P_j^0 + p_j$. P_j^0 is set to the corrected value for P_j and the procedure is repeated. Successive iterations were performed until the values for p_j were less than the selected convergence test value,

$$p_j \leq C_{\text{test}} \cdot P_j.$$

C_{test} was typically 0.0001 and 3 to 10 iterations were required depending on the initial estimates for the various parameters, before this condition was met.

The errors on each parameter were determined from the statistical variations in the data,

$$\sigma_{P_j}^2 = \sum_i \left(\frac{\partial P_j}{\partial Y_i} \sigma_i \right)^2 . \quad (\text{A-10})$$

The D_{jk} are assumed independent of the Y_i and inserting (A-9) into (A-10) yields,

$$\sigma_{P_j}^2 = \sum_i DI_{jk} \frac{\partial S_k}{\partial Y_i} DI_{j\ell} \frac{\partial S_\ell}{\partial Y_i} \sigma_i^2 , \quad (\text{A-11})$$

where summation over j is suppressed.

From (A-6) we obtain:

$$\frac{\partial S_k}{\partial Y_i} = f_k(t_i) / \sigma_i^2$$

and

$$\frac{\partial S_\ell}{\partial Y_i} = f_\ell(t_i) / \sigma_i^2 ,$$

which when substituted into (A-11) give:

$$\begin{aligned} \sigma_{P_j}^2 &= DI_{jk} D_{k\ell} DI_{j\ell} \\ &= \delta_{j\ell} DI_{j\ell} \\ &= DI_{jj} . \end{aligned}$$

This simple definition of the statistical error on the parameters does not include the off-diagonal contributions linking the parameters to each other. It is the error reported here where

$$\text{Error } P_j = \sqrt{DI_{jj}}. \quad (\text{A-12})$$

This procedure was coded in Fortran language for execution on an IBM/360 Os Computing system at the College of William and Mary and subsequently modified for an IBM/1130 DOS system at the Virginia Associated Research Campus. An important feature of the procedure was the subprogram which defined the derivatives $f_j(t)$. By isolating this part of the calculation the number and type of the parameters to be used in the fit could be easily modified.

The values for χ^2 reported are normally expressed as χ_v^2 where

$$\chi_v^2 = \chi^2 / (\text{number of data points} - N).$$

It should be noted that in two cases the data were able to be expressed in a linear form.

(1) Stainless steel backgrounds were evaluated by

$$N(t) = N_{ss} e^{-\lambda_{ss} t} + N_0 e^{-\lambda t} \{1 + a' \cos(\omega t + \phi)\} + B, \quad (\text{A-13})$$

where precession was assumed known and only N_{ss} , N_0 and B were fit.

(2) Fits for N_0 and a' only resulted in an expression for the data

$$N(t) = N_0 e^{-\lambda t} + A' \cdot e^{-\lambda t} \cdot \cos(\omega t + \phi) + B, \quad (\text{A-14})$$

where $A' = a' \cdot N_0$.

If we identify the terms in (A-2) as the products of parameters and analytic functions rather than corrections and derivatives, then the results for the procedure after only one iteration will be the values of the parameters. Since none of the functions f_j were dependent on the fitted parameters N_{SS} , N_0 , A' or B a linear procedure could be used. Since all of the sums are the same, with the new identifications of the functions, the same computer procedure could be used. Using this procedure the computer running time was halved. If a non-linear procedure was used, after two iterations the results were identical to the linear modification results. By substituting P_j for p_j and the appropriate functions from either (A-13) or (A-14) for $N(t) |_0$ and $f_j(t)$ in the preceding discussion the linear analysis is obtained.

APPENDIX B

Corrections to Asymmetry

1. Solid Angle Correction

In equation (2) the parameter a' is experimentally determined from the data. For a telescope of finite dimension a correction must be made for the following effect. For electrons decaying into the solid angle element, $d\Omega(\theta)$, the expression becomes:

$$dn(\theta) = \{N_0(1 + a'' \cdot \cos(\theta)) + B\} d\Omega(\theta), \quad (B-1)$$

where θ is the angle between the muon spin and the direction of the element of solid angle $d\Omega(\theta)$. If we assume a uniform distribution of stopping muons the total expression is obtained by integrating $dn(\theta)$ over the target volume and the telescope solid angle.

$$N(\theta) = \int dr^3 \int dr'^2 \frac{d\Omega(r',r)}{dr'^2 dr^3} \{N_0(1+a'\cos(\theta(r,r')))\},$$

$$\text{or } N(\theta) = N_0 \{ \int \int 1 + a'' \int \int \cos(\theta(r,r')) \}. \quad (B-2)$$

The expression, $\int \int 1$, represents the product of the average solid angle and total volume. This reduces to:

$$N(\theta) = N_0 \{ 1 + a' F(\Omega) \cos(\bar{\theta}) \}, \quad (B-3)$$

where $F(\Omega) = \int \int \cos\theta(r,r') / \{ \cos\bar{\theta} \cdot \int \int 1 \}$,

where $\bar{\theta}$ is the angle between the muon spin and the symmetric target-telescope axis, which was the beam axis.

$F(\Omega)$ presents a correction factor reducing the value of the observed asymmetry. The parameter a' was then given by the following expression:

$$a' = a''F(\Omega).$$

$F(\Omega)$ was calculated by two methods. The first estimates were made by employing a Monte-Carlo selection of values for all five coordinates. Later a program was written for a Wang programmable calculator which performed a numerical integration over the target area and telescope solid angle using cylindrical geometry along the beam axis. In this way cylindrical target elements could be used and most of the calculation could be completed analytically. The corners of the telescope were included by numerical integration. The results for both methods of calculation were the same within variations of the values obtained by the Monte-Carlo technique. And typical results were:

$$\frac{\bar{\Omega}}{4\pi} = 0.13$$

$$\text{and } F(\Omega) = 0.86.$$

2. Energy Corrections

In Section I the dependence of the decay electron distribution on electron energy was given by:

$$dN(\theta, x) = 2x^2\{(3-2x) + (1-2x)\cos(\theta)\}dx d\Omega/4\pi.$$

When the above expression is integrated over all possible energies ($0 \leq x \leq 1$), the result,

$$dN(\theta) = (1 + a_0 \cos\theta) d\Omega / 4\pi,$$

is obtained, where $a_0 = -1/3$. If the integration is limited to values of x above some minimum value x_0 the result can be written in the following form:

$$a''(x_0) = a_0 \cdot F(x_0).$$

The integration over energy is straightforward and gives:

$$F(x_0) = 1 + \frac{4x_0^3(1 - x_0)}{1 - 2x_0^3 + x_0^4}.$$

Values for x_0 were calculated based on electron range-energy relationships. The range was assumed to be one-half of the target thickness plus the thickness of any material between the target and the second telescope counter (counter 5). Values for x_0 and $F(x_0)$ are also given in Table II. The energy correction was not included in an analytical way during the solid angle calculation. This is justified by the relative size of this correction as compared to the solid angle correction. The energy corrections are small and can be approximated well by an average value for each target. These corrections are also much smaller than the statistical errors on the parameter a' for every run.

Combining both corrections we obtain the following simple relationship:

$$a' = a_0 \cdot F(x_0) \cdot F(\Omega).$$

VIII. REFERENCES

1. J. R. Kane, Carnegie Institute of Technology Report No. 882-9, 1964 (unpublished).
2. R. Prepost, V. W. Hughes, S. P. Penman, D. McCohn, and K. Ziock, *Bull. Am. Phys. Soc.* 5, 75 (1960).
3. I. M. Shmushkevich, *Nucl. Phys.* 11, 419 (1959).
4. R. A. Mann and M. E. Rose, *Phys. Rev.* 121, 293 (1961).
5. T. E. Lee and C. N. Yang, *Phys. Rev.* 105, 1671 (1957).
6. C. S. Wu, E. Ambler, R. W. Hayward, D. D. Hoppes, and R. F. Hudson, *Phys. Rev.* 105, 1413 (1957).
7. R. L. Garwin, L. M. Lederman, and M. Weinrich, *Phys. Rev.* 105, 1415 (1957).
8. M. Goldhaber, L. Grodzins, and A. W. Sunyar, *Phys. Rev.* 109, 1015 (1958).
9. M. Goldhaber, L. Grodzins, and A. W. Sunyar, *Phys. Rev.* 106, 826 (1957).
10. R. P. Feynman and M. Gell-Mann, *Phys. Rev.* 109, 193 (1958).
11. Burgy, Krohn, Novey, Ringo, and Telegdi, *Phys. Rev.* 110, 1214 (1958).
12. C. S. Wu and S. A. Meszkowski, Monographs and Texts in Physics and Astronomy XVI ("Beta Decay"), John Wiley & Sons, New York (1966).
13. Sergio DeBenedetti, Nuclear Interactions, John Wiley & Sons, New York (1964).
14. G. W. Ford and C. J. Mullin, *Phys. Rev.* 108, 477 (1957).
15. A. E. Ignatenko, L. B. Egorov, B. Khalupa, and D. Chulthem, *Soviet Physics JETP* 35, 894 (1958).

16. A. E. Ignatenko, E. B. Egorov, B. Khalupa, and D. Chulthem, *Soviet Physics JETP* 35, 1131 (1958).
17. H. Uberall, *Phys. Rev.* 114, 1640 (1959).
18. E. Lubkin, *Phys. Rev.* 119, 815 (1960).
19. L. B. Egorov, G. V. Zhuravlev, A. E. Ignatenko, Li Syuang-Ming, M. G. Petrashku, and D. Chulthem, *Nucl. Phys.* 23, 62 (1961).
20. V. W. Hughes, *Phys. Rev.* 108, 1106 (1957).
21. S. S. Gershtein, V. I. Petrukhin, L. I. Ponomarev, and Yu. D. Prokoshkin, *Usp. Fiz. Nank. (U.S.S.R.)* 97, 3 (1969). (Translation: *Soviet Physics USPEKHI* 97, 1 (1969).
22. L. I. Ponomarev, *Ann. Rev. Nucl. Sci.* 23, 395 (1973).
23. J. B. Birks, *The Theory and Practice of Scintillation Counting*, Pergamon Press, New York (1964).
24. M. Eckhause, R. T. Siegel, and R. E. Welsh, *Nucl. Instr. and Meth.* 43, 365 (1966).
25. D. C. Buckle, J. R. Kane, B. D. Orrick, R. T. Siegel, and R. J. Wetmore, *Nucl. Instr. and Meth.* 77, 249 (1970).
26. D. P. Hutchinson, J. Menes, and G. Shapiro, *Phys. Rev. Letters* 9, 516 (1962).
27. V. W. Hughes, D. W. McCohn, K. Ziock, and R. Prepost, *Phys. Rev. Letters* 5, 63 (1960).
28. M. Eckhause, R. T. Siegel, R. E. Welsh, and T. A. Filippas, *Nucl. Phys.* 81, 575 (1966).
29. V. W. Evseev, V. S. Roganov, V. A. Chernogorova, G. G. Myasishcheva, and Yu. V. Obukhov, *Yad. Fiz. (U.S.S.R.)* 8, 741 (1968). (Translation: *Sov. J. Nucl. Phys.* 8, 431 (1969).
30. D. C. Buckle, J. R. Kane, R. T. Siegel, and R. J. Wetmore, *Phys. Rev. Letters* 20, 705 (1968).
31. G. McD. Bingham (private communication) based on UCRL report 10107 (1962).

32. J. E. Russell, *Phys. Rev. A* 1, 742 (1970).
33. D. N. Michael, *Phys. Rev.* 158, 1343 (1967).
34. G. T. Condo, *Phys. Letters* 9, 65 (1964).
35. M. M. Block, J. B. Kopelman, and C. R. Sun, *Phys. Rev.* 140B, 143 (1965).
36. B. D. Orrick, College of William and Mary, Ph.D. Thesis.
37. R. J. Wetmore, D. C. Buckle, J. R. Kane, and R. T. Siegel, *Phys. Rev. Letters* 19, 1003 (1967).
38. J. G. Fetkovitch and E. G. Pewitt, *Phys. Rev. Letters* 11, 290 (1963).
39. T. W. Crane, D. E. Casperson, H. Chang, V. W. Hughes, J. R. Kane, H. F. Kaspar, B. Lovett, A. Schiz, P. Souder, R. D. Stambaugh, and G. Zu. Putlitz, to be published.
40. G. Backenstoss, H. Daniel, K. Jentzsch, H. Koch, H. P. Povel, F. Schmeissner, K. Springer, and R. L. Stearns, *Phys. Letters* 36B, 422 (1971).
41. V. G. Zinov, A. D. Konin, A. I. Mukhin and P. V. Polyakova, *Yad. Fiz. (U.S.S.R.)* 5, 591 (1967). (Translation: *Sov. J. Nucl. Phys.* 5, 420 (1968).
42. W. K. Panofsky, R. L. Aamodt and J. Hadley, *Phys. Rev.* 81, 565 (1951).
43. E. Fermi and E. Teller, *Phys. Rev.* 62, 399 (1947).
44. R. Arit, V. S. Evseev, G. H. Orthlepp, V. S. Roganov, B. M. Sabirov, and H. Haupt, JINR, Dubna, USSR, to be published.
45. P. R. Berington, Data Reduction and Error Analysis for the Physical Sciences, McGraw-Hill (1969).

IX. ACKNOWLEDGEMENTS

The author would like to express appreciation to the following people for their contribution to this work.

Dr. John R. Kane, his advisor, for help and advice in preparing and performing this experiment, and for many useful suggestions during the preparation of the manuscript.

Drs. R. T. Siegel, R. E. Welsh, W. J. Kossler, and J. B. Delos for reading the manuscript and offering many helpful suggestions.

Dr. R. L. Kiefer for reading the manuscript.

His wife, Claire, for careful typing of the manuscript.

Drs. W. J. Wetmore and B. Orrick Sapp for help in preparing and performing the experiment.

Dr. F. R. Crownfield for suggestions concerning the construction of the Helmholtz precession coils.

Mr. S. G. Hummel and the staff of the William and Mary machine shop for the construction of much of the experimental equipment and especially for the modifications to the helium dewar.

The staff of the Space Radiation Effects Laboratory.

The author also wishes to express thanks for financial support to the College of William and Mary and to the National Aeronautics and Space Administration.

X. FIGURES

Figure Captions

1. Experimental Arrangement - He Counter in Place.
2. Experimental Arrangement - Targets Other than He.
3. a. Bending Magnet Curve
b. Muon Differential Range Curve and Decay Event ("STORES") Range Curve.
4. Electronic Logic. For Targets Other than Liquid He.
5. Cross Section of He Target - Counter.
6. Sapphire Window - Vacuum Seal Detail.
7. Data for Typical High Field C Run and Summed High Field He Runs. The plotted points are two channel sums.
8. H₂O Data, High Fields (runs 112 and 114). Plotted points are the values of the expression
$$\bar{N}(t) = \frac{(\bar{Y} - B) \cdot e^{+\lambda t}}{N_0},$$
where \bar{Y} is the average of the data points Y_i for an 8 channel interval, and t is the time at the center of each interval. A C data run (15) is included for comparison.
9. Paraffin Data - High Fields (runs 103, 113), and C Run 102. (cf. Figure 8.).
10. Pilot B (Plastic Scintillant) Data, High Field (run 14), Low Field (run 18) and C Run 13. (cf. Figure 8).
11. Polyethylene Data, High Field (run 12), Low Field (run 19), and C run 11. (cf. Figure 8).
12. Toluene Data, High Field (run 110), Low Field (run 120), and C run 117. (cf. Figure 8).
13. Liquid O₂ Data, High Field (run 118), Low Field (run 119), and C run 117. (cf. Figure 8).

14. Liquid He Data, High Fields (runs 24, 26, 28 summed), Low Fields (runs 25, 27 summed), and C run 22. (cf. Figure 8). The C target was located inside the He target cylinder.
15. High Field Frequency Resonance Plots for C (run 107), Pilot B (109), Toluene (115), Paraffin (113), and Polyethylene (104). The result for asymmetry a' is plotted vs. the value of ω used in the fitting procedure.
16. Frequency and Phase Angle Contour Plot. A single C run (117) was analyzed for the best value of asymmetry a' for a range of values of both parameters ω , and ϕ . The asymmetry results are the contours.
17. High Field Frequency Resonance Plots for Liquid He (run 26), Mg (108), H₂O (112), and Liquid O₂ (118). (cf. Figure 15).
18. Time Dependence of Asymmetry - High Fields H₂O and C. The results of analysis for the parameter a' are plotted vs. the first channel (I1) used in the fitting procedure for a fixed data window of 80 channels or 1.6 μ sec. The C runs are plotted singly. The results for H₂O are the means of the results from each for the same first channel.
19. Time Dependence of Asymmetry - High Fields. Toluene and Paraffin Data. Results plotted are means of all runs of the same target. (cf. Figure 18).
20. Time Dependence of Asymmetry - High Fields. Pilot B and Polyethylene Data. (cf. Figure 18).
21. Low Field Frequency Resonance Plots for C (3-23), He (25), Pilot B (18), Toluene (120) and Polyethylene (19). (cf. Figure 15).

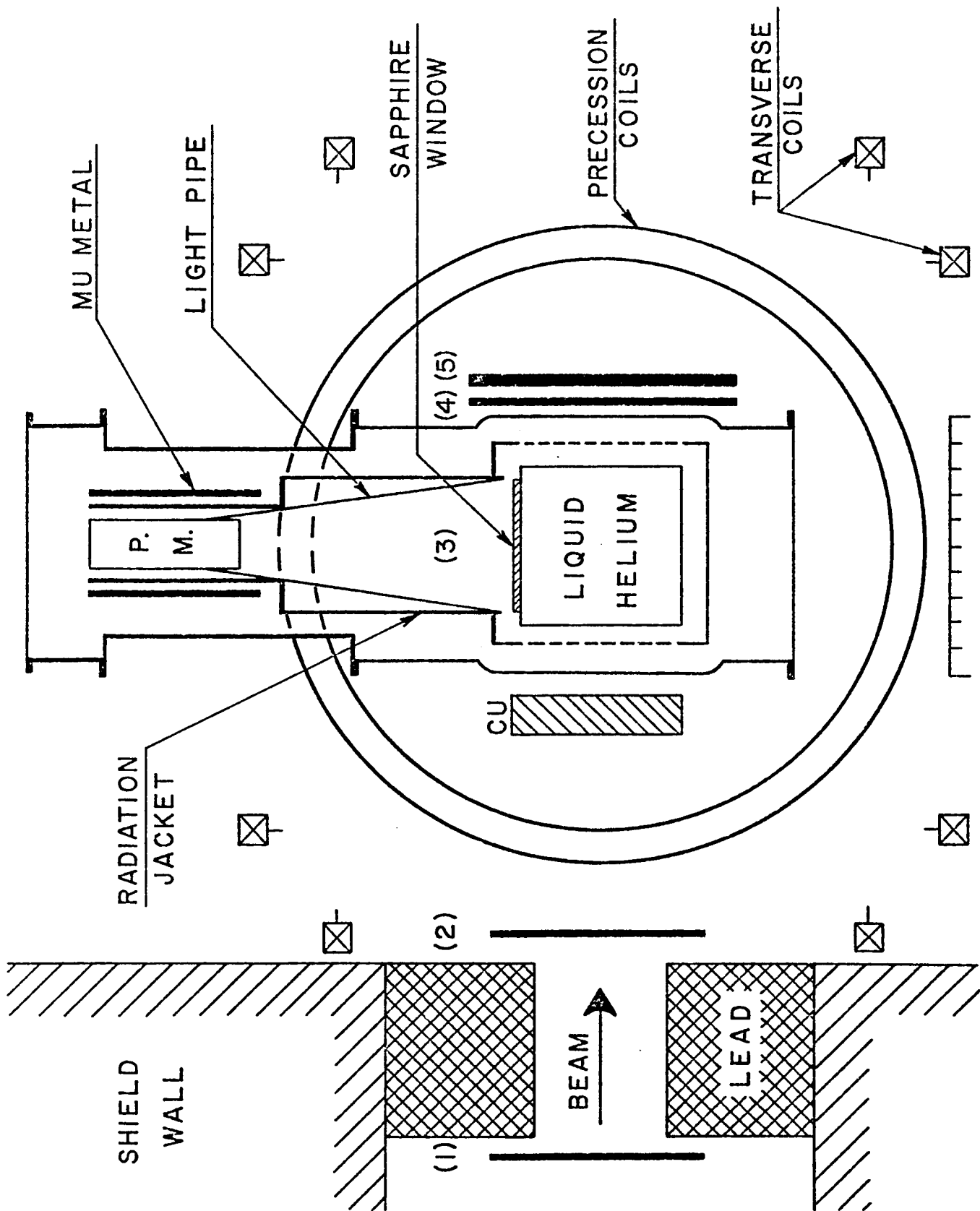


Figure 1

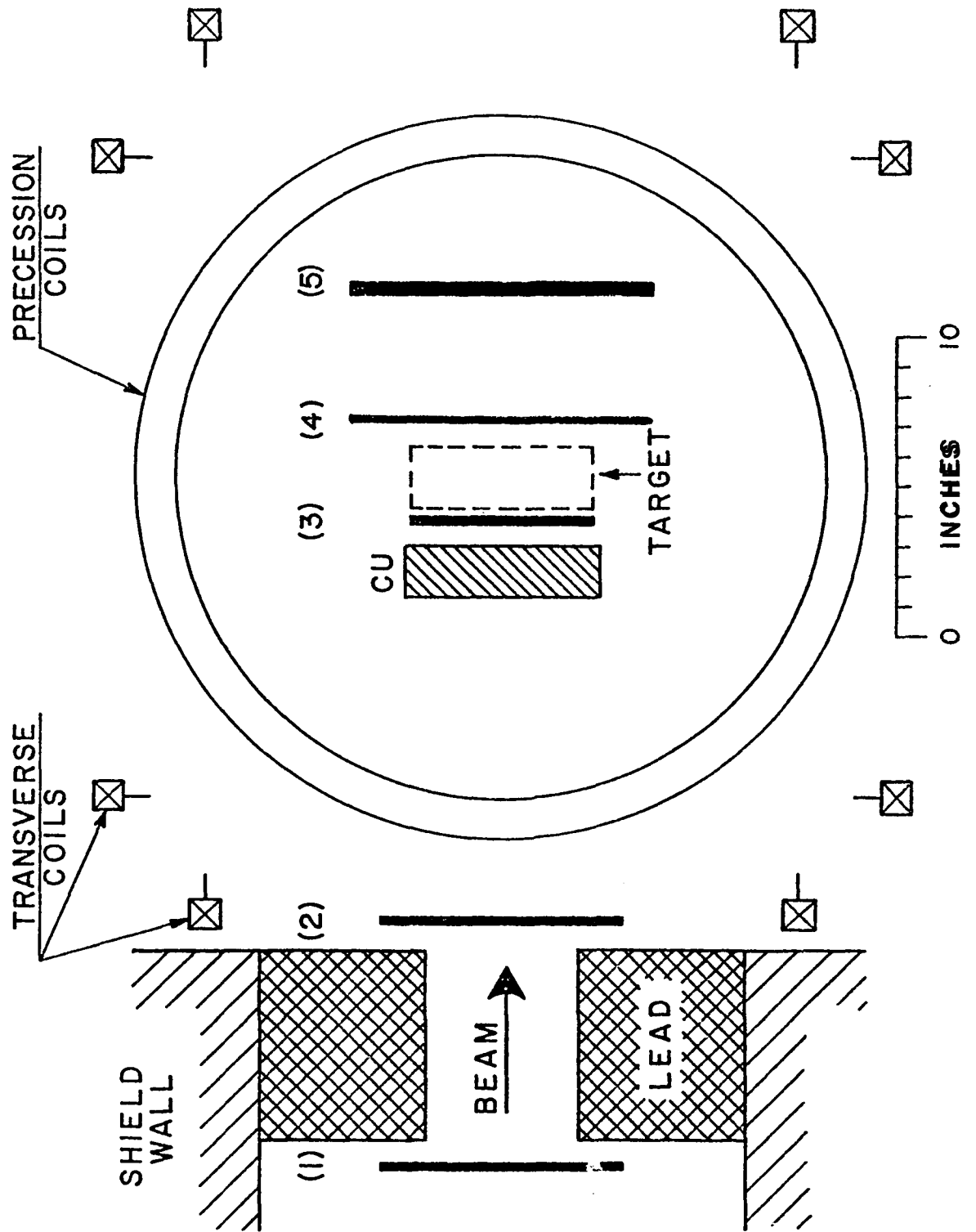


Figure 2

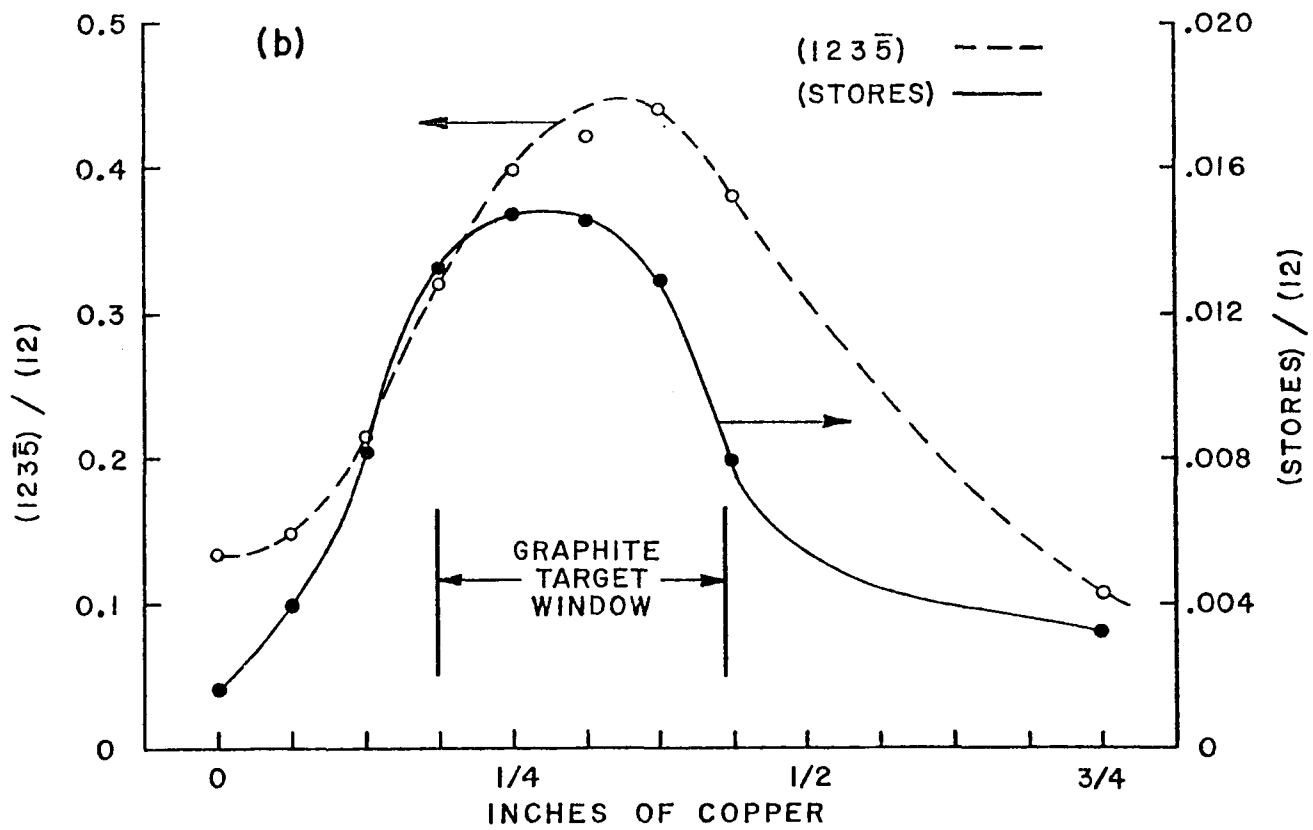
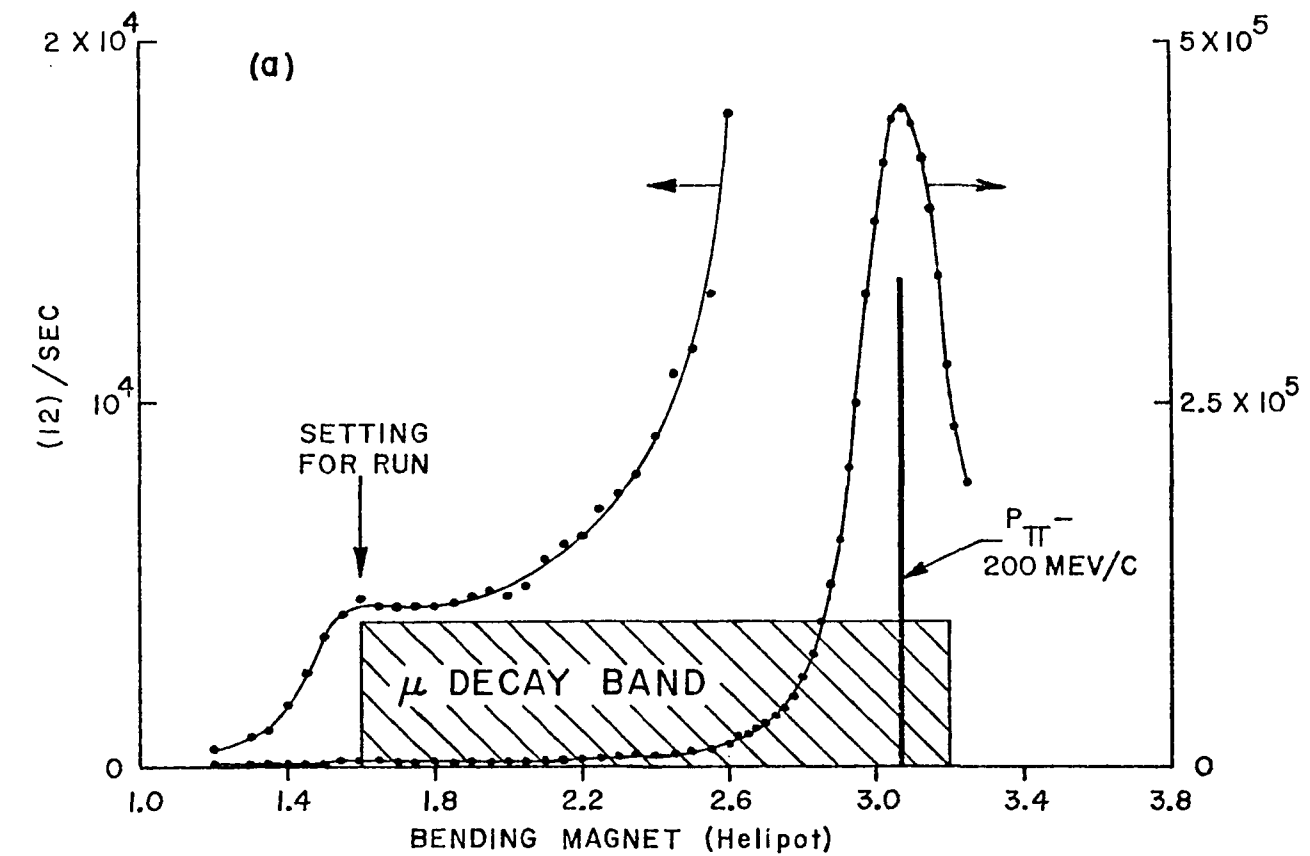


Figure 3

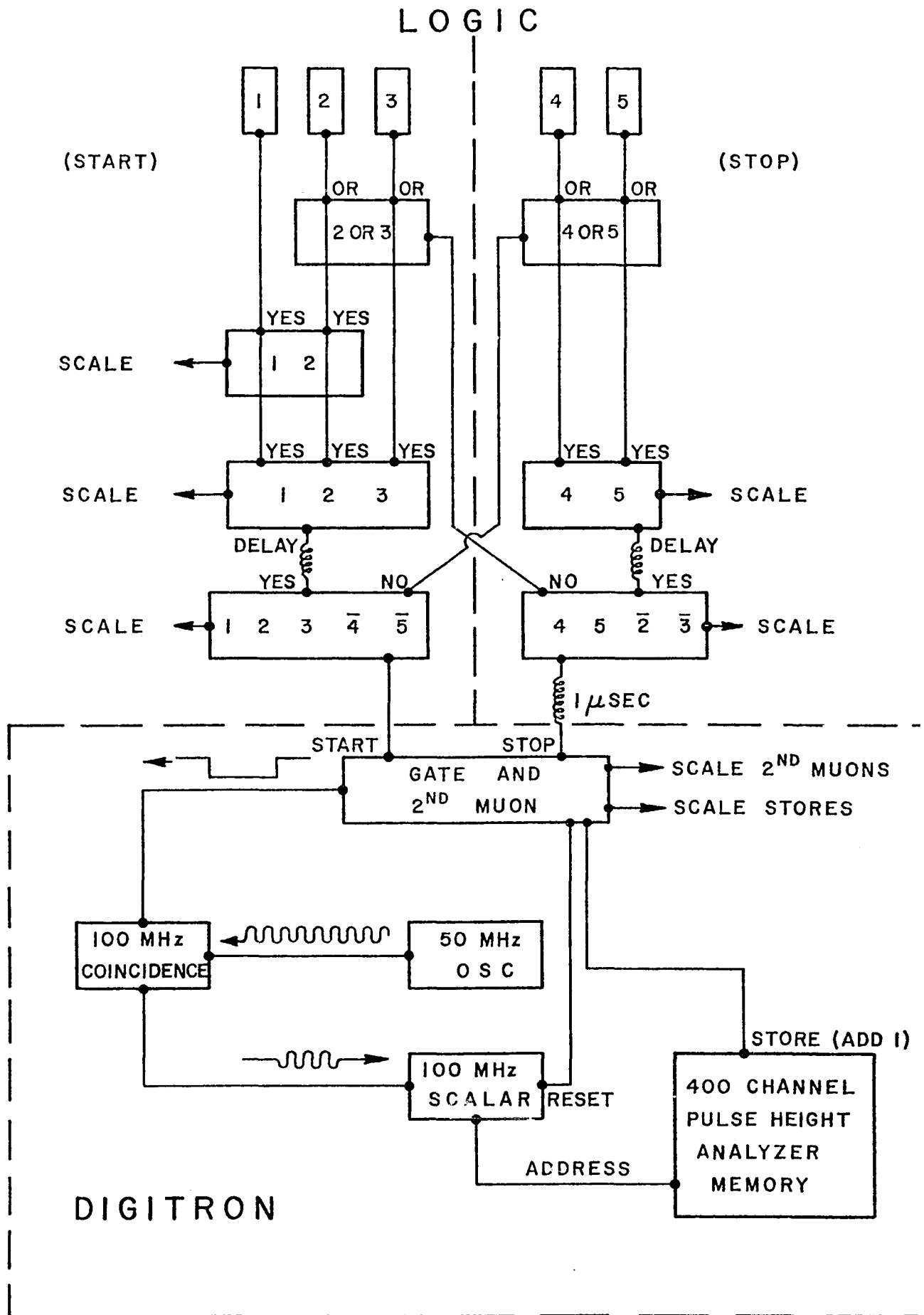


Figure 4

HELIUM TARGET ASSEMBLY

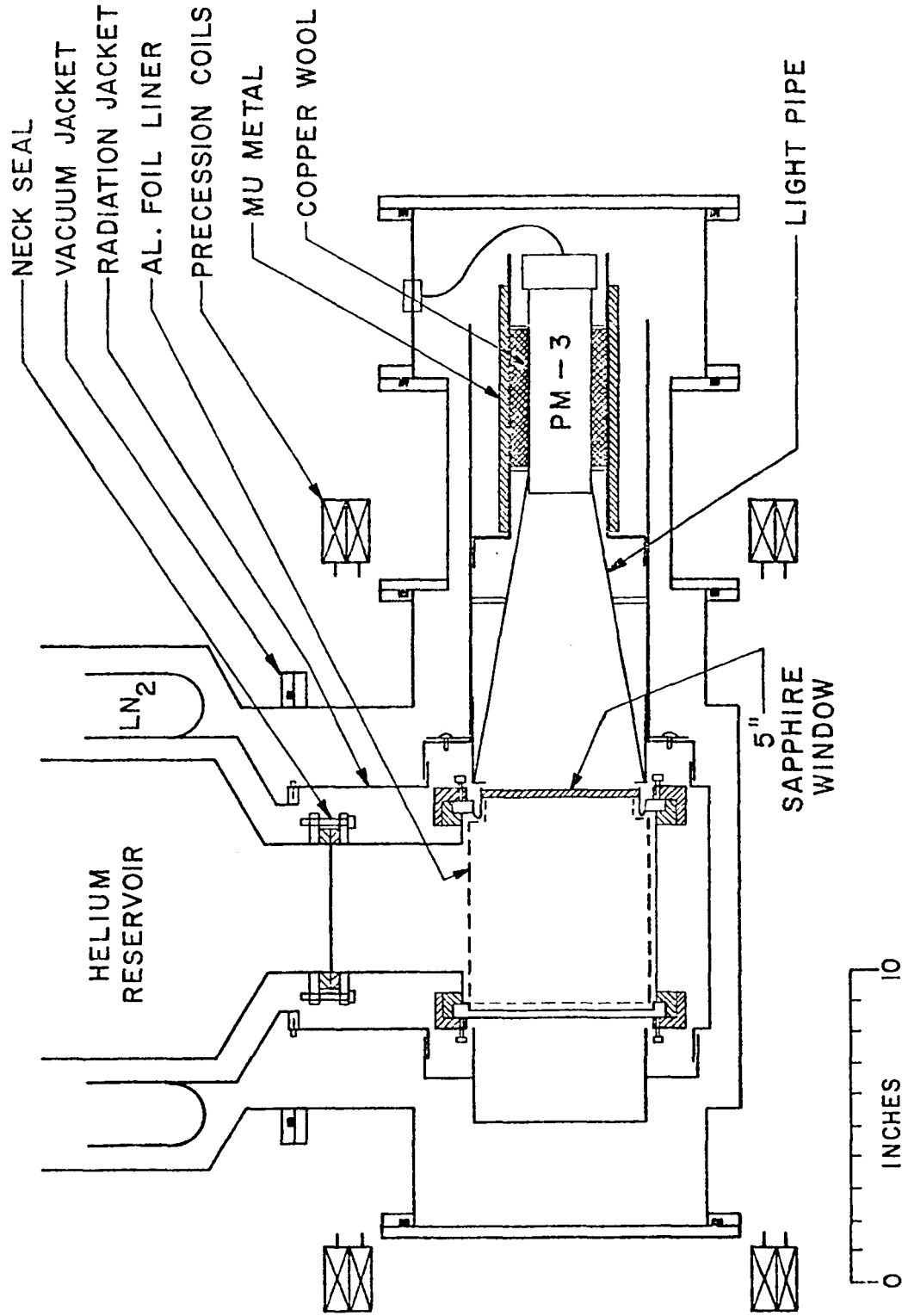


Figure 5

SAPPHIRE WINDOW ASSEMBLY VACUUM SEAL DETAIL

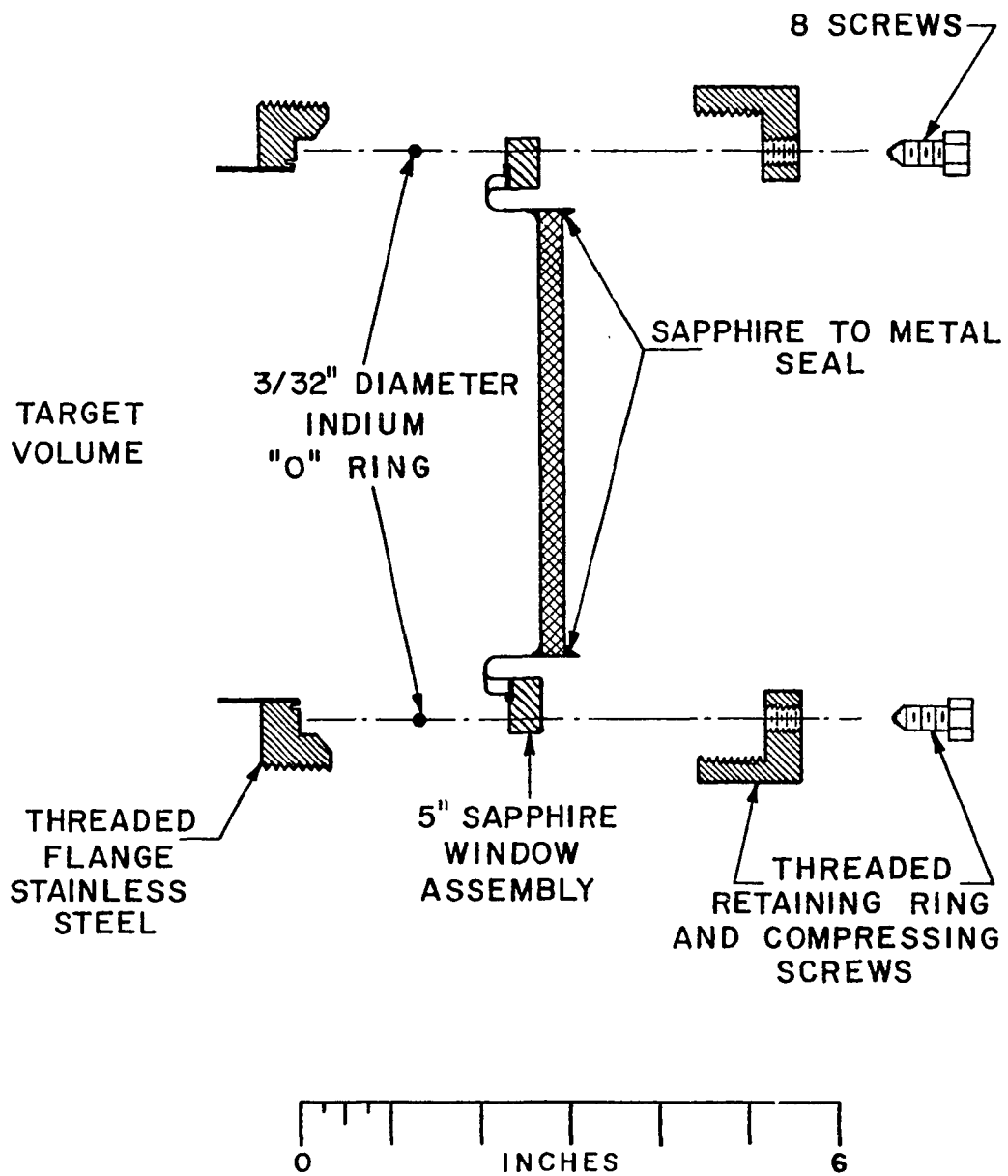


Figure 6

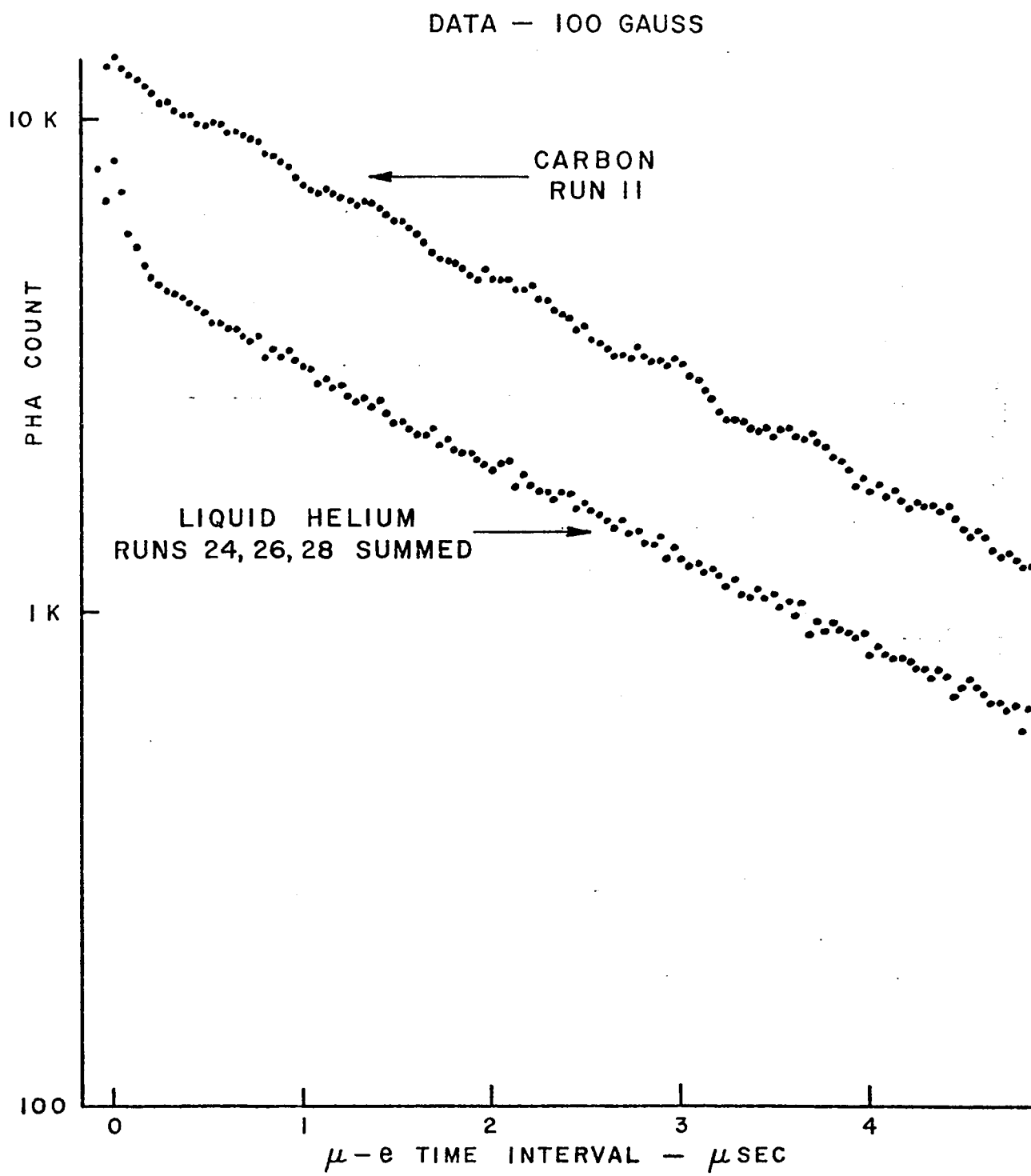


Figure 7

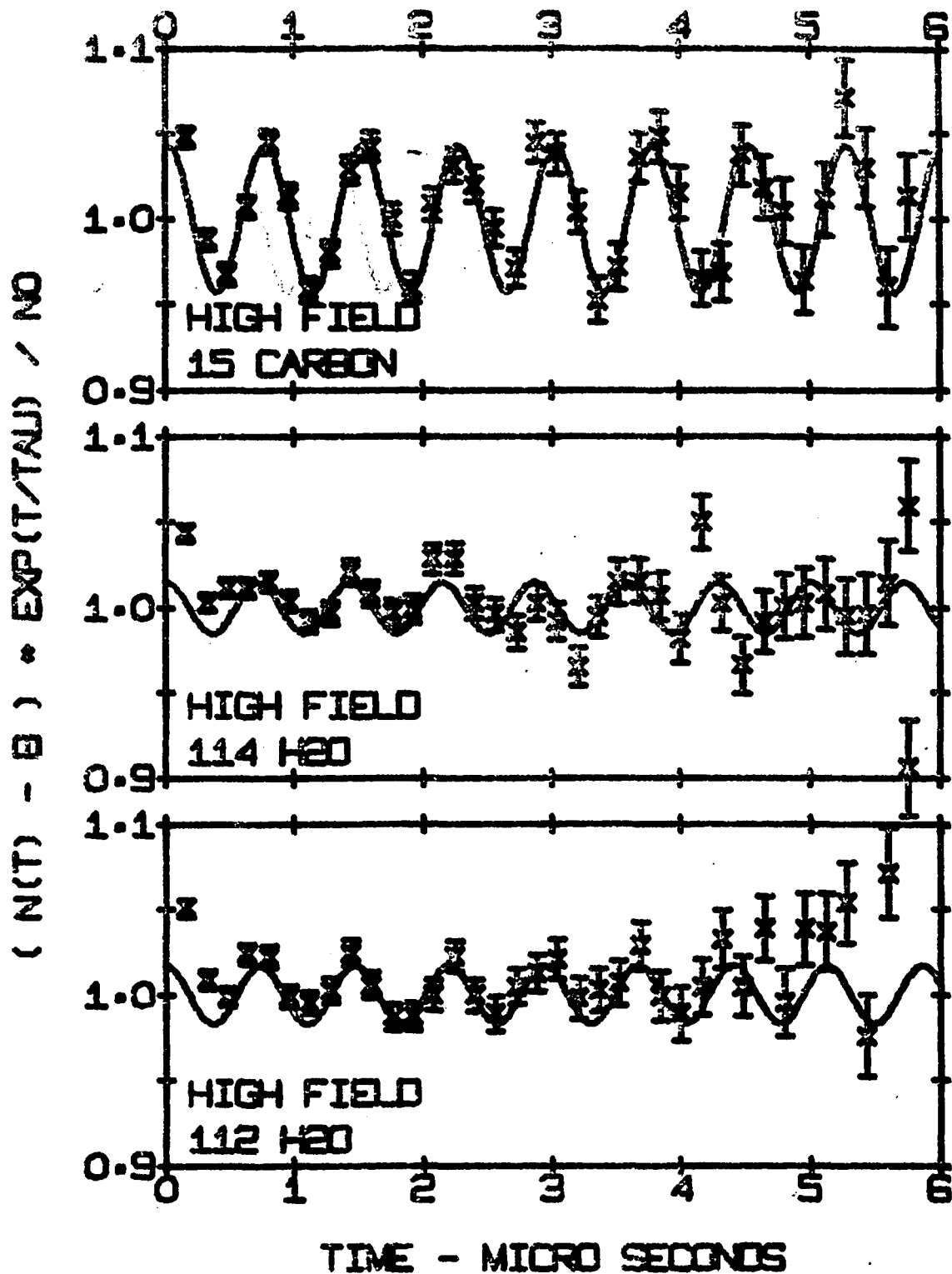


Figure 8

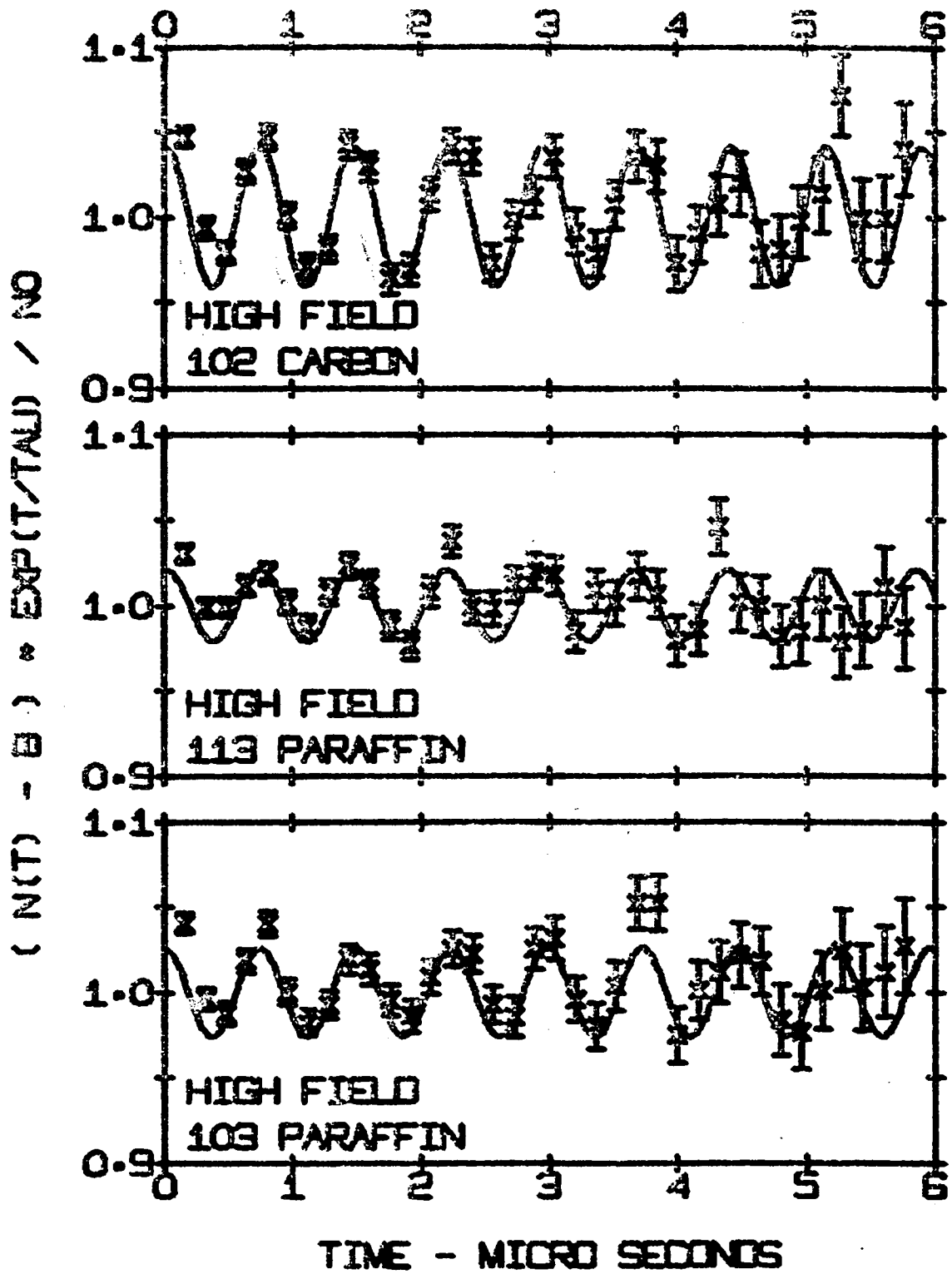


Figure 9

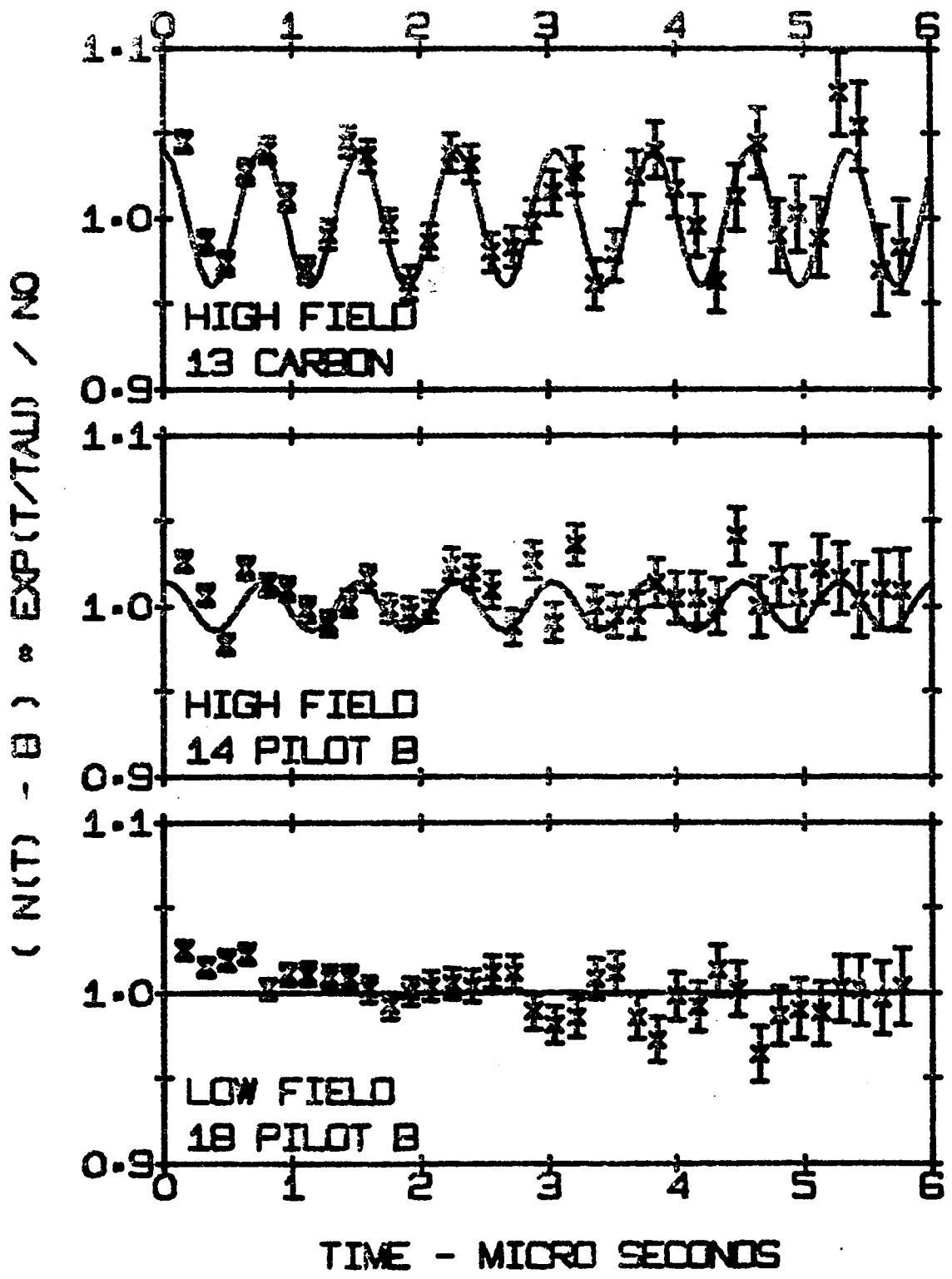


Figure 10

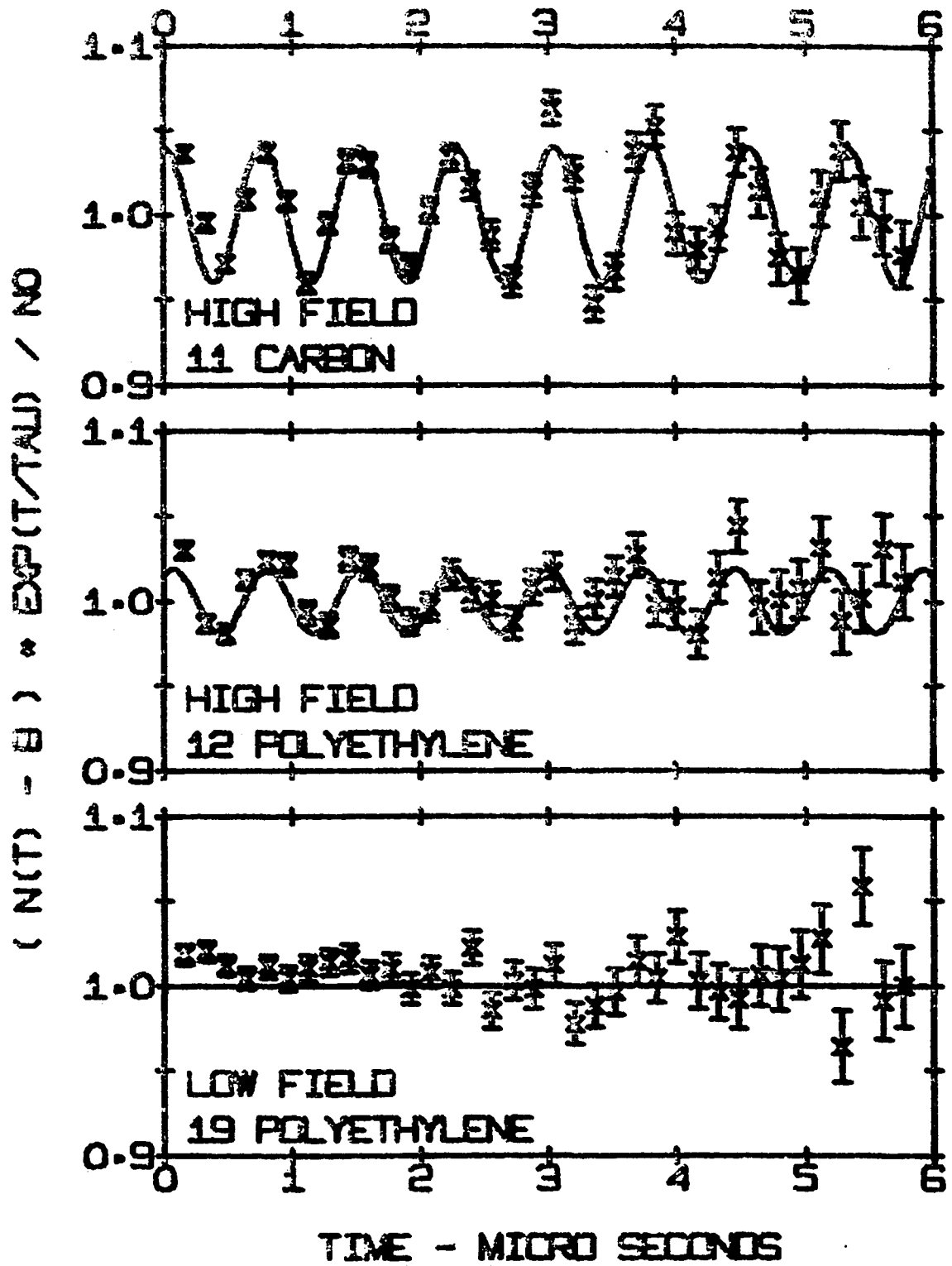


Figure 11

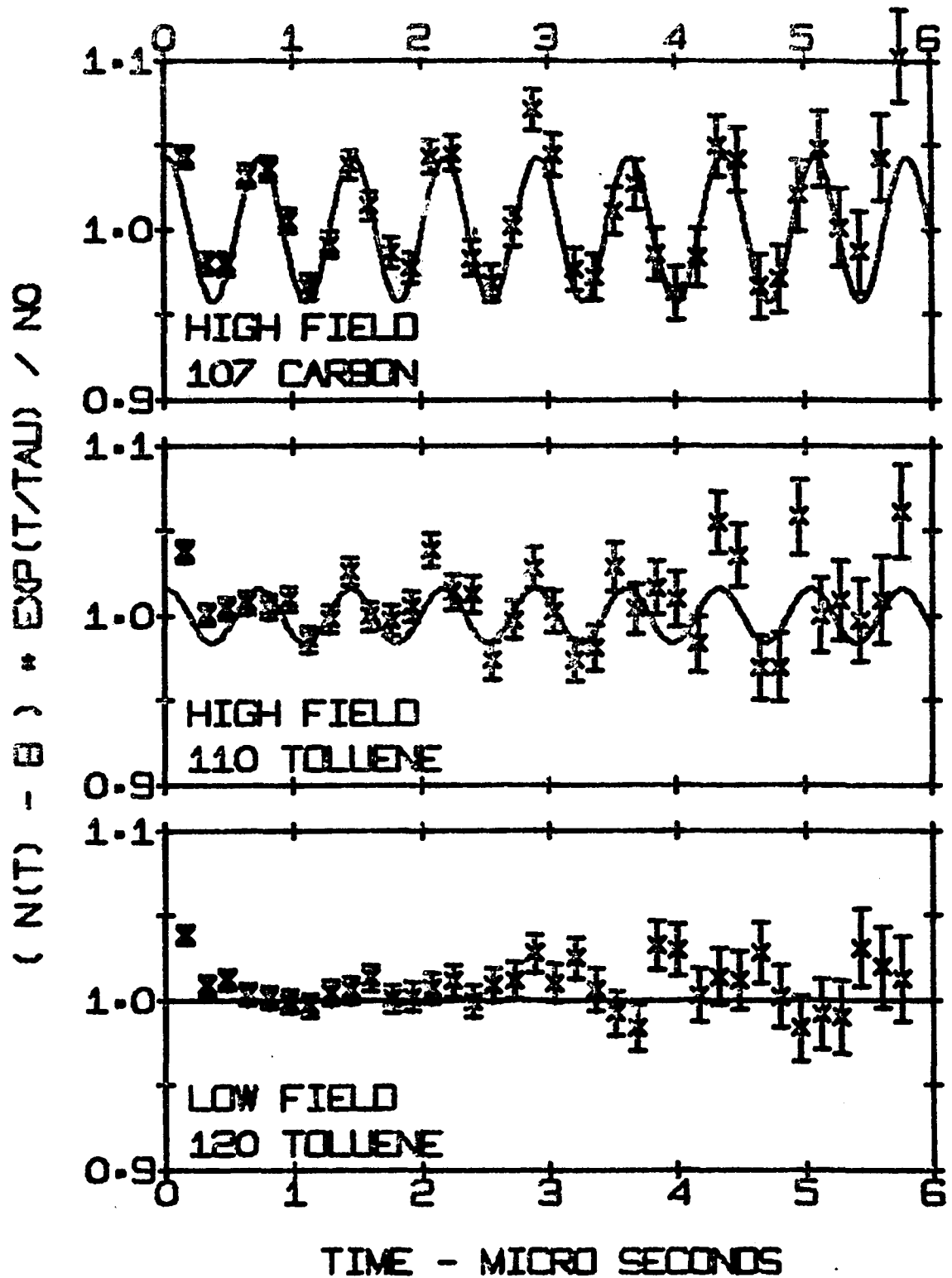


Figure 12

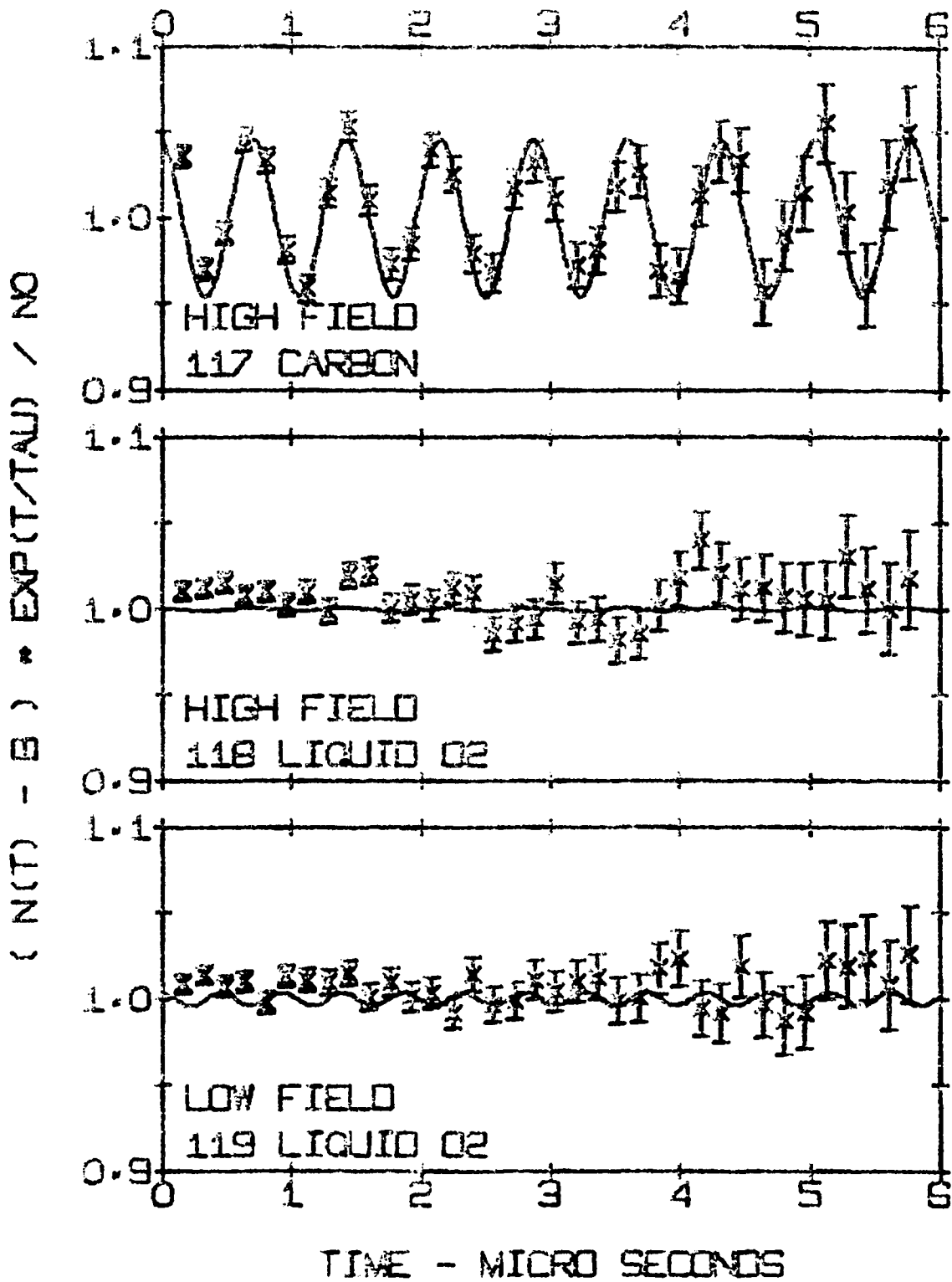


Figure 13

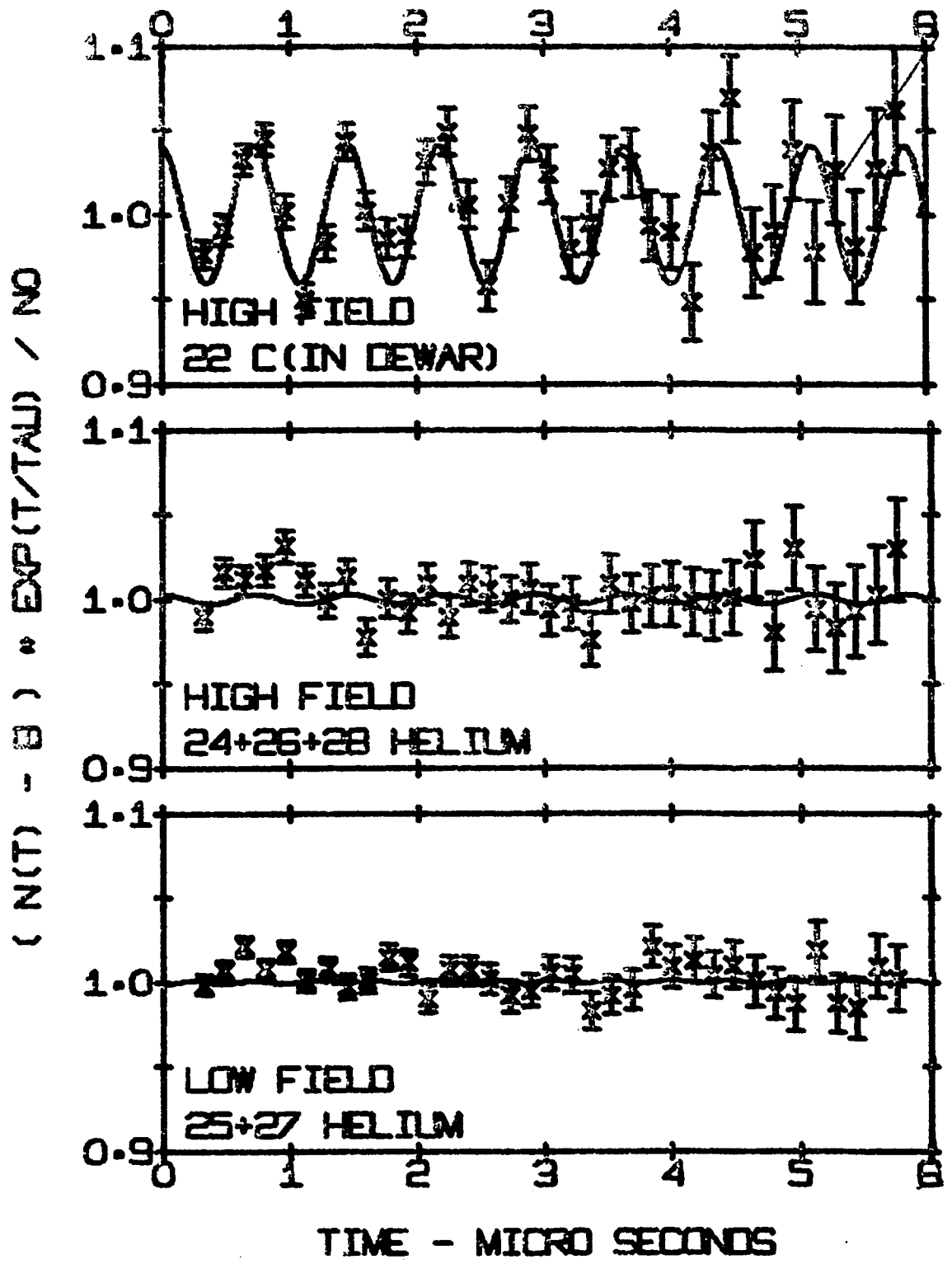
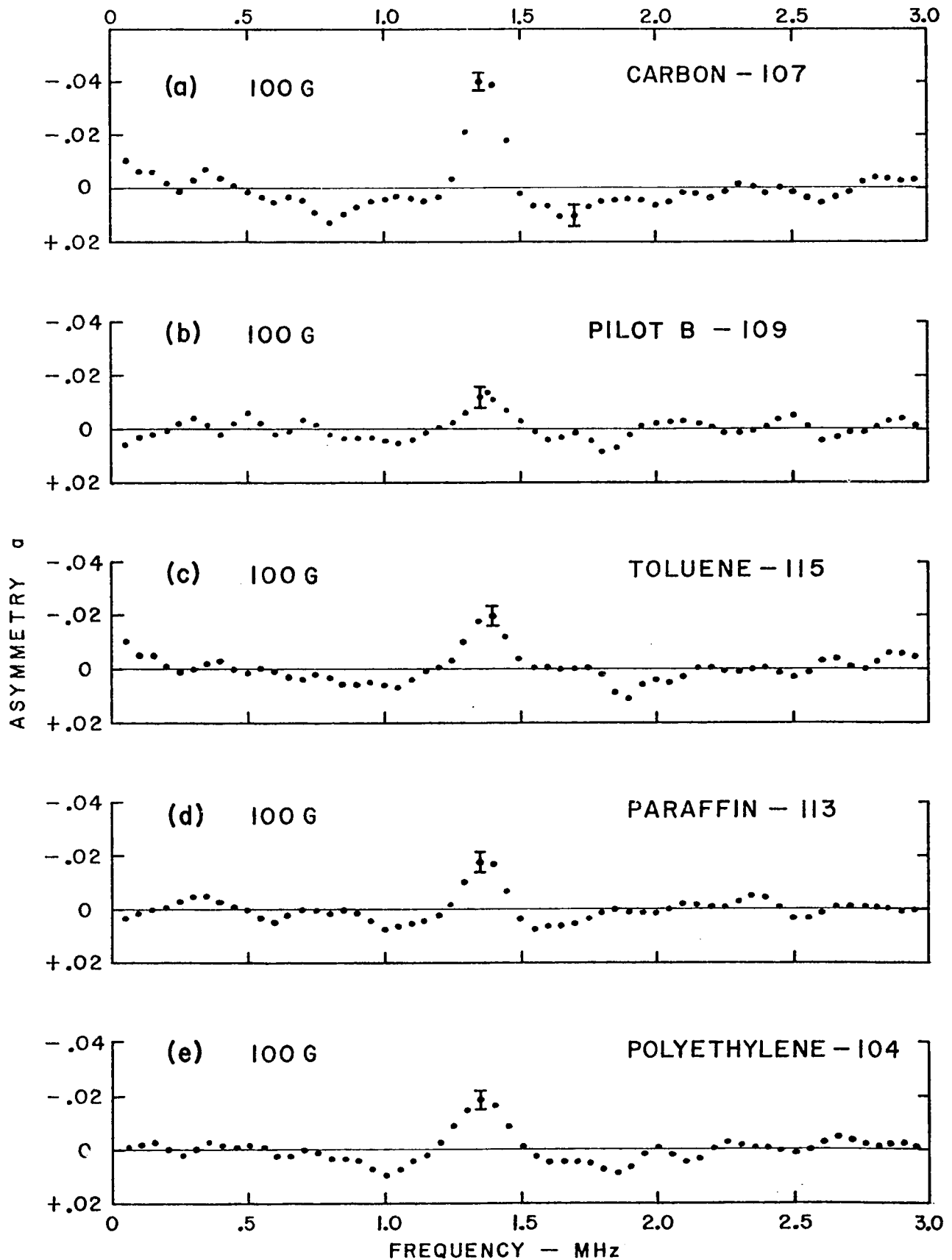


Figure 14



DATA WINDOW = CHANNELS 20 - 220

Figure 15

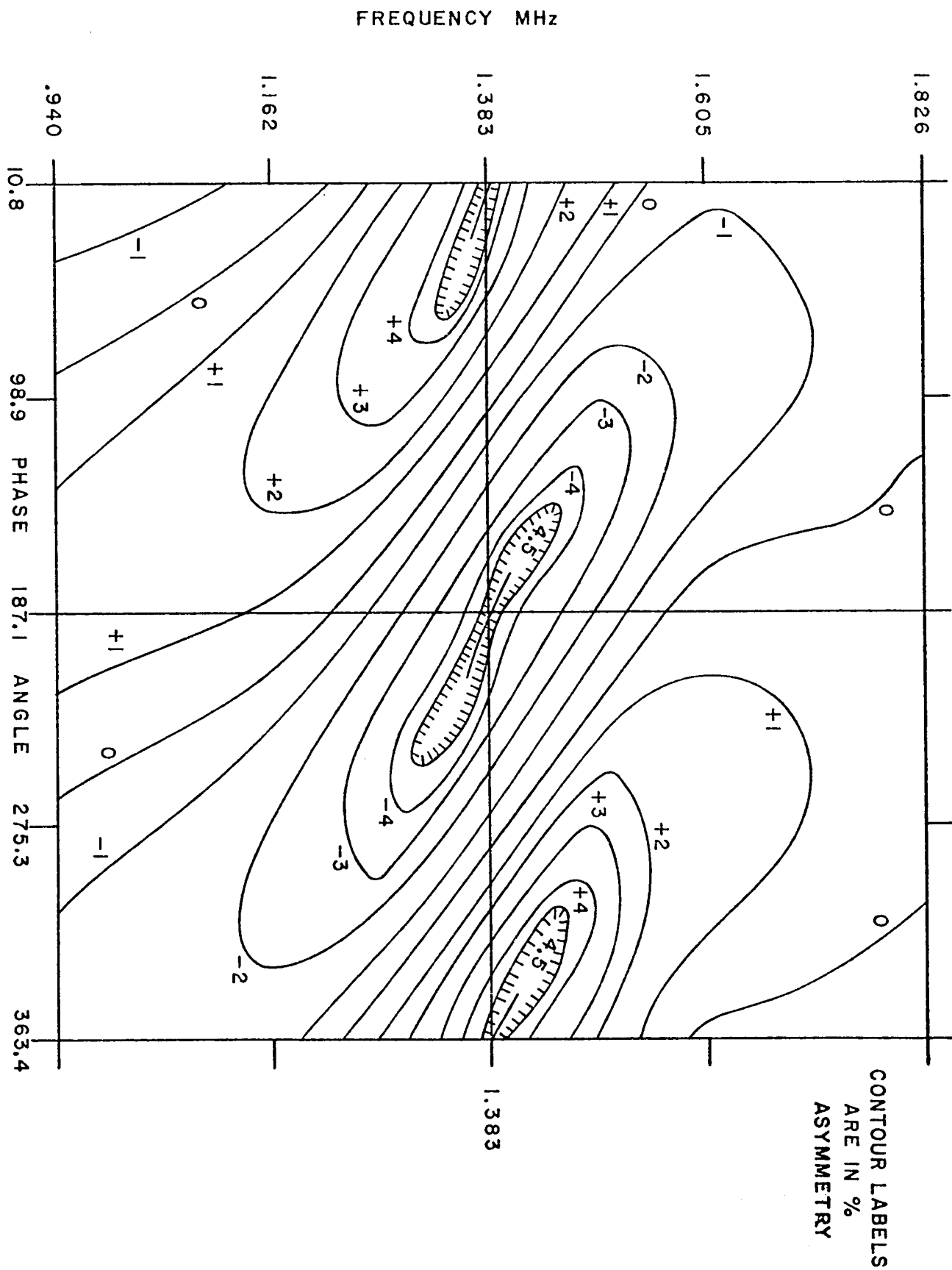


Figure 16

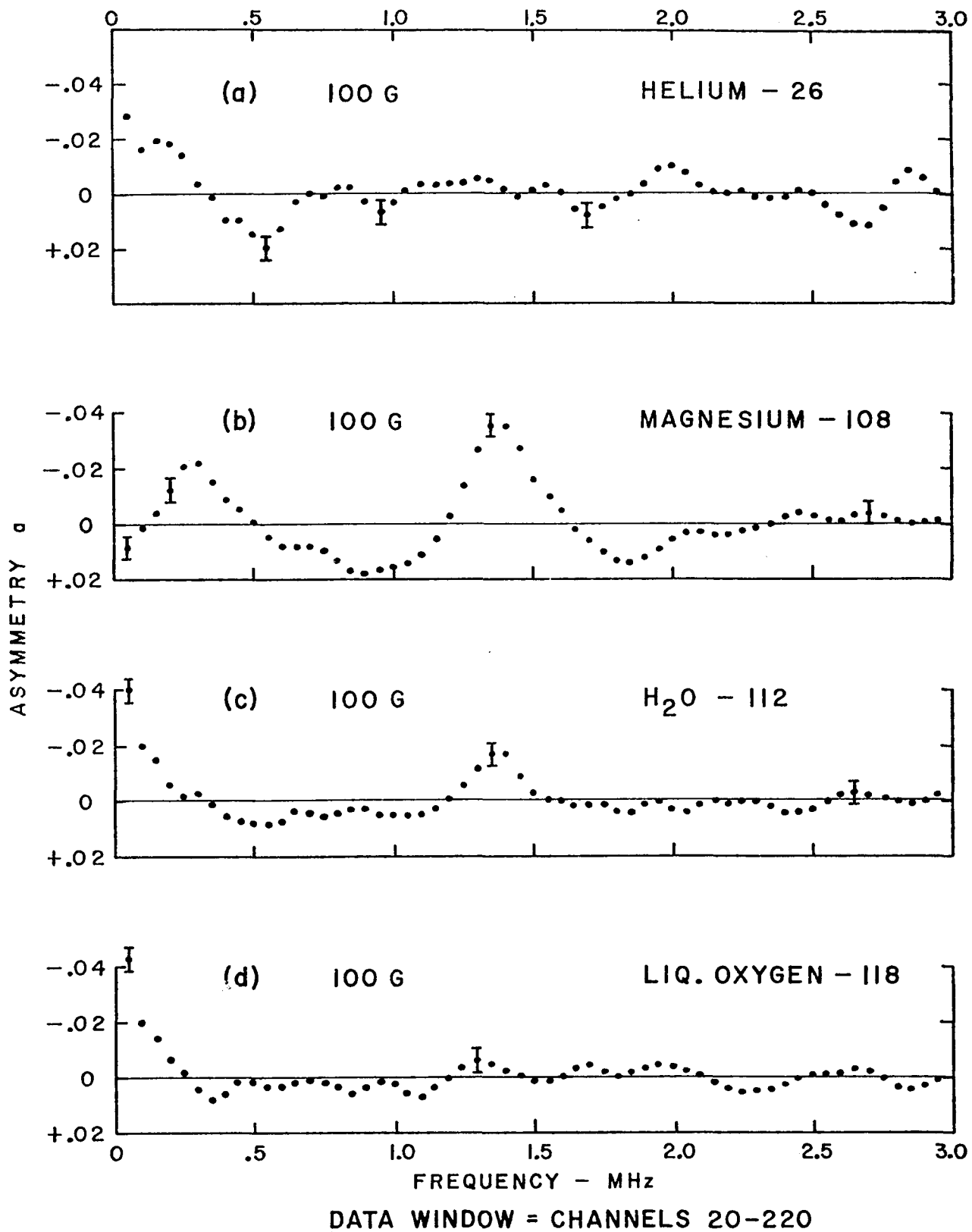


Figure 17

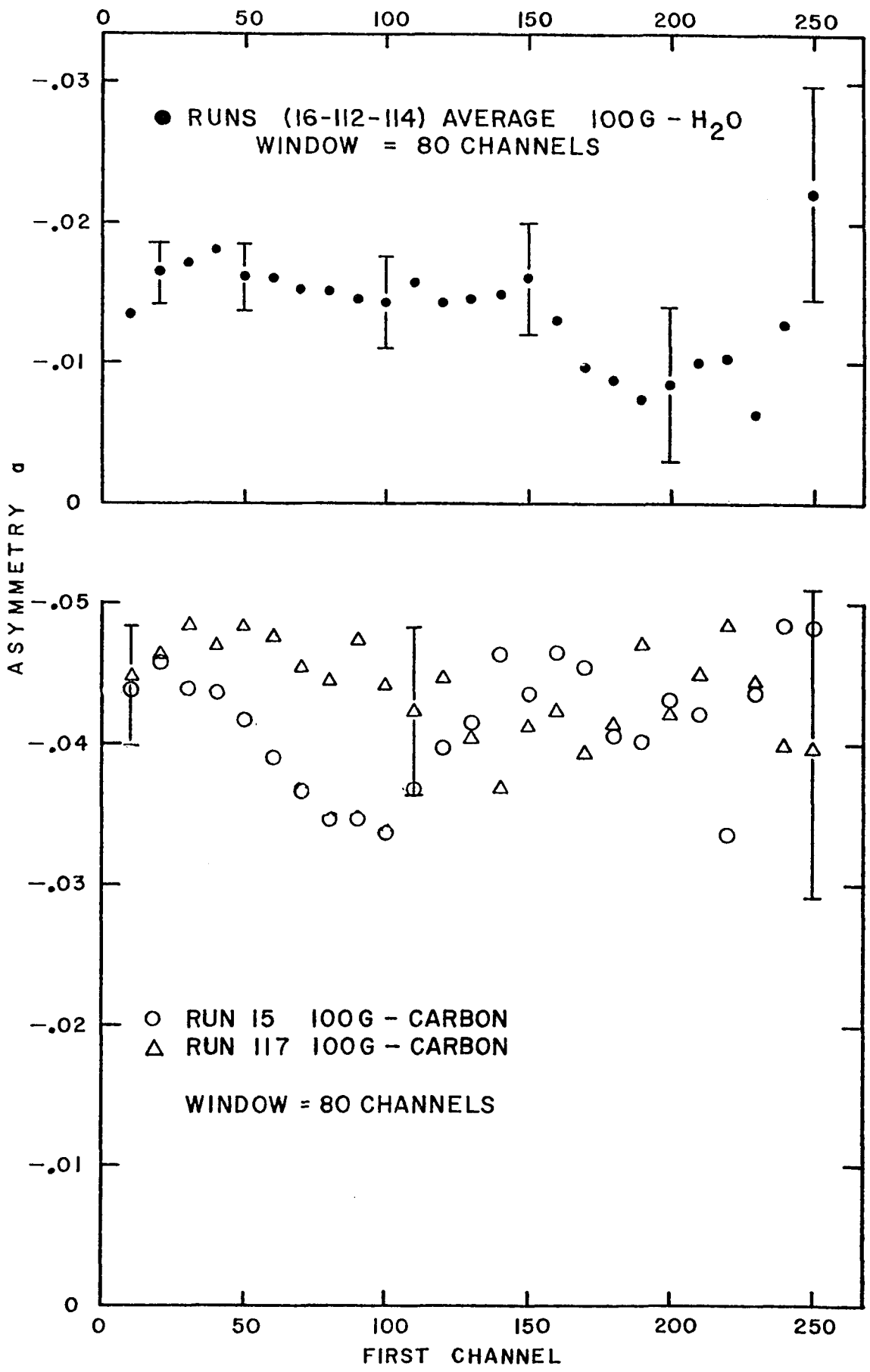


Figure 18

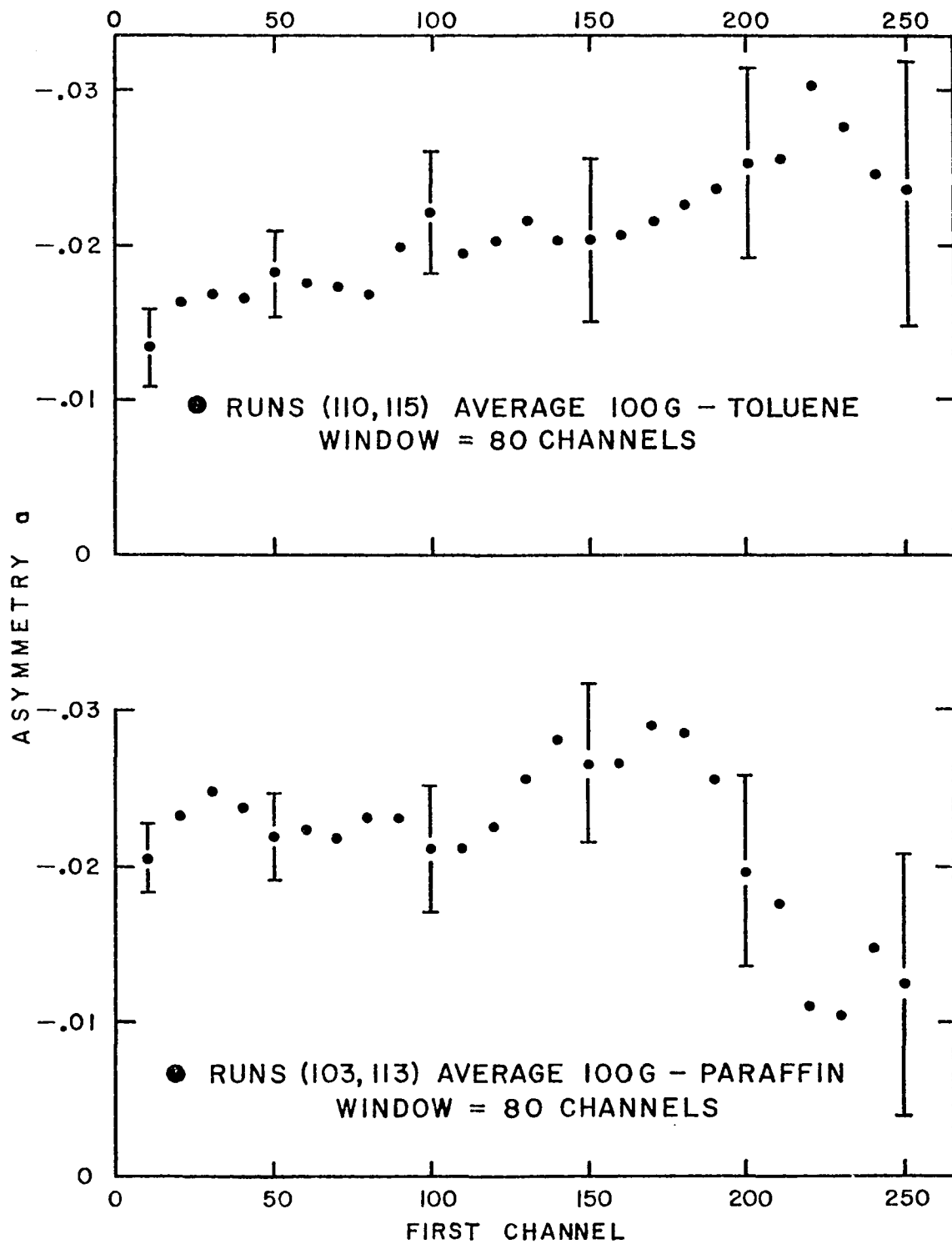


Figure 19

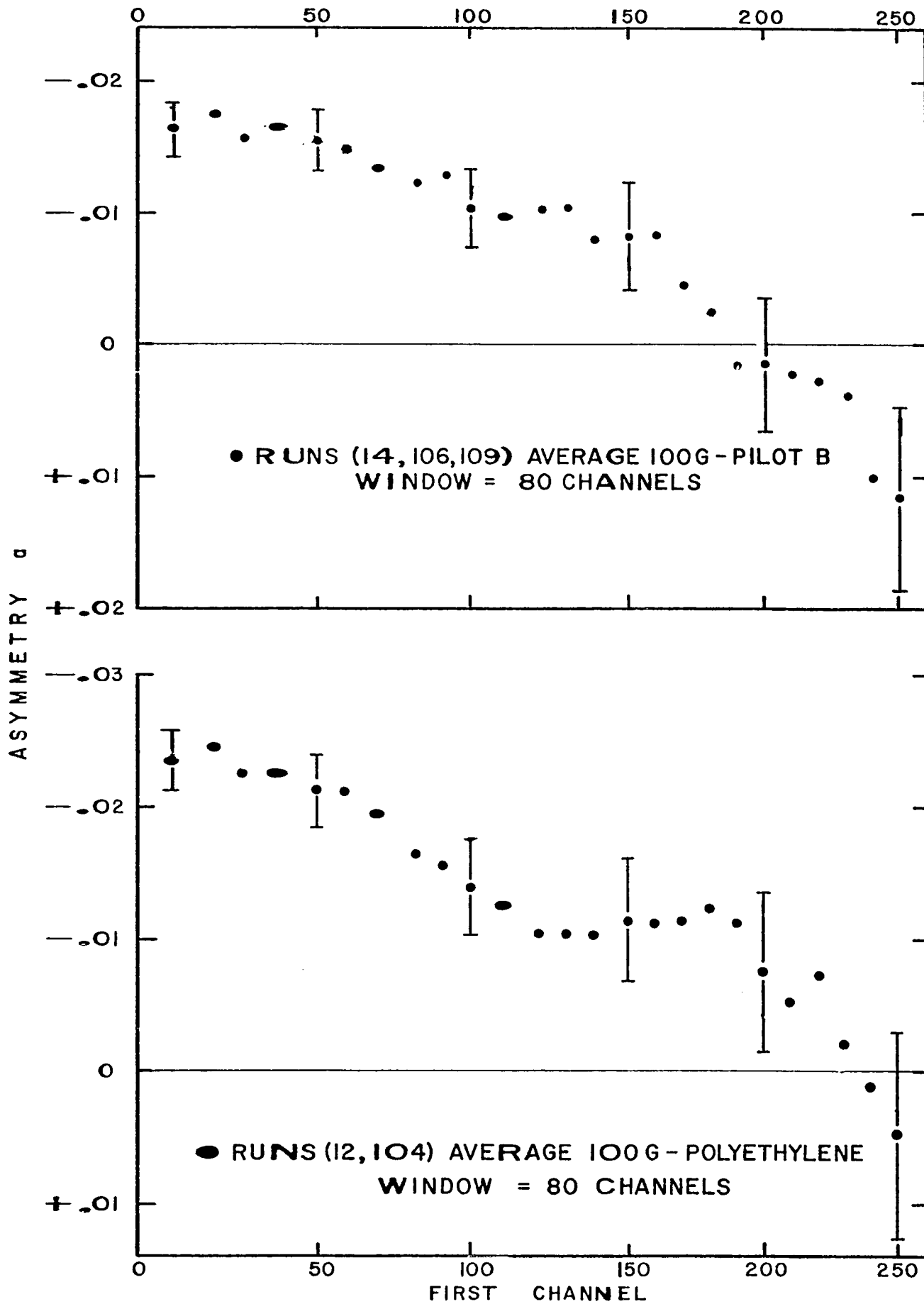
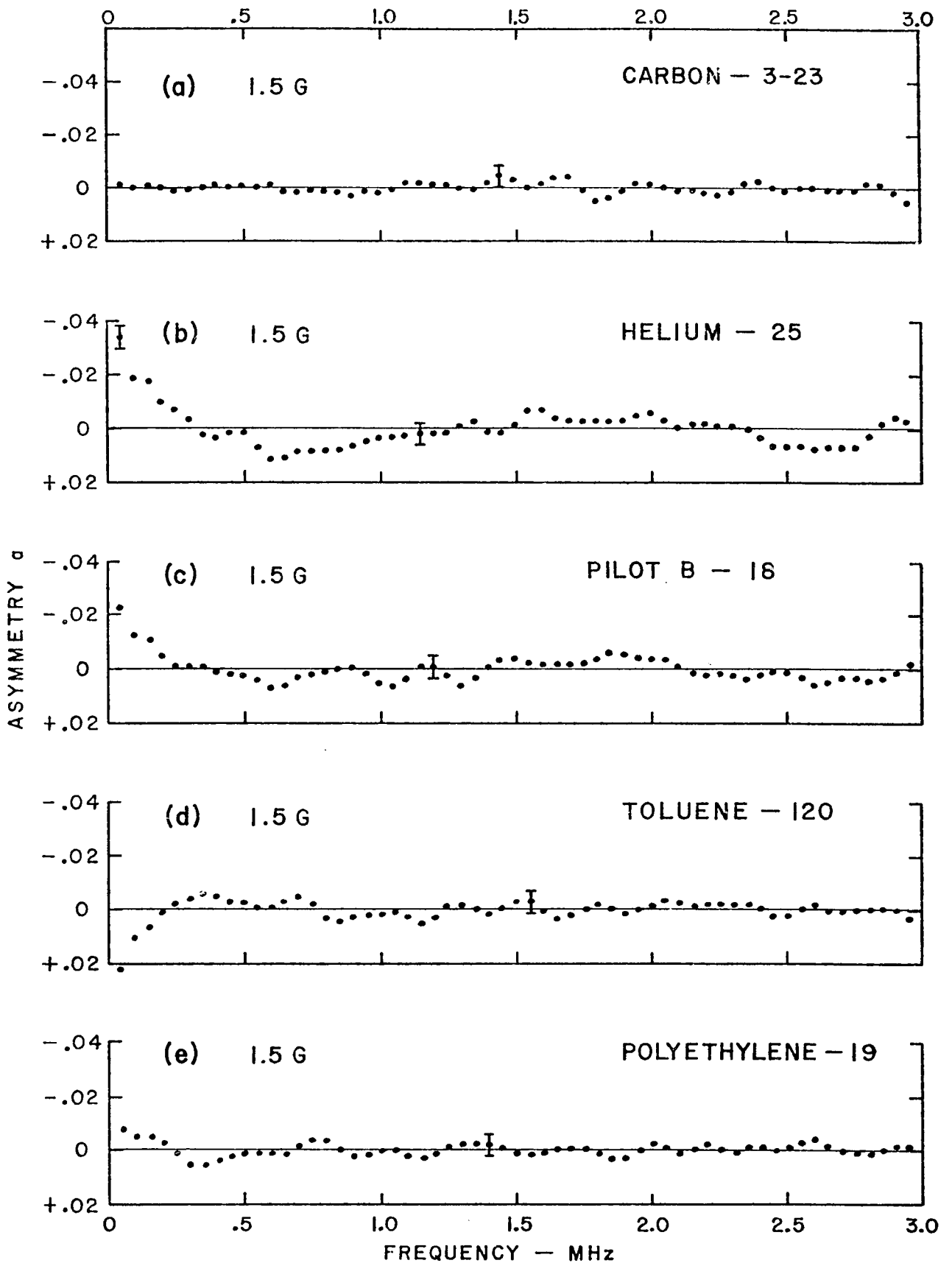


Figure 20



DATA WINDOW = CHANNELS 20-220

Figure 21